The Existence and Stability of Spike Equilibria in the One-Dimensional Gray-Scott Model: The Low Feed Rate Regime

Theodore Kolokolnikov*, Michael J. Ward†, Juncheng Wei‡

Abstract

In a singularly perturbed limit of small diffusivity ε of one of the two chemical species, equilibrium spike solutions to the Gray-Scott model on a bounded one-dimensional domain in the low feed-rate regime are constructed asymptotically using the method of matched asymptotic expansions. Two classes of such equilibrium solutions are constructed: symmetric spike patterns where the spikes have equal heights, and asymmetric patterns where each spike can have two different heights. The solution branches of symmetric k-spike patterns are found to have a saddle-node bifurcation structure in terms of certain non-dimensional parameters in the Gray-Scott model. To determine the stability of these branches of symmetric spike patterns, it is shown that there are two classes of eigenvalues in the spectrum of the linearization that need to be analyzed: the large eigenvalues for which $\lambda = O(1)$ as $\varepsilon \to 0$, and the small eigenvalues for which $\lambda = O(\varepsilon^2)$ as $\varepsilon \to 0$. Precise conditions in terms of the non-dimensional parameters for the stability of symmetric k-spike equilibrium solutions with respect to both classes of eigenvalues are obtained. For a symmetric k-spike pattern with $k > 1$, it is shown that an instability with respect to the large eigenvalues leads either to a competition instability, whereby certain spikes in a sequence are annihilated, or an oscillatory instability (typically synchronous) of the spike amplitudes as a result of a Hopf bifurcation. In contrast, an instability with respect to the small eigenvalues leads to a slow drift of spike layer locations away from their equilibrium values. As a control parameter is increased we show that such an instability, which results in the birth of a traveling wave, can occur as a result of a Hopf bifurcation. Finally, we show that there is a precise and surprising equivalence between spectral properties of the Gray-Scott model in the low feed-rate regime and the Gierer-Meinhardt model of morphogenesis.

*Department of Mathematics, University of British Columbia, Vancouver, Canada V6T 1Z2

†Department of Mathematics, University of British Columbia, Vancouver, Canada V6T 1Z2, (corresponding author)

‡Department of Mathematics, Chinese University of Hong Kong, New Territories, Hong Kong

1 Introduction

We study the existence and stability of spike patterns in the one-dimensional Gray-Scott model in the low feed-rate regime. The Gray-Scott system, introduced in [10], models an irreversible reaction involving two reactants in a gel reactor, where the reactor is maintained in contact with a reservoir of one of the two chemicals in the reaction. In nondimensional variables, this system can be written as

$$V_T = D_v V_{XX} - (F+k)V + UV^2\,, \qquad 0 < X < L\,, \quad T > 0\,, \tag{1.1a}$$

$$U_T = D_u U_{XX} + F(1-U) - UV^2\,, \qquad 0 < X < L\,, \quad T > 0\,, \tag{1.1b}$$

$$U_X = V_X = 0\,, \qquad X = 0, L\,. \tag{1.1c}$$

Here $D_u > 0$, $D_v > 0$ are the constant diffusivities, $F > 0$ is the feed rate, and $k > 0$ is a reaction-time constant. For various ranges of these parameters, (1.1) and its two-dimensional counterpart, are known to posses a rich solution structure including the existence of stable standing pulses, the propagation of traveling waves, pulse-replication behavior, and spatio-temporal chaos (cf. [2]–[5], [7], [15], [17], [18], [26], [29], [30], [31], [32], [33], [34], and [36]).

We will analyze (1.1) in the singularly perturbed limit where D_v/D_u is asymptotically small. In our formulation, it is convenient to introduce the change of variables

$$v = V/\sqrt{F}\,, \qquad x = -1 + 2X/L\,, \qquad t = (F+k)T\,. \tag{1.2}$$

This leads to the dimensionless system

$$v_t = \varepsilon^2 v_{xx} - v + Auv^2\,, \qquad -1 < x < 1\,, \quad t > 0\,, \tag{1.3a}$$

$$\tau u_t = Du_{xx} + (1-u) - uv^2 \qquad -1 < x < 1\,, \quad t > 0\,, \tag{1.3b}$$

$$v_x(\pm 1, t) = u_x(\pm 1, t) = 0\,; \qquad v(x,0) = v_0(x)\,, \qquad u(x,0) = u_0(x)\,. \tag{1.3c}$$

Here $A > 0$, D, $\tau > 1$, and $\varepsilon \ll 1$, are defined in terms of D_u, D_v, L, F, and k, by

$$D \equiv \frac{4D_u}{FL^2}\,, \qquad \varepsilon^2 \equiv \frac{4D_v}{L^2(F+k)}\,, \qquad \tau \equiv \frac{F+k}{F}\,, \qquad A \equiv \frac{\sqrt{F}}{F+k}\,. \tag{1.4}$$

The non-dimensional system (1.3) is particularly convenient in that it shows that, for $\varepsilon \ll 1$, the construction of equilibrium solutions depends only on the two parameters A and D, while the reaction-time constant $\tau > 1$ only influences the stability of these solutions. The parameter D measures the effect of the finite domain and the strength of the inter-spike interactions. For a k-spike pattern,

the finite domain and the inter-spike interactions are only significant when $k\sqrt{D} = O(1)$. When $k\sqrt{D} \ll 1$, an equilibrium k-spike pattern for (1.3) is composed, to leading order, of k identical copies of a one-spike solution for the infinite-line problem, where (1.3) is defined on $-\infty < x < \infty$.

We will analyze the existence and stability of equilibrium k-spike patterns for (1.3) in the limit $\varepsilon \to 0$ and for $D = O(1)$, where the finite domain and inter-spike coupling cannot be neglected. There are three regimes for A where different behaviors are obtained. For the parameter range $A = O(\varepsilon^{1/2})$, referred to here as the low feed-rate regime, there is a saddle-node bifurcation structure of equilibrium k-spike patterns, and we find that the stability of these solutions depends intricately on A, D, and τ. For the intermediate regime, where $O(\varepsilon^{1/2}) \ll A \ll O(1)$, there are certain scaling laws in terms of a universal nonlocal eigenvalue problem that determine the stability of equilibrium spike patterns. In this regime, the finite domain and inter-spike coupling do not play a central role. Finally, in the regime where $A = O(1)$, the equilibrium spike patterns again exhibit a saddle-node bifurcation structure, and this regime is intimately connected with a pulse-splitting behavior of spike patterns. In this regime, which is studied in the companion paper [16], the effect of the finite domain is crucial in the analysis.

We now summarize some of our findings for the low feed-rate regime. In the low feed-rate regime, we introduce new variables $\mathcal{A}$ and ν defined by

$$A = \varepsilon^{1/2}\mathcal{A}\,, \qquad v = \varepsilon^{-1/2}\nu\,. \tag{1.5}$$

In terms of (1.5), (1.3) is transformed to

$$\nu_t = \varepsilon^2\nu_{xx} - \nu + \mathcal{A}u\nu^2\,, \qquad -1 < x < 1\,, \quad t > 0\,, \tag{1.6a}$$

$$\tau u_t = Du_{xx} + (1-u) - \varepsilon^{-1}u\nu^2 \qquad -1 < x < 1\,, \quad t > 0\,, \tag{1.6b}$$

$$\nu_x(\pm 1, t) = u_x(\pm 1, t) = 0\,; \qquad \nu(x,0) = \varepsilon^{1/2}v_0(x)\,, \qquad u(x,0) = u_0(x)\,. \tag{1.6c}$$

For symmetric k-spike equilibrium patterns where the spikes in ν have a common amplitude, we show that for each $k = 1, 2\ldots$ there are two branches of such solutions for (1.6) when $\mathcal{A} > \mathcal{A}_{ke}$. These branches are referred to as the small and large solution branches. They meet at the saddle-node bifurcation value

$$\mathcal{A}_{ke} \equiv \sqrt{\frac{12\theta_0}{\tanh\left(\theta_0/k\right)}}\,, \qquad \theta_0 \equiv D^{-1/2}\,. \tag{1.7}$$

These solution branches are conveniently parameterized in terms of a parameter s, with $0 < s < \infty$, defined by

$$s = \frac{1-U_\pm}{U_\pm}\,, \qquad U_\pm = \frac{1}{2}\left[1 \pm \sqrt{1 - \frac{\mathcal{A}_{ke}^2}{\mathcal{A}^2}}\right]\,. \tag{1.8}$$

Our next result concerns the existence of asymmetric k-spike patterns where the spikes have different heights. The resulting spike patterns have the form $SB..BS$, where there are $k_1 > 0$ small spikes S and $k_2 = k - k_1 > 0$ large spikes B arranged in any order across the interval. Neglecting the orientation of large and small spikes in a spike sequence, we show that there are $k-1$ asymmetric k-spike equilibrium patterns that bifurcate from the symmetric k-spike small solution branch at the value $\mathcal{A} = \mathcal{A}_{ka}$, where

$$\mathcal{A}_{ka} \equiv \mathcal{A}_{ke}\left[\tanh\left(\frac{2\theta_0}{k}\right)\right]^{-1}. \tag{1.9}$$

The $k-1$ bifurcating branches correspond to the number of small spikes S in a spike sequence $SB...BS$. In Fig. 1, for $D = 0.75$, we plot a bifurcation diagram of the norm of ν versus $\mathcal{A}$ for the symmetric k-spike solution branches for $k = 1, \ldots, 4$. The dotted curves in Fig. 1 show the asymmetric k-spike patterns that bifurcate off of the symmetric k-spike solution branch at $\mathcal{A} = \mathcal{A}_{ka}$. The asymptotic construction of symmetric and asymmetric k-spike equilibrium patterns is given in §2. The construction of asymmetric patterns, and symmetric k-spike patterns on a finite domain, are new results, although similar techniques have been used in [37] and [14] to construct equilibrium spike patterns in the Gierer Meinhardt (GM) model. A dynamical systems approach to construct asymmetric patterns for the GM model is given in [6].

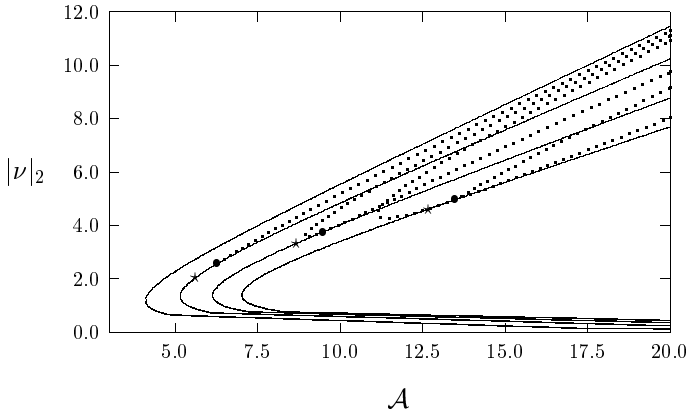

Figure 1: Bifurcation diagram of symmetric (solid curves) and asymmetric (dotted curves) spike patterns in the low feed-rate regime $A = \mathcal{A}\varepsilon^{1/2}$ for $D = 0.75$ and $k = 1, 2, 3, 4$. The saddle-node values $\mathcal{A}_{ke}$ increase with k.

In §3 we derive a nonlocal eigenvalue problem that governs the stability of the symmetric k-spike

equilibrium solutions constructed in §2 with respect to eigenvalues of order $O(1)$ in the spectrum of the linearization. These eigenvalues, referred to here as the large eigenvalues, are associated with the initiation of profile instabilities, whereby the spike amplitudes will either oscillate, typically with a common frequency and phase, or else undergo a competition instability leading to the monotonic annihilation of spikes in a spike sequence. From this nonlocal eigenvalue problem, we prove in Proposition 3.10 that the large solution branch is unconditionally unstable for any $\tau > 0$ and $D > 0$. The stability properties of the small solution branch is significantly more intricate. In particular, for each $k = 1, 2 \ldots$ and $D > 0$ fixed, we prove that there exists a threshold value $\mathcal{A}_{kL}$, with $\mathcal{A}_{kL} > \mathcal{A}_{ke}$, such that the small solution branch is stable with respect to profile instabilities for $\mathcal{A} > \mathcal{A}_{kL}$ provided that $\tau < \tau_{hL}$. An explicit formula for $\mathcal{A}_{kL}$ is given below in (3.27b). For the range $\mathcal{A} > \mathcal{A}_{kL}$, there is a Hopf bifurcation as τ exceeds some critical value τ_{hL}. This bifurcation typically leads to a synchronous oscillatory instability in the spike amplitudes. The precise results are given below in Propositions 3.11 and 3.13-3.15. On the range $\mathcal{A}_{ke} < \mathcal{A} < \mathcal{A}_{kL}$ for the small solution branch, the spectrum of the linearization of (1.6) around a symmetric k-spike equilibrium solution contains at least one (unstable) real and positive eigenvalue. The existence of real positive eigenvalues in this parameter range is the mechanism for the initiation of competition instabilities whereby certain spikes in a spike sequence are annihilated. Precise results for the spectrum of the linearization for this range of $\mathcal{A}$ is given below in Proposition 3.12. We believe that these competition instabilities, due to real eigenvalues crossing into the right half-plane, are closely related to the *overcrowding effect* discussed in [17] for multiple spot patterns in the two-dimensional Gray-Scott model, and observed experimentally in the ferrocyanide-iodate-sulphite reaction.

We now illustrate these instabilities for (1.6) for the parameter set $k = 4$, $D = 0.1$, and $\varepsilon = 0.01$ (this is Example 3 of §3.3). For this example, our theory yields $\mathcal{A}_{kL} = 8.127$. For the value $\mathcal{A} = 8.0$, in Fig. 2(a) we show a 1% perturbation in the equilibrium pattern, which we use as the initial condition for (1.6). Since $\mathcal{A} < \mathcal{A}_{kL}$, our theory predicts the initiation of a spike competition process. In Fig. 2(b) we plot the spike amplitudes, defined as the values of ν at its local maxima, versus time showing a spike competition process leading to the annihilation of two spikes. In Fig. 3(a) where $\mathcal{A} = 8.302 > \mathcal{A}_{kL}$ we show a synchronous decaying oscillation in the spike amplitudes when $\tau = 3.8$. In Fig. 3(b), where $\tau = 4.1$ exceeds the Hopf bifurcation value, we show a synchronous oscillatory instability leading to the simultaneous collapse of the four spikes. A mathematical theory to characterize the initiation of these fast instabilities is given in §3. For $D = O(1)$, this intricate spectral behavior of competition and oscillatory instabilities in the Gray-Scott model (1.6), which have not been observed previously, occurs as a result of the finite domain and a strong inter-spike coupling mediated by the concentration field u.

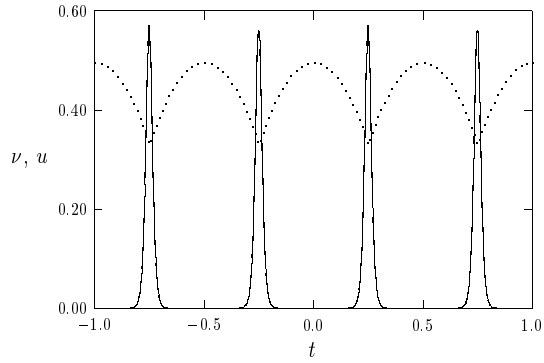

(a) The initial condition

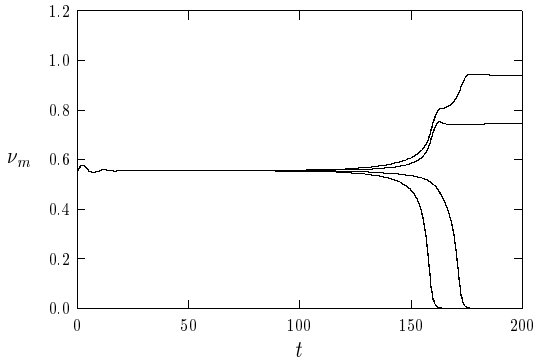

(b) ν_m versus t

Figure 2: The parameters are $k = 4$, $D = 0.1$, $\mathcal{A} = 8.0$, $\varepsilon = 0.01$, and $\tau = 2.0$. Left figure: the initial condition for ν (solid curve) and u (dashed curve). Right figure: The spike amplitudes ν_m. The second and fourth spikes are annihilated by a spike competition. Of the two remaining spikes, the third spike has the largest amplitude.

Similar types of competition and synchronous oscillatory instabilities of equilibrium spike patterns have been analyzed in [38] for the Gierer Meinhardt (GM) model of morphogenesis introduced in [9]. This model, which has been widely used to model localization processes in nature, such as cell differentiation and morphogenesis (cf. [11]), biological pattern formation (cf. [20]), and the formation of sea-shell patterns (cf. [21]), can be written in dimensionless form for an activator a and an inhibitor h concentration field as

$$a_t = \varepsilon^2 a_{xx} - a + \frac{a^p}{h^q}\,, \qquad -1 < x < 1\,, \quad t > 0\,, \tag{1.10a}$$

$$\tau h_t = D h_{xx} - h + \varepsilon^{-1}\frac{a^m}{h^s}\,, \qquad -1 < x < 1\,, \quad t > 0\,, \tag{1.10b}$$

$$a_x(\pm 1, t) = h_x(\pm 1, t) = 0\,; \qquad a(x,0) = a_0(x)\,, \qquad h(x,0) = h_0(x)\,. \tag{1.10c}$$

Here $0 < \varepsilon^2 \ll 1$, $D > 0$, and $\tau \geq 0$, represent the activator diffusivity, inhibitor diffusivity, and reaction-time constant, respectively. The usual assumption on the exponents (p, q, m, s) of the GM model (cf. [9]) are that they satisfy

$$p > 1\,, \qquad q > 0\,, \qquad m > 1\,, \qquad s \geq 0\,, \qquad \text{with} \qquad \zeta \equiv \frac{qm}{(p-1)} - (s+1) > 0\,. \tag{1.11}$$

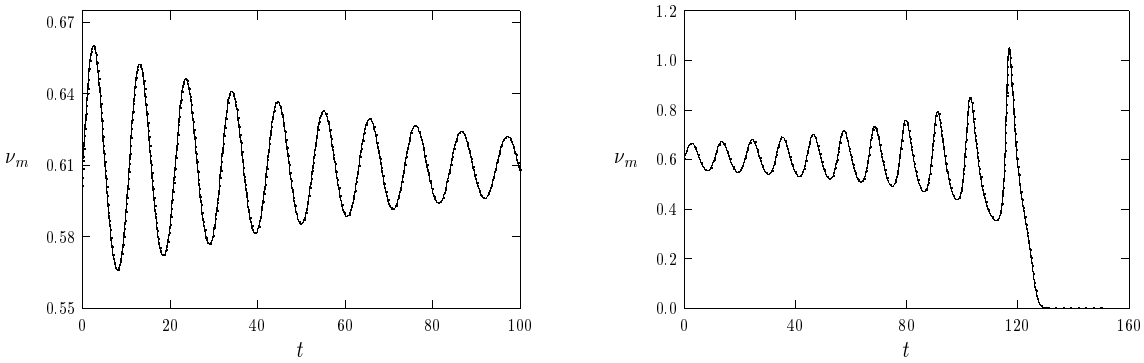

(a) ν_m versus t

(b) ν_m versus t

Figure 3: Spike amplitudes for $k = 4$, $D = 0.1$, $\mathcal{A} = 8.302$, and $\varepsilon = 0.01$. Left figure: synchronous decaying oscillation in the spike amplitudes for $\tau = 3.8$. Right figure: synchronous oscillatory instability for $\tau = 4.1$, leading to a collapse of the four spikes. In these figures, the amplitudes of the spikes trace out identical trajectories.

The relationship between oscillatory and competition instabilities in the Gray-Scott and Gierer Meinhardt models is made clear in Proposition 3.3 below where we prove that the nonlocal eigenvalue problem for instabilities in the Gray-Scott model in the low feed-rate regime is identical to the nonlocal eigenvalue problem for the Gierer Meinhardt model with exponent set $(p, q, m, s) = (2, s, 2, s)$, where s is defined in (1.8). This spectral equivalence principle is a new result, and allows us to use many of the detailed spectral results derived in [38] for the GM model.

For the low feed-rate regime $A = O(\varepsilon^{1/2})$ (or equivalently $\mathcal{A} = O(1)$), in §4 we analyze the stability of symmetric k-spike equilibrium patterns with respect to the small eigenvalues of order $O(\varepsilon^2)$ that govern instabilities with respect to translations of the spike profile. In Proposition 4.4 we prove that, for any $\tau = O(1)$, the k-spike pattern is stable with respect to translations only when $\mathcal{A} > \mathcal{A}_{ka}$, where $\mathcal{A}_{ka}$ is the critical threshold for the emergence of asymmetric k-spike patterns from a symmetric k-spike small solution branch. As $\mathcal{A}$ decreases below $\mathcal{A}_{ka}$, there are $k-1$ small eigenvalues that simultaneously cross into the unstable right half-plane $\mathrm{Re}(\lambda) > 0$ along the real axis. We prove that $\mathcal{A}_{ka} > \mathcal{A}_{kL}$. Hence, when $\mathcal{A}_{kL} < \mathcal{A} < \mathcal{A}_{ka}$, an equilibrium spike profile is stable with respect to fast $O(1)$ instabilities when τ is sufficiently small, but that there is a slow $O(\varepsilon^2)$ instability with respect to translations of the profile. Numerical computations are performed to illustrate spike

dynamics for (1.6) in this range of $\mathcal{A}$. This analysis of the small eigenvalues for the Gray-Scott model is new, although a similar analysis has been done previously in [14] for the GM model.

The intermediate regime where $O(1) \ll \mathcal{A} \ll O(\varepsilon^{-1/2})$ is analyzed in §5. In this regime, there are no competition instabilities, and we show in Proposition 5.2 that there is a universal nonlocal eigenvalue problem, independent of D and k, that governs the stability of a symmetric k-spike equilibrium solution with respect to oscillatory instabilities. In terms of a certain critical value of this universal nonlocal eigenvalue problem, a scaling law for the Hopf bifurcation value of τ is derived in Proposition 5.3 that yields the Hopf bifurcation value in terms of D and k. In this regime for $\mathcal{A}$, the Hopf bifurcation value is $\tau = O(\mathcal{A}^4)$, and so there are no oscillatory instabilities when $\tau = O(1)$. For $\tau = O(1)$, we show in Proposition 5.4 that the small solution branch is stable with respect to the small (translation) eigenvalues of order $O(\varepsilon^2)$ in the spectrum of the linearization.

Since the Hopf bifurcation value has the scaling $\tau = O(\mathcal{A}^4) \gg 1$ in the intermediate regime, we may observe an instability with respect to the small eigenvalues before the onset of the Hopf bifurcation for large values of τ. This interchange in the instability mechanism as τ is increased was suggested in [23] and [24] in the context of the infinite-line problem. For a one-spike equilibrium solution, in §5.1 we show that there is a traveling wave, or drift, instability that is associated with a small $O(\varepsilon^2)$ eigenvalue when $\tau = O(\mathcal{A}^{-2}\varepsilon^{-2})$. As τ increases past some critical value, this instability with respect to translations of the profile occurs from a Hopf bifurcation and leads to oscillations in the spike layer location. As τ is increased even further, the oscillations in the spike location ceases due to a complex conjugate pair of eigenvalues merging onto the positive real axis. When this occurs there is a slow monotonic drift of the spike to the boundary of the domain. A related type of Hopf bifurcation, followed by a monotonic drift instability, as a reaction-time constant is increased has been analyzed in [12] and [22] for hyperbolic tangent-type interfaces associated with a two-component reaction diffusion system with bistable nonlinearities. Alternatively, for a three-component reaction-diffusion system it was shown numerically in [28] that the Hopf bifurcation occurs *after* the onset of a monotonic drift instability as a reaction-time parameter is increased.

The previous equilibrium and spectral results for the Gray-Scott model in [4], [5], [7], [2], and [3], have been based on a different nondimensionalization of the Gray-Scott model. This alternative formulation is presented in detail in §6, where we give a precise discussion of the relationship between our results and theirs. In §6, §5.1, and in §3.4 we also relate our results to those in [23] and [24]. The main point is that our results have a clear overlap with these previous results only in the intermediate parameter regime for $\mathcal{A}$ and for the infinite-line problem. Our analysis of synchronous spike oscillations and competition instabilities, which occur on a finite domain with $k\sqrt{D} \ll 1$, and instabilities resulting from the small eigenvalues, is novel. In §6 we also list a few open problems.

2 Symmetric and Asymmetric k-Spike Equilibria: $\mathcal{A} = O(1)$

For $\varepsilon \to 0$, and with $\mathcal{A} = O(1)$ and $D = O(1)$, we construct a symmetric k-spike equilibrium solution to (1.6) using the method of matched asymptotic expansions. The spike locations x_j, for $j = 1, \ldots, k$, for this pattern satisfy

$$x_j = -1 + \frac{(2j-1)}{k}\,, \qquad j = 1, \ldots, k\,. \tag{2.1}$$

For a symmetric spike pattern the spikes have equal height. Hence, we have $u(x_j) = U$, where U is independent of j.

Since the asymptotic construction of a symmetric k-spike pattern to (1.6) for $\varepsilon \ll 1$ is similar to that done in [14] for the Gierer Meinhardt model, we will only sketch the derivation of the result. In §5, where we consider the intermediate regime $O(1) \ll \mathcal{A} \ll O(\varepsilon^{-1/2})$ we will give a detailed derivation of the equilibrium solutions for (1.3) and (1.6) and include formal error estimates associated with the inner and outer expansions.

In the inner region near the j^{th} spike, we let $y = \varepsilon^{-1}(x - x_j)$. In each inner region, we obtain that $u \sim U + O(\varepsilon)$. Therefore, from (1.6a), the leading-order inner solution for ν is

$$\nu \sim \frac{1}{\mathcal{A}U} w(y)\,, \tag{2.2}$$

where $w(y) = \frac{3}{2}\mathrm{sech}^2\,(y/2)$ is the homoclinic solution to

$$w'' - w + w^2 = 0\,, \qquad -\infty < y < \infty\,, \tag{2.3a}$$

$$w \to 0 \quad \text{as} \quad |y| \to \infty\,; \qquad w'(0) = 0\,, \quad w(0) > 0\,. \tag{2.3b}$$

In the outer region, defined away from $O(\varepsilon)$ regions near the union of the x_j, for $j = 1, \ldots, k$, we obtain that ν is exponentially small and that the term $\varepsilon^{-1} u\nu^2$ in (1.6b) can be approximated by a delta function. Consequently, the outer solution for u satisfies

$$D u_{xx} + (1 - u) - \frac{6}{\mathcal{A}^2 U} \sum_{j=1}^{k} \delta(x - x_j) = 0\,, \tag{2.4a}$$

$$u_x(-1) = u_x(1) = 0\,. \tag{2.4b}$$

In obtaining (2.4a), we used $\int_{-\infty}^{\infty} w^2\, dy = 6$. The solution to (2.4) is

$$u(x) = 1 - \frac{6}{\mathcal{A}^2 U} \sum_{j=1}^{k} G(x; x_j)\,, \tag{2.5}$$

where $G(x;x_j)$ is the Green's function, satisfying

$$DG_{xx} - G = -\delta(x - x_j)\,, \qquad -1 < x < 1\,; \qquad G_x(\pm 1; x_j) = 0\,. \tag{2.6}$$

A simple calculation gives,

$$G(x;x_j) = \begin{cases} g_j \cosh\left[\theta_0(1+x)\right] / \cosh\left[\theta_0(1+x_j)\right], & -1 < x < x_j\,, \\ g_j \cosh\left[\theta_0(1-x)\right] / \cosh\left[\theta_0(1-x_j)\right], & x_j < x < 1\,, \end{cases} \tag{2.7a}$$

where

$$g_j \equiv \frac{1}{\sqrt{D}} \left(\tanh\left[\theta_0(1-x_j)\right] + \tanh\left[\theta_0(1+x_j)\right]\right)^{-1}\,, \qquad \theta_0 \equiv D^{-1/2}\,. \tag{2.7b}$$

We define $a_g \equiv \sum_{i=1}^{k} G(x_j;x_i)$, where the spike locations satisfy (2.1). A simple calculation using (2.7) shows that a_g is independent of j, and that

$$a_g \equiv \sum_{i=1}^{k} G(x_j;x_i) = \left[2\sqrt{D}\tanh\left(\theta_0/k\right)\right]^{-1}\,. \tag{2.8}$$

Evaluating (2.5) at $x = x_j$, where $u(x_j) = U$, we obtain a quadratic equation for U

$$U(U-1) = -\frac{6a_g}{\mathcal{A}^2}\,. \tag{2.9}$$

In this way, we obtain the following result for symmetric k-spike equilibrium solutions to (1.6):
Proposition 2.1: *Let $\varepsilon \to 0$, with $\mathcal{A} = O(1)$ and $D = O(1)$ in (1.6). Then, when $\mathcal{A} > \mathcal{A}_{ke}$, there are two symmetric k-spike equilibrium solutions to (1.6) given asymptotically by*

$$\nu_{\pm}(x) \sim \frac{1}{\mathcal{A}U_{\pm}} \sum_{j=1}^{k} w\left[\varepsilon^{-1}(x - x_j)\right]\,, \tag{2.10a}$$

$$u_{\pm}(x) \sim 1 - \frac{(1-U_{\pm})}{a_g} \sum_{j=1}^{k} G(x;x_j)\,. \tag{2.10b}$$

We label u_+, ν_+ and u_-, ν_- as the large and small solution, respectively. In (2.10), w and G satisfy (2.3) and (2.6), respectively. In addition, $U_{\pm}$ are the roots of (2.9) given by

$$U_{\pm} = \frac{1}{2}\left[1 \pm \sqrt{1 - \frac{\mathcal{A}_{ke}^2}{\mathcal{A}^2}}\right]\,, \tag{2.11}$$

where the existence threshold is $\mathcal{A}_{ke} = \sqrt{24 a_g}$, *so that*

$$\mathcal{A}_{ke} \equiv \sqrt{\frac{12\theta_0}{\tanh\left(\theta_0/k\right)}}\,, \qquad \theta_0 \equiv D^{-1/2}\,. \tag{2.12}$$

The existence threshold (2.12) for a finite domain with k spikes is a new result. It shows that we have a saddle-node bifurcation of symmetric k-spike equilibria on the finite line when $\mathcal{A} = \mathcal{A}_{ke}$. These existence thresholds correspond to the fold points in Fig. 1 separating the upper and lower branches of symmetric k-spike equilibria (solid curves in this figure). As a remark, we notice that $\mathcal{A}_{ke}$ is an increasing function of k. For $D \ll 1$ and with $\sqrt{D}k \ll 1$, we get that $\mathcal{A}_{ke} \sim \sqrt{12} D^{-1/4}$. Thus, when $D \ll 1$, the saddle-node bifurcation value $\mathcal{A}_{ke}$ for symmetric k-spike equilibria is roughly independent of k provided that $\sqrt{D}k \ll 1$.

To display our results graphically, it is convenient to define a norm of ν by

$$|\nu|_2 \equiv \left(\varepsilon^{-1}\int_{-1}^{1} \nu^2\, dx\right)^{1/2}\,. \tag{2.13}$$

Using (2.10a) and (2.11), we calculate

$$|\nu|_2 \sim \frac{2\sqrt{6k}}{\mathcal{A}}\left[1 \pm \sqrt{1 - \frac{\mathcal{A}_{ke}^2}{\mathcal{A}^2}}\right]^{-1}\,. \tag{2.14}$$

For $\mathcal{A} = 9.0$ and $\varepsilon = 0.02$, in Fig. 4(a) and Fig. 4(b) we plot the small solution when $D = 0.75$ and $D = 0.1$, respectively. Notice that as D decreases, the Green's function in (2.10b) decays more rapidly away from the spike locations. Hence, for D small, u should approach the asymptotic value $u = 1$ in the outer regions. This asymptotic value $u = 1$ in the outer region is also relevant to the infinite-line problem, where we seek a one-spike solution to (1.6) on $-\infty < x < \infty$. However, as seen from Fig. 4(b), even with $D = 0.1$, u is not so close to its asymptotic value in the outer regions. Therefore, this suggests that there is range of values of D for which boundary effects due to the finite domain will be important in the analysis.

The classification of large and small solution refers to high and low concentrations of u in the core of the spike. Smaller concentrations of u in the core of the spike generate larger amplitudes for ν. Hence, each upper branch (upper solid curve) in Fig. 1 corresponds to the small solution, while each lower branch corresponds to the large solution. As shown in §3 – §5, a particularly convenient way to parameterize these symmetric k-spike solution branches is to introduce a parameter s defined by

$$s = \frac{1 - U_{\pm}}{U_{\pm}}\,, \qquad 0 < s < \infty\,. \tag{2.15a}$$

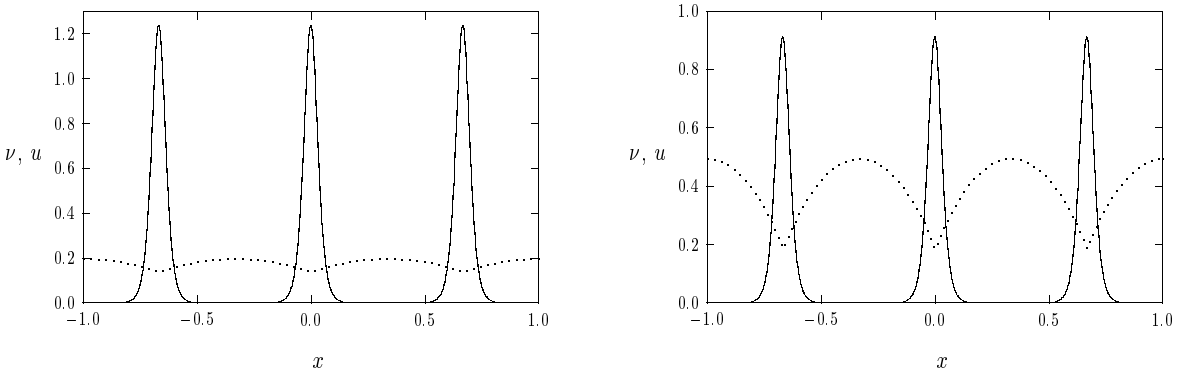

(a) $D = 0.75$ (b) $D = 0.1$

Figure 4: Left figure: three-spike small solution when $D = 0.75$, $\mathcal{A} = 9.0$, and $\varepsilon = 0.02$. Right figure: three-spike small solution when $D = 0.1$, $\mathcal{A} = 9.0$, and $\varepsilon = 0.02$.

Using (2.11), we can write $\mathcal{A}$ in terms of s as

$$\frac{\mathcal{A}}{\mathcal{A}_{ke}} = \frac{(1+s)}{2\sqrt{s}}\,. \tag{2.15b}$$

Hence the small solution u_-, ν_- corresponds to the range $1 < s < \infty$, while the large solution corresponds to $0 < s < 1$. The existence threshold $\mathcal{A}_{ke}$ corresponds to $s = 1$.

To analyze the stability of symmetric k-spike equilibrium solutions we let

$$u(x,t) = u_\pm(x) + e^{\lambda t}\eta(x)\,, \qquad \nu(x,t) = \nu_\pm(x) + e^{\lambda t}\phi(x)\,, \tag{2.16}$$

where $\eta \ll 1$ and $\phi \ll 1$. Substituting (2.16) into (1.6) and linearizing, we obtain the eigenvalue problem

$$\varepsilon^2\phi_{xx} - \phi + 2\mathcal{A}u_\pm\nu_\pm\phi + \mathcal{A}\eta\nu_\pm^2 = \lambda\phi\,, \qquad -1 < x < 1\,, \tag{2.17a}$$

$$D\eta_{xx} - \eta - \varepsilon^{-1}\nu_\pm^2\eta - 2\varepsilon^{-1}u_\pm\nu_\pm\phi = \tau\lambda\eta\,, \qquad -1 < x < 1\,, \tag{2.17b}$$

$$\phi_x(\pm 1) = \eta_x(\pm 1) = 0\,. \tag{2.17c}$$

In §3 we analyze the spectrum of (2.17) corresponding to those eigenfunctions that are not locally odd functions near each spike. The corresponding eigenvalues, which determine the stability of the symmetric k-spike profile with respect to instabilities occurring on a fast $O(1)$ time-scale, are referred to as the large eigenvalues. We will show that the large solution u_+ and ν_+ is always unstable. For the small solution, we show that there are two different types of instabilities that can occur depending on the parameter ranges of D, $\mathcal{A}$, τ, and k. A competition instability, whereby spikes in a spike sequence are destroyed, can occur only for $k > 1$ when $\mathcal{A}$ is close to $\mathcal{A}_{ke}$. This instability results from a certain eigenvalue on the positive real axis $\mathrm{Re}(\lambda) > 0$. On the other hand, oscillatory instabilities in the amplitudes of the spikes as a result of a Hopf bifurcation can occur for any $\mathcal{A} > \mathcal{A}_{ke}$ when τ is sufficiently large.

In §4 we analyze the spectrum of (2.17) corresponding to those eigenvalues that approach zero as $\varepsilon \to 0$. To leading order, the corresponding eigenfunction is locally an odd function near each spike. These eigenvalues, referred to as the small eigenvalues, are $O(\varepsilon^2)$ as $\varepsilon \to 0$. These eigenvalues are related to translational instabilities, and are intimately connected with the small-scale dynamics of spike locations near their equilibrium positions. They are also related to the bifurcation of asymmetric k-spike equilibria from a symmetric k-spike solution branch.

2.1 Asymmetric Spike Patterns

We now construct asymmetric equilibrium spike patterns, where the spikes can have different heights. To determine how spikes of different heights can arise, we proceed as in the analysis of [37] for the GM model (1.10) by first constructing a one-spike solution centered at the origin for (1.6) posed on $-l < x < l$, with $u_x(\pm l) = \nu_x(\pm l) = 0$. For $\varepsilon \ll 1$, such a solution has the property that ν and u are even, that $\nu(l)$ is exponentially small, and that $u(l) = O(1)$. We would like to find all different values of l, labeled by l_1,..,l_n, such that $u(l_1) =, \ldots, = u(l_n)$. For a certain range of the parameters as obtained below there are exactly two such values of l. These "local" solutions are then used to construct a global asymmetric equilibrium k-spike pattern for (1.6) on $[-1, 1]$.

To construct a solution to (1.6) on $-l < x < l$ with a spike at the origin, we proceed in a similar way as was done earlier for the symmetric pattern. We obtain that

$$\nu(x) \sim \frac{1}{\mathcal{A}U} w\left(x/\varepsilon\right), \qquad u(x) \sim 1 - \frac{6}{\mathcal{A}^2 U} G_l(x;0)\,. \tag{2.18}$$

Here $w(y)$ satisfies (2.3), and $G_l(x;0)$ is the Green's function on $-l < x < l$ satisfying

$$DG_{lxx} - G_l = -\delta(x)\,, \quad -l < x < l\,; \qquad G_{lx}(\pm l;0) = 0\,. \tag{2.19}$$

A simple calculation gives,

$$G_l(x;0) = \left(\frac{\theta_0}{2}\right) \frac{\cosh\left[(l-|x|)\theta_0\right]}{\sinh\left(l\theta_0\right)} \,. \tag{2.20}$$

The constant U in (2.18), representing the leading-order approximation for u in the inner region, is obtained by setting $u(0) = U$ in (2.18). Solving the resulting quadratic equation we get

$$U = \frac{1}{2}\left(1 \pm \sqrt{1 - \frac{\coth(\theta_0 l)}{\tilde{\mathcal{A}}^2}}\right) \,, \qquad \mathcal{A} \equiv \sqrt{12\theta_0}\tilde{\mathcal{A}} \,. \tag{2.21}$$

To construct asymmetric patterns, we must calculate $u(l)$. Using (2.18) and (2.20), we get

$$\frac{u(l)-1}{U-1} = \frac{G_l(l;0)}{G_l(0;0)} = \mathrm{sech}\left(l\theta_0\right) \,. \tag{2.22}$$

Combining (2.22) and (2.21), we obtain the key formula for $u(l)$,

$$u(l) = E_{\pm}(z) \equiv 1 + \frac{1}{2}\mathrm{sech}(z)\left[-1 \pm \sqrt{1 - \frac{\coth(z)}{\tilde{\mathcal{A}}^2}}\right] \,, \qquad z \equiv \theta_0 l \,. \tag{2.23}$$

The minus and plus signs in (2.23) refer to small and large solutions, respectively. In (2.23), we require $\tilde{\mathcal{A}} > 1$. Moreover, when $\tilde{\mathcal{A}} > 1$, the function $E_{\pm}(z)$ is defined only on the range where $\coth(z) < \tilde{\mathcal{A}}^2$. This yields that $z > z_0$, where

$$z_0 \equiv \frac{1}{2}\ln\left[\frac{\tilde{\mathcal{A}}^2+1}{\tilde{\mathcal{A}}^2-1}\right] \,. \tag{2.24}$$

Clearly $E_{\pm}(z) > 0$ for $z > z_0$. For $z > z_0$, we readily derive some key properties of $E_{\pm}(z)$.

Proposition 2.2: *Let $\tilde{\mathcal{A}} > 1$. Then, on the range $z > z_0$ we have that $E_+^{'}(z) > 0$ with $E_+(z_0) < 1$ and $E_+(z) \to 1$ as $z \to \infty$. Alternatively, we have $E_-(z_0) < 1$ with $E_-^{'}(z) < 0$ for $z_0 < z < z_m$, and $E_-^{'}(z) > 0$ for $z > z_m$. Moreover, $E_-(z) \to 1$ as $z \to \infty$. The point z_m where $E_-(z)$ has its minimum value is the unique root of*

$$\tilde{\mathcal{A}} = \left[\tanh z\right]^{-1/2}\left[\tanh(2z)\right]^{-1} \,. \tag{2.25}$$

Proof: Clearly $E_{\pm}(z_0) < 1$ and $E_{\pm}(z) \to 1$ as $z \to \infty$. In addition, by differentiating (2.23) it is immediately clear that $E_+^{'}(z) > 0$ for $z > z_0$. For $E_-(z)$, we calculate

$$E_-^{'}(z) = \frac{\sinh z}{2\cosh^2 z}\left[1 + \sqrt{1 - \frac{\coth z}{\tilde{\mathcal{A}}^2}}\right] - \frac{\mathrm{sech}z}{\tilde{\mathcal{A}}^2}\frac{\mathrm{csch}^2 z}{\sqrt{1 - \frac{\coth z}{\tilde{\mathcal{A}}^2}}} \,. \tag{2.26}$$

Therefore, $E_-^{'}(z) < 0$ only when

$$2\tilde{\mathcal{A}}^2 \tanh z \left[\sqrt{1 - \frac{\coth z}{\tilde{\mathcal{A}}^2}} + 1 - \frac{\coth z}{\tilde{\mathcal{A}}^2} \right] > \operatorname{csch}^2 z \,. \tag{2.27}$$

Manipulating (2.27), we get that $E_-^{'}(z) < 0$ if and only if

$$\sqrt{1 - \frac{\coth z}{\tilde{\mathcal{A}}^2}} > \frac{\cosh(2z)}{2\tilde{\mathcal{A}}^2 \sinh^2 z} \coth z - 1 \,. \tag{2.28}$$

It is easy to see from (2.28) that there exists a z_m such that $E_-^{'}(z) < 0$ for $z_0 < z < z_m$, and $E_-^{'}(z) > 0$ for $z > z_m$. To determine where $E_-^{'}(z) = 0$, we square both sides of (2.28) to obtain

$$1 - t = \left(\frac{t \cosh(2z)}{2 \sinh^2 z} - 1 \right)^2 , \qquad t \equiv \frac{\coth z}{\tilde{\mathcal{A}}^2} \,. \tag{2.29}$$

Solving for $t > 0$ we get $t = \tanh^2(2z)$. Since, $\tilde{\mathcal{A}}^2 = \coth z / t$, we obtain (2.25) for $\mathcal{A}$. ■

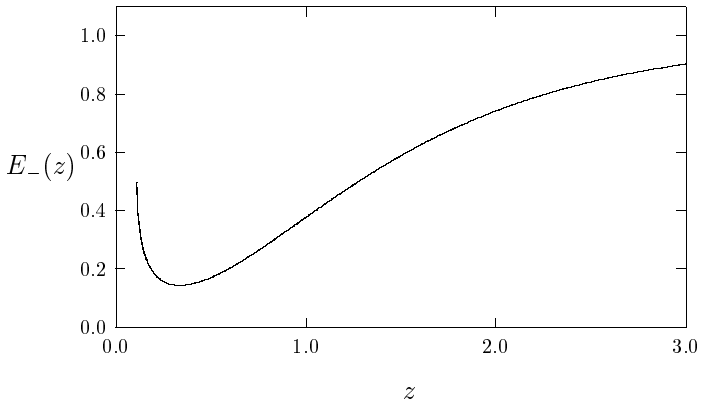

Figure 5: Plot of E_- versus z for $z \geq z_0$ when $\tilde{\mathcal{A}} = 3$.

Therefore, when $\tilde{\mathcal{A}} > 1$, we conclude that for any z in $z_0 < z < z_m$, there exists a unique $\tilde{z}$, with $\tilde{z} > z_m$, such that $E_-(z) = E_-(\tilde{z})$. In Fig. 5 we plot $E_-(z)$ versus z when $\tilde{\mathcal{A}} = 3$. Since $z = \theta_0 l$ and $\tilde{z} = \theta_0 \tilde{l}$, the implication of this result is the following: Given any l with $z_0 < l\theta_0 < z_m$, there exists a unique $\tilde{l}$, with $\tilde{l}\theta_0 > z_m$, such that $u(l) = u(\tilde{l})$. This implies that in any asymmetric pattern of this

form using $E_-(z)$ there are only two distinct values for the heights of the spikes. Furthermore, since $E_+(z)$ is monotonically increasing we cannot construct asymmetric patterns for the large solution.

For $E_-(z)$, we refer to solutions of length l and $\tilde{l}$ as S-type and B-type spikes, respectively. We now construct asymmetric k-spike equilibrium solutions to the global problem (1.6) on the interval $[-1,1]$ with $k_1 > 0$ spikes of type S and $k_2 = k - k_1 > 0$ spikes of type B arranged in any particular order from left to right across the interval as

$$\text{SBSSB....B}\,, \qquad k_1 \ - \ \text{S's}\,, \qquad k_2 \ - \ \text{B's}. \tag{2.30}$$

To do so, we use translation invariance and the fact that $u(l) = u(\tilde{l})$ to glue S and B type spikes together to satisfy C^1 continuity for the global function u defined on $[-1,1]$. The global function ν is exponentially close to being C^1 continuous since the local function is such that $\nu(l)$ and $\nu(\tilde{l})$ are exponentially small when $\varepsilon \ll 1$.

Since the supports of an S-spike and a B-spike are $2l$ and $2\tilde{l}$, respectively, we get the length constraint $2k_1 l + 2k_2\tilde{l} = 2$. This condition can be written as

$$k_1 z + k_2 \tilde{z} = \theta_0 \equiv D^{-1/2}\,. \tag{2.31a}$$

The other condition, which ensures that u is C^1 continuous is

$$E_-(z) = E_-(\tilde{z})\,, \tag{2.31b}$$

where $E_-(z)$ is defined in (2.23). Equations (2.31a) and (2.31b) are a coupled nonlinear system for z and $\tilde{z}$. In terms of this solution, the half-lengths of the supports of the spikes are given by

$$l = z\theta_0^{-1}\,, \qquad \tilde{l} = \tilde{z}\theta_0^{-1}\,, \qquad \theta_0 = D^{-1/2}\,. \tag{2.31c}$$

This leads to the following result for asymmetric k-spike patterns:

Proposition 2.3: *Let l and $\tilde{l}$ be found from the coupled system (2.31) for a given $\tilde{\mathcal{A}} > 1$ and $D > 0$. Then, for $\varepsilon \to 0$, an asymmetric equilibrium k-spike pattern for (1.6) with k_1 spikes of type S and $k_2 = k - k_1$ spikes of type B is characterized by*

$$\nu_-(x) \sim \sum_{j=1}^{k} \frac{1}{\mathcal{A}U(l_j)} w\left[\varepsilon^{-1}(x - x_j)\right]\,, \tag{2.32a}$$

where $U(l_j)$ satisfies

$$U(l_j) \equiv \frac{1}{2}\left(1 - \sqrt{1 - \frac{\coth(\theta_0 l_j)}{\tilde{\mathcal{A}}^2}}\right)\,, \qquad \mathcal{A} \equiv \sqrt{12\theta_0}\tilde{\mathcal{A}}\,. \tag{2.32b}$$

Here for each j, $l_j = l$ or $l_j = \tilde{l}$, where l and $\tilde{l}$ are determined in terms of k_1, k_2, θ_0, and $\tilde{\mathcal{A}}$ by (2.31). The value $l_j = l$ must occur $k_1 > 0$ times, while $l_j = \tilde{l}$ must occur $k_2 = k - k_1 > 0$ times. The small and large spikes can be arranged in any sequence. Finally, the equilibrium outer solution $u(x)$ is given asymptotically by

$$u(x) = 1 - \sum_{j=1}^{k} \frac{2}{\theta_0 \coth(\theta_0 l_j)} \left[1 - U(l_j)\right] G(x; x_j)\,, \tag{2.32c}$$

where $G(x; x_j)$ satisfies (2.6). The spike locations x_j are found from

$$x_1 = l_1 - 1\,, \qquad x_k = 1 - l_k\,, \qquad x_{j+1} = x_j + l_{j+1} + l_j\,, \qquad j = 1, .., k-2\,. \tag{2.32d}$$

To recover the symmetric k-spike equilibrium solutions constructed earlier, we set $z = \tilde{z} = \theta_0/k$, which solves (2.31a). Then, (2.31b) has a solution only when $z = \tilde{z} = z_m$. Therefore, setting $z = \theta_0/k$ in (2.25) we obtain the critical value of $\tilde{\mathcal{A}}$ for the emergence of the asymmetric branch. This leads to the following bifurcation result:

Proposition 2.4: *The asymmetric k-spike equilibrium solutions bifurcate from the k-spike symmetric small equilibrium solution branch of Proposition 2.1 at the value $\mathcal{A} = \mathcal{A}_{ka}$, where*

$$\mathcal{A}_{ka} \equiv \mathcal{A}_{ke} \left[\tanh\left(\frac{2\theta_0}{k}\right)\right]^{-1}\,. \tag{2.33a}$$

Here $\mathcal{A}_{ke}$ are the existence thresholds for the symmetric branch given in (2.12). Alternatively, for a fixed $\mathcal{A} > \mathcal{A}_{ke}$, the asymmetric k-spike branches bifurcate off of the small symmetric k-spike solution branch when $D = D_k^*$, where

$$D_k^* \equiv \frac{4}{k^2 \left[\ln\left(r + \sqrt{r^2 - 1}\right)\right]^2}\,, \qquad r \equiv \left[1 - \frac{\mathcal{A}_{ke}^2}{\mathcal{A}^2}\right]^{-1/2}\,. \tag{2.33b}$$

By solving the system (2.31) using Newton's method, we plot two different asymmetric 3-spike patterns from (2.32) when $\varepsilon = 0.02$ and $D = 0.75$. In Fig. 6(a) we show a BSB pattern with $k_1 = 1$, $k_2 = 2$, when $\mathcal{A} = 10.5$. In Fig. 6(b), we show a SSB pattern with $k_1 = 2$, $k_2 = 1$, and $\mathcal{A} = 9.0$. To display the bifurcation diagram for the asymmetric branches for $D = 0.75$, we calculate the norm in (2.13) using (2.32a) to get

$$|\nu|_2 \sim \frac{1}{\mathcal{A}} \left(\frac{6k_1}{\left[U(l)\right]^2} + \frac{6k_2}{\left[U(\tilde{l})\right]^2}\right)^{1/2}\,. \tag{2.34}$$

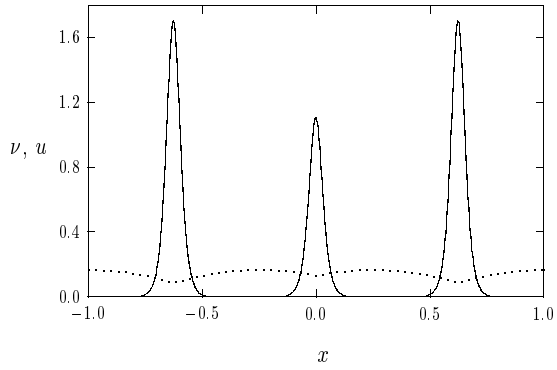

(a) BSB pattern

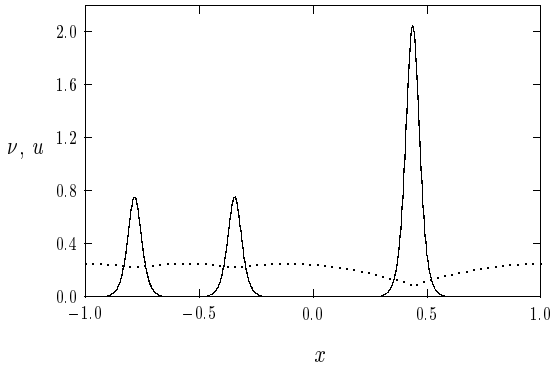

(b) SSB pattern

Figure 6: Left figure: BSB pattern with $D = 0.75$, $\mathcal{A} = 10.5$, $\varepsilon = 0.02$. Right figure: SSB pattern with $D = 0.75$, $\mathcal{A} = 9.0$, and $\varepsilon = 0.02$.

The dashed lines in the bifurcation diagram Fig. 1 of §1 correspond to plots of (2.34) versus $\mathcal{A}$ for all of the asymmetric branches that emerge from the symmetric branches at the bifurcation values $\mathcal{A} = \mathcal{A}_{ka}$, for $k = 1, \ldots, 4$. In this bifurcation diagram, the key relevant quantity is k_1 and k_2, as the ordering of spikes on the interval is invisible to the norm (2.34). From (2.31), (2.34), and Fig. 1, it can be seen that an asymmetric branch with k_1 small spikes asymptotes to the symmetric branch with $k - k_1$ spikes as $\mathcal{A} \to \infty$.

3 Large Eigenvalues: Fast Profile Instabilities for $\mathcal{A} = O(1)$

In this section we analyze the stability of the symmetric k-spike equilibrium solutions of Proposition 2.1 with respect to the large eigenvalues.

3.1 The Nonlocal Eigenvalue Problem

We begin by deriving a nonlocal eigenvalue problem that is central to the stability analysis. This derivation is similar to that done in [38] for the GM model (1.10), and was originally motivated by the approach used in [27] to analyze pulses in the Fitzhugh-Nagumo system. As in [38], we look for

a localized eigenfunction for ϕ in (2.17) in the form

$$\phi(x) \sim \sum_{j=1}^{k} c_j \Phi\left[\varepsilon^{-1}(x - x_j)\right] , \tag{3.1}$$

for some coefficients c_j. These coefficients are determined below to be related to eigenvectors of a certain matrix eigenvalue problem. The large eigenvalues are characterized by eigenfunctions $\Phi(y)$ for which $\int_{-\infty}^{\infty} w(y)\Phi(y)\,dy \neq 0$. Alternatively, the small eigenvalues of order $O(\varepsilon^2)$, studied in §4, correspond to translation modes for which this condition is not asymptotically satisfied.

Since ϕ is localized near each x_j, the coefficients in (2.17b) can be approximated by certain Dirac masses. In particular, using (3.1) and (2.10), we obtain near $x = x_j$ that

$$\varepsilon^{-1}\nu_{\pm}^2 \sim \frac{6}{\mathcal{A}^2 U_{\pm}^2}\delta(x - x_j)\,, \tag{3.2a}$$

$$2\varepsilon^{-1}u_{\pm}\nu_{\pm}\phi \sim \frac{2c_j}{\mathcal{A}}\left(\int_{-\infty}^{\infty} w(y)\Phi(y)\,dy\right)\delta(x - x_j)\,. \tag{3.2b}$$

Here $\delta(x)$ is the delta function, and we have used $\int_{-\infty}^{\infty} w^2\,dy = 6$. Substituting (3.2) into (2.17b), we obtain that η satisfies

$$D\eta_{xx} - \left(1 + \tau\lambda + \frac{6}{\mathcal{A}^2 U_{\pm}^2}\sum_{i=1}^{k}\delta(x - x_i)\right)\eta = \frac{2}{\mathcal{A}}\left(\int_{-\infty}^{\infty} w\Phi\,dy\right)\sum_{i=1}^{k} c_i\delta(x - x_i)\,, \quad |x| < 1\,, \tag{3.3a}$$

$$\eta_x(-1) = \eta_x(1) = 0\,. \tag{3.3b}$$

This problem for η is equivalent to

$$D\eta_{xx} - (1 + \tau\lambda)\,\eta = 0\,, \qquad \eta_x(\pm 1) = 0\,, \tag{3.4a}$$

$$[\eta]_i = 0\,, \qquad i = 1, .., k\,, \tag{3.4b}$$

$$[D\eta_x]_i = -\omega_i + \frac{6}{\mathcal{A}^2 U_{\pm}^2}\eta(x_i)\,, \qquad i = 1, .., k\,. \tag{3.4c}$$

In (3.4), we have defined $[\xi]_i \equiv \xi(x_{i+}) - \xi(x_{i-})$, and ω_i by

$$\omega_i \equiv -\frac{2c_i}{\mathcal{A}}\int_{-\infty}^{\infty} w(y)\Phi(y)\,dy\,. \tag{3.4d}$$

To determine the eigenvalue problem for λ, we first need to compute $\eta(x_i)$ from (3.4). To do so, we solve (3.4a) on each subinterval and use the jump conditions (3.4b) and (3.4c) to patch the

solution together across each subinterval. This calculation results in the matrix problem

$$\mathcal{B}\boldsymbol{\eta} = [(1+\tau\lambda)D]^{-1/2}\,\boldsymbol{\omega}\,, \qquad \boldsymbol{\omega} = -\frac{2\boldsymbol{c}}{\mathcal{A}}\int_{-\infty}^{\infty} w(y)\Phi(y)\,dy\,. \tag{3.5}$$

Here we have defined the vectors $\boldsymbol{\omega}$, $\boldsymbol{c}$, and $\boldsymbol{\eta}$, by $\boldsymbol{\omega}^t = (\omega_1,\ldots,\omega_k)$, $\boldsymbol{c}^t = (c_1,\ldots,c_k)$, and $\boldsymbol{\eta}^t = (\eta_1,\ldots,\eta_k)$, where t denotes transpose. The matrix $\mathcal{B}$ in (3.5) is given in terms of a tridiagonal matrix $\mathcal{B}_0$ by

$$\mathcal{B} = \mathcal{B}_0 + \frac{6}{\mathcal{A}^2 U_\pm^2\sqrt{(1+\tau\lambda)D}}I\,. \tag{3.6}$$

Here I is the $k\times k$ identity matrix, and $\mathcal{B}_0$ has the form

$$\mathcal{B}_0 \equiv \begin{pmatrix} d_\lambda & f_\lambda & 0 & \cdots & 0 & 0 & 0 \\ f_\lambda & e_\lambda & f_\lambda & \cdots & 0 & 0 & 0 \\ 0 & f_\lambda & e_\lambda & \ddots & 0 & 0 & 0 \\ \vdots & \vdots & \ddots & \ddots & \ddots & \vdots & \vdots \\ 0 & 0 & 0 & \ddots & e_\lambda & f_\lambda & 0 \\ 0 & 0 & 0 & \cdots & f_\lambda & e_\lambda & f_\lambda \\ 0 & 0 & 0 & \cdots & 0 & f_\lambda & d_\lambda \end{pmatrix}, \tag{3.7a}$$

with matrix entries

$$d_\lambda \equiv \coth\left(\frac{2\theta_\lambda}{k}\right) + \tanh\left(\frac{\theta_\lambda}{k}\right); \qquad e_\lambda \equiv 2\coth\left(\frac{2\theta_\lambda}{k}\right); \qquad f_\lambda \equiv -\operatorname{csch}\left(\frac{2\theta_\lambda}{k}\right). \tag{3.7b}$$

In (3.7b), θ_λ is the principal branch of the square root function defined by

$$\theta_\lambda \equiv \theta_0\sqrt{1+\tau\lambda}\,, \qquad \theta_0 \equiv D^{-1/2}\,. \tag{3.7c}$$

Next, we substitute (3.1) and (3.6) into (2.17a). This yields the nonlocal eigenvalue problem for $\Phi(y)$, for $i = 1,..,k$,

$$c_i\left(\Phi'' - \Phi + 2w\Phi\right) - \frac{12w^2}{\mathcal{A}^2U_\pm^2}\left[(1+\tau\lambda)\,D\right]^{-1/2}\left(\mathcal{B}^{-1}\boldsymbol{c}\right)_i\left(\frac{\int_{-\infty}^{\infty} w\Phi\,dy}{\int_{-\infty}^{\infty} w^2\,dy}\right) = \lambda c_i\Phi\,, \tag{3.8}$$

with $\Phi(y)\to 0$ as $|y|\to\infty$. Therefore, we must calculate the spectrum of the matrix eigenvalue problem

$$\mathcal{B}\boldsymbol{c} = \kappa\boldsymbol{c}\,. \tag{3.9}$$

From (3.6), we have

$$\kappa = \kappa_0 + \frac{6}{\mathcal{A}^2 U_\pm^2} \left[(1 + \tau\lambda)\, D \right]^{-1/2} , \tag{3.10}$$

where κ_0 and $\boldsymbol{c}$ is an eigenpair of $\mathcal{B}_0$. The eigenpairs of $\mathcal{B}_0$ were calculated explicitly in Proposition 2 of [14], where the following result was obtained:

Lemma 3.1: *The eigenvalues κ_{0j}, ordered as $0 < \kappa_{01} < \ldots < \kappa_{0k}$, and the normalized eigenvectors $\boldsymbol{c}_j$ of $\mathcal{B}_0$ are*

$$\kappa_{0j} = 2 \tanh\left(\theta_\lambda / k\right) + 2 \left[1 - \cos\left(\frac{\pi(j-1)}{k} \right) \right] \operatorname{csch}\left(2\theta_\lambda / k\right) , \qquad j = 1, \ldots, k , \tag{3.11a}$$

$$\boldsymbol{c}_1^t = \frac{1}{\sqrt{k}} \left(1, \ldots, 1\right) ; \quad c_{l,j} = \sqrt{\frac{2}{k}} \cos\left(\frac{\pi(j-1)}{k} \left(l - 1/2\right) \right) , \quad j = 2, \ldots, k . \tag{3.11b}$$

Here $\boldsymbol{c}^t$ denotes transpose and $\boldsymbol{c}_j^t = (c_{1,j}, \ldots, c_{k,j})$.

Substituting (3.9), (3.10), and (3.11), into (3.8), we obtain the following spectral problem for the large $O(1)$ eigenvalues of (2.17):

Proposition 3.2: *Assume that $0 < \varepsilon \ll 1$. Then, with $\Phi = \Phi(y)$, the $O(1)$ eigenvalues of (2.17) satisfy the nonlocal eigenvalue problem*

$$L_0 \Phi - \chi w^2 \left(\frac{\int_{-\infty}^{\infty} w\Phi \, dy}{\int_{-\infty}^{\infty} w \, dy} \right) = \lambda \Phi , \qquad -\infty < y < \infty , \tag{3.12a}$$

$$\Phi \to 0 , \qquad \text{as} \quad |y| \to \infty . \tag{3.12b}$$

Here the operator L_0, referred to as the local operator, is defined by

$$L_0 \Phi \equiv \Phi'' - \Phi + 2w\Phi . \tag{3.12c}$$

The multiplier $\chi = \chi(z; j)$ in (3.12) is given explicitly by

$$\chi = \chi(z; j) \equiv 2s \left(s + \frac{\sqrt{1+z}}{\tanh\left(\theta_0 / k\right)} \left[\tanh\left(\theta_\lambda / k\right) + \frac{\left(1 - \cos\left[\pi(j-1)/k\right]\right)}{\sinh\left(2\theta_\lambda / k\right)} \right] \right)^{-1} , \tag{3.13a}$$

where

$$z \equiv \tau\lambda , \qquad \theta_\lambda \equiv \theta_0 \sqrt{1+z} , \qquad \theta_0 \equiv D^{-1/2} , \tag{3.13b}$$

and s is defined by

$$s \equiv \frac{1 - U_\pm}{U_\pm} . \tag{3.14}$$

Here $U_\pm$ is determined in terms of $\mathcal{A}/\mathcal{A}_{ke}$ by (2.11). The global eigenfunction $\phi(x)$ is given by (3.1), where the coefficients $\boldsymbol{c}^t = (c_1, \ldots, c_k)$ are the eigenvectors of $\mathcal{B}_0$ given in (3.11b).

We now establish an important spectral equivalence principle between the nonlocal eigenvalue problem (3.12) and a corresponding nonlocal eigenvalue problem derived in Proposition 2.3 of [38] for the GM model (1.10) with exponent set (p, q, m, s). For this general exponent set, Proposition 2.3 of [38] shows that the nonlocal eigenvalue problem for the GM model with exponent set $(2, q, 2, s)$ has exactly the same form as in (3.12), except that χ in (3.13) is to be replaced with

$$\chi = \chi(z; j) \equiv 2q \left(s + \frac{\sqrt{1+z}}{\tanh(\theta_0/k)} \left[\tanh(\theta_\lambda/k) + \frac{(1 - \cos[\pi(j-1)/k])}{\sinh(2\theta_\lambda/k)} \right] \right)^{-1} . \tag{3.15}$$

Therefore, we conclude that the nonlocal eigenvalue problems for the GM model and the Gray-Scott model are identical if we take $q = s$, to get the GM exponent set $(p, q, m, s) = (2, s, 2, s)$, where s is given in (3.14). However, in the GM model, the usual assumption on the exponents (p, q, m, s) are that they satisfy $\zeta \equiv qm/(p-1) - (1+s) > 0$. The spectral results in [38] for the GM model were obtained under this condition. With the exponent set $(2, s, 2, s)$, we calculate $\zeta = s - 1$. Since $0 < s < 1$ corresponds to the large solution, while $s > 1$ corresponds to the small solution, we obtain the following spectral equivalence principle between the Gray-Scott and the GM models:

Proposition 3.3: *In the limit $\varepsilon \ll 1$, consider the large eigenvalues of (2.17). The nonlocal eigenvalue problem for the stability of the small k-spike symmetric equilibrium solution u_-, ν_- of the Gray-Scott problem (1.6) is identical to the related nonlocal eigenvalue problem for the GM model with exponent set $(p, q, m, s) = (2, s, 2, s)$, where $s > 1$ is given in (3.14). The spectral problem for the large solution of the Gray-Scott model is also equivalent to that for a GM model with exponents $(2, s, 2, s)$, except that $\zeta < 0$ in (1.11).*

In the context of the Gray-Scott model, the eigenvalue problem (3.12) is new. The equivalence principle of Proposition 3.3 allows us to immediately analyze the stability of the small solution of the Gray-Scott model by directly appealing to the results of [38] obtained for the GM model with arbitrary exponent set (p, q, m, s) satisfying (1.11). For the large solution u_+, ν_+, we have to extend the analysis in [38] to allow for a GM model with exponent set $(2, s, 2, s)$, but with $\zeta = s - 1 < 0$.

Next, we reformulate (3.12) into a form more amenable to analysis. Let $\psi(y)$ be the solution to

$$L_0\psi \equiv \psi'' - \psi + 2w\psi = \lambda\psi + w^2 ; \qquad \psi \to 0 \quad \text{as} \quad |y| \to \infty . \tag{3.16}$$

Then, the eigenfunctions of (3.12) can be written as

$$\Phi = \chi(\tau\lambda; j)\psi J , \qquad J \equiv \frac{\int_{-\infty}^{\infty} w\Phi \, dy}{\int_{-\infty}^{\infty} w^2 \, dy} . \tag{3.17}$$

We then multiply both sides of (3.17) by w and integrate over the domain. Assuming, as mentioned earlier, that $\int_{-\infty}^{\infty} w\Phi\, dy \neq 0$, we then obtain that the eigenvalues of (3.12) are the union of the zeros of the functions $g_j(\lambda) = 0$ for $j = 1, .., k$, where

$$g_j(\lambda) \equiv C_j(\lambda) - f(\lambda)\,, \qquad f(\lambda) \equiv \frac{\int_{-\infty}^{\infty} w\,(L_0 - \lambda)^{-1}\, w^2\, dy}{\int_{-\infty}^{\infty} w^2\, dy}\,. \tag{3.18}$$

Here we have defined $C_j(\lambda) \equiv [\chi(\tau\lambda; j)]^{-1}$, so that from (3.13a) we get

$$C_j(\lambda) = \frac{1}{2} + \frac{\sqrt{1+\tau\lambda}}{2s\tanh(\theta_0/k)}\left[\tanh(\theta_\lambda/k) + \frac{(1-\cos[\pi(j-1)/k])}{\sinh(2\theta_\lambda/k)}\right]\,. \tag{3.19}$$

After establishing the theoretical results in §3.2, in §3.3 we numerically determine the roots of (3.18) by following a similar approach as in [38]. We use a combination of Newton's method coupled to the numerical solution to the boundary value problem (3.16) obtained by COLSYS [1]. Although (3.16) can be solved explicitly in terms of hypergeometric functions [4], we avoid this approach since with these special functions it is then difficult to prove rigorous results for the spectrum of (3.12).

3.2 Theoretical Results on the Spectrum: Large Eigenvalues

We begin by looking for roots of (3.18) on the non-negative real axis $\lambda = \lambda_R \geq 0$. The first observation is that $f(\lambda_R)$ has a singularity on the positive real axis as a consequence of Theorem 2.12 of [19].

Lemma 3.4: (From [19]): *Consider the local eigenvalue problem $L_0\phi_l = \sigma\phi_l$ for $\phi_l \in \mathcal{H}^1(R)$. This problem admits the eigenvalues $\sigma_0 > 0$, $\sigma_1 = 0$, and $\sigma_j < 0$ for $j > 1$. The eigenvalue σ_0 is simple, and the corresponding eigenfunction ϕ_{l0} has one sign.*

A simple calculation yields $\sigma_0 = 5/4$. Therefore, $f(\lambda_R) \to +\infty$ as $\lambda_R \to \sigma_0^-$. In [38] a detailed study of the behavior of $f(\lambda_R)$ on the positive real axis was given. The following rigorous result is a consequence of Proposition 3.5 of [38]:

Proposition 3.5: (From [38]): *For $\lambda_R \geq 0$, the function $f(\lambda_R)$ in (3.18) has the local behavior,*

$$f(\lambda_R) \sim 1 + \frac{3\lambda_R}{4} + \kappa_c\lambda_R^2 + O(\lambda_R^3)\,, \quad \text{as} \quad \lambda_R \to 0\,; \qquad \kappa_c \equiv \frac{\int_{-\infty}^{\infty}\left(L_0^{-1}w\right)^2\, dy}{\int_{-\infty}^{\infty} w^2\, dy} > 0\,. \tag{3.20a}$$

In addition, we have the global behavior

$$f'(\lambda_R) > 0 \quad \text{and} \quad f''(\lambda_R) > 0\,, \quad \text{for} \quad 0 < \lambda_R < \sigma_0\,. \tag{3.20b}$$

Moreover, $f(\lambda_R) \to +\infty$ as $\lambda_R \to \sigma_0^-$. On the other side of the singularity we have

$$f(\lambda_R) < 0\,, \quad \text{for} \quad \lambda_R > \sigma_0\,. \tag{3.20c}$$

Proof: This result is simply Proposition 3.5 of [38] for a GM model with exponents $p = m = 2$. ■

Next, we summarize the key properties of $C_j(\lambda)$ when $\lambda = \lambda_R \geq 0$ is real.

Proposition 3.6: *For any fixed $\tau > 0$, we have a monotonicity result for $\lambda_R \geq 0$ that*

$$C_k(\lambda_R) > C_{k-1}(\lambda_R) > \ldots > C_1(\lambda_R) > 0\,, \qquad C_k^{'}(\lambda_R) < C_{k-1}^{'}(\lambda_R) < \ldots < C_1^{'}(\lambda_R)\,. \tag{3.21a}$$

In addition, for $\tau > 0$, and for each $j = 1, \ldots, k$, we have for $\lambda_R > 0$ that

$$C_j^{'}(\lambda_R) > 0\,, \qquad C_j^{''}(\lambda_R) < 0\,, \qquad C_j^{'}(\lambda_R) = O(\tau^{1/2})\,, \quad \text{as} \quad \tau \to +\infty\,. \tag{3.21b}$$

Define the coefficients B_j by $B_j = C_j(0)$ for $j = 1, .., k$. These coefficients are independent of τ and have the following properties:

$$B_1 < B_2 < \ldots < B_k\,, \qquad B_1 = \frac{(s+1)}{2s}\,, \tag{3.21c}$$

$$\frac{dB_j}{dD} > 0\,, \quad \text{for} \quad j = 2, \ldots, k\,; \qquad \frac{dB_j}{ds} < 0\,, \quad \text{for} \quad j = 1, \ldots, k\,. \tag{3.21d}$$

Proof: This is Proposition 5.1 of [38] for a GM model with exponents $(p, q, m, s) = (2, s, 2, s)$. The monotonicity result for B_j with respect to s is immediate from (3.19). ■

As shown below, the critical values of D and $\mathcal{A}$ where $B_j = 1$ for $j = 2, \ldots, k$ play a central role in the analysis. We now calculate these values. The first observation is that for the large solution branch where $0 < s < 1$, we have from (3.21c) that $B_j > 1$ for $j = 1, \ldots, k$. Therefore,

$$1 < C_1(0) < C_2(0) < \ldots < C_k(0)\,, \qquad \text{for} \quad 0 < s < 1\,. \tag{3.22}$$

For the small solution branch where $s > 1$ we calculate the values $D = D_j$ for which $B_j = 1$ for $j = 2, \ldots, k$. Note that since $B_1 < 1$ for any D, there is no threshold value D_1. A simple calculation using (3.19) and $B_j = C_j(0)$, yields that

$$B_j = \frac{1}{2}\left(1 + \frac{1}{s}\right) + \frac{\gamma_j}{4s\sinh^2(\theta_0/k)}\,, \qquad \gamma_j \equiv 1 - \cos\left(\frac{\pi(j-1)}{k}\right)\,. \tag{3.23}$$

Setting $B_j = 1$, for $j = 2, \ldots, k$, and solving for the thresholds D_j, we get

$$D_j \equiv \frac{4}{k^2 \left[\ln\left(r_j + \sqrt{r_j^2 - 1}\right)\right]^2}, \quad j = 2, \ldots, k; \qquad r_j \equiv \frac{\gamma_j}{s-1} + 1, \qquad j = 2, \ldots, k. \tag{3.24}$$

Alternatively, for a fixed D, we can calculate thresholds $\mathcal{A} = \mathcal{A}_j$ for which $B_j = 1$. Using (2.15b), which relates s in terms of $\mathcal{A}$, we set $B_j = 1$ in (3.23) to get

$$\mathcal{A}_j = \mathcal{A}_{ke} \frac{\left[(\gamma_j/2) + 2\sinh^2(\theta_0/k)\right]}{\left(\left[(\gamma_j/2) + 2\sinh^2(\theta_0/k)\right]^2 - (\gamma_j/2)^2\right)^{1/2}}, \qquad j = 2, \ldots, k. \tag{3.25}$$

Here $\mathcal{A}_{ke}$ are the existence thresholds for symmetric k-spike patterns given in (2.12). Since $\mathcal{A}$ is an increasing function of s for $s > 1$, it follows from (3.21c), (3.21d), (3.24), and (3.25), that

$$\mathcal{A}_2 < \mathcal{A}_3 < \ldots < \mathcal{A}_k, \qquad D_k < D_{k-1} < \ldots < D_2. \tag{3.26}$$

Therefore, when $D < D_k$, or when $\mathcal{A} > \mathcal{A}_k$, we have that $B_j < 1$ for $j = 2, \ldots, k$. We label these important critical values as

$$D_k \equiv D_{kL} \equiv \frac{4}{k^2 \left[\ln\left(r_k + \sqrt{r_k^2 - 1}\right)\right]^2}, \qquad r_k \equiv \frac{\gamma_k}{s-1} + 1, \quad \gamma_k \equiv 1 + \cos\left(\frac{\pi}{k}\right), \tag{3.27a}$$

$$\mathcal{A}_k \equiv \mathcal{A}_{kL} \equiv \mathcal{A}_{ke} \frac{\left((\gamma_k/2) + 2\sinh^2(\theta_0/k)\right)}{\left(\left[(\gamma_k/2) + 2\sinh^2(\theta_0/k)\right]^2 - (\gamma_k/2)^2\right)^{1/2}}. \tag{3.27b}$$

Next, we look for roots of (3.18), or equivalently eigenvalues of (3.12), on the non-negative imaginary axis $\lambda = i\lambda_I$, with $\lambda_I > 0$. Substituting $\lambda = i\lambda_I$ into (3.16) and (3.18), and extracting real and imaginary parts, we obtain that the eigenvalues of (3.12) with $\lambda = i\lambda_I$ and $\lambda_I \geq 0$ are the roots of the coupled system $g_{Rj} = g_{Ij} = 0$, where

$$g_{Rj}(\lambda_I) \equiv C_{Rj}(\lambda_I) - f_R(\lambda_I), \qquad g_{Ij}(\lambda_I) \equiv C_{Ij}(\lambda_I) - f_I(\lambda_I), \qquad j = 1, \ldots, k, \tag{3.28a}$$

and

$$f_R(\lambda_I) \equiv \frac{\int_{-\infty}^{\infty} wL_0 \left[L_0^2 + \lambda_I^2\right]^{-1} w^2\, dy}{\int_{-\infty}^{\infty} w^2\, dy}, \qquad f_I(\lambda_I) \equiv \frac{\lambda_I \int_{-\infty}^{\infty} w \left[L_0^2 + \lambda_I^2\right]^{-1} w^2\, dy}{\int_{-\infty}^{\infty} w^2\, dy}. \tag{3.28b}$$

Here we have defined $g_{Rj}(\lambda_I) \equiv \mathrm{Re}\left[g_j(i\lambda_I)\right]$, $g_{Ij}(\lambda_I) \equiv \mathrm{Im}\left[g_j(i\lambda_I)\right]$, and

$$C_{Rj}(\lambda_I) \equiv \mathrm{Re}\left[C_j(i\lambda_I)\right], \qquad C_{Ij}(\lambda_I) \equiv \mathrm{Im}\left[C_j(i\lambda_I)\right]. \tag{3.28c}$$

To analyze the spectrum of (3.12) on the imaginary axis, we need some qualitative properties of the functions f_R, f_I, C_{Rj}, and C_{Ij}. The key properties are summarized as follows.

Proposition 3.7: *The functions f_R and f_I in (3.28b) have the asymptotic behavior*

$$f_R(\lambda_I) \sim 1 - \kappa_c \lambda_I^2 + O(\lambda_I^4), \quad \text{as} \quad \lambda_I \to 0; \qquad f_R(\lambda_I) = 0\left(\lambda_I^{-2}\right), \quad \text{as} \quad \lambda_I \to \infty, \tag{3.29a}$$

$$f_I(\lambda_I) \sim \frac{3\lambda_I}{4} + O(\lambda_I^3), \quad \text{as} \quad \lambda_I \to 0; \qquad f_I(\lambda_I) = 0\left(\lambda_I^{-1}\right), \quad \text{as} \quad \lambda_I \to \infty. \tag{3.29b}$$

Here κ_c is given in (3.20a). Moreover, the functions $f_R(\lambda_I)$ and $f_I(\lambda_I)$ have the global behavior

$$f_R'(\lambda_I) < 0, \qquad f_I(\lambda_I) > 0, \quad \text{for} \quad \lambda_I > 0. \tag{3.29c}$$

For $\lambda_I > 0$ and $\tau > 0$, the functions C_{Rj} and C_{Ij} satisfy

$$C_{Rj}(0) = B_j, \quad C_{Rj}'(\lambda_I) > 0; \qquad C_{Ij}(0) = 0, \qquad C_{Ij}'(\lambda_I) > 0, \tag{3.30a}$$

$$C_{Rj}'(\lambda_I) = O(\tau^{1/2}), \qquad C_{Ij}'(\lambda_I) = O(\tau^{1/2}), \quad \text{as} \quad \tau \to \infty, \tag{3.30b}$$

$$C_{Rj}(\lambda_I) = C_{Rj}(0) + O(\tau\lambda_I), \qquad C_{Ij}(\lambda_I) = O(\tau\lambda_I), \quad \text{as} \quad \tau \to 0. \tag{3.30c}$$

Here B_j are the values $C_j(0) = B_j$, whose properties were given in (3.21c) and (3.21d).

Proof: The proof of the results in (3.29) are a special case of Propositions 3.1 and 3.2 of [38] corresponding to setting $p = m = 2$ in the GM model (1.10). The proof of (3.30) is immediate from setting $\lambda = i\lambda_I$ in the definition of $C_j(\lambda)$ in (3.19). ■

A critical ingredient for determining the number of eigenvalues in the right half-plane $\mathrm{Re}(\lambda) > 0$ is to derive a winding number criterion. Specifically, we calculate the winding number of $g_j(\lambda)$, with $\lambda = \lambda_R + i\lambda_I$ in (3.18) over the counterclockwise contour composed of the imaginary axis $-iR \le \mathrm{Im}\lambda \le iR$ and the semi-circle Γ_R, given by $|\lambda| = R > 0$, for $-\pi/2 \le \arg\lambda \le \pi/2$. Assuming that there are no zeros of $g_j(\lambda)$ on the imaginary axis, we let $R \to \infty$ and use the argument principle to determine the number of zeros of $g_j(\lambda)$ in the right half-plane. The function $g_j(\lambda)$ in (3.18) is analytic in the right half-plane, except at the simple pole $\lambda = \sigma_0 > 0$, where $\sigma_0 = 5/4$ is the unique positive eigenvalue of the operator L_0 (see Lemma 3.4 above). For any $\tau > 0$, we have from (3.19) that $C_j(\lambda) \sim O(\sqrt{\lambda})$ as $|\lambda| \to \infty$ in the right half-plane. Moreover, $f(\lambda) \to 0$ as $|\lambda| \to \infty$. Thus, for any $\tau > 0$, the change in the argument of $g_j(\lambda)$ over Γ_R as $R \to \infty$ is $\pi/2$. By using the argument principle, and $g_j(\overline{\lambda}) = \overline{g_j(\lambda)}$, we then obtain the following winding number criterion:

Proposition 3.8: *Let $\tau > 0$ and assume that there are no zeros of $g_j(\lambda)$ on the imaginary axis for*

$j = 1, \ldots, k$. *Then, the number of eigenvalues* M *of (3.12) in* $Re(\lambda) > 0$ *satisfies*

$$M = \frac{5k}{4} + \frac{1}{\pi} \sum_{j=1}^{k} [\arg g_j]_{\Gamma_I} \, . \tag{3.31}$$

Here $[arg\, g_j]_{\Gamma_I}$ *denotes the change in the argument of* $g_j(\lambda)$ *along the semi-infinite imaginary axis* $\Gamma_I = i\lambda_I$, $0 \le \lambda_I < \infty$, *traversed in the downwards direction.*

Using the properties given in Propositions 3.6 and 3.7, there are only a few possible values for $[\arg g_j]_{\Gamma_I}$. This leads to a more specific winding number criterion.

Proposition 3.9: *Let* $\tau > 0$. *Then, there are three distinct possibilities:*

$$\text{(1): if } \quad g_{Ij} < 0 \quad \text{when} \quad g_{Rj} = 0\,, \qquad \text{then} \quad [\arg g_j]_{\Gamma_I} = -5\pi/4\,, \tag{3.32a}$$

$$\text{(2): if } \quad g_{Ij} > 0 \quad \text{when} \quad g_{Rj} = 0\,, \qquad \text{then} \quad [\arg g_j]_{\Gamma_I} = 3\pi/4\,, \tag{3.32b}$$

$$\text{(3): if } \quad g_{Rj} > 0 \quad \text{for all } \lambda_I \ge 0\,, \qquad \text{then} \quad [\arg g_j]_{\Gamma_I} = -\pi/4\,. \tag{3.32c}$$

Proof: Let $\tau > 0$. From (3.30) and (3.29) we have that $C_{Rj}(\lambda_I)$ is a positive monotone increasing function, whereas $f_R(\lambda_I)$ is a positive monotone decreasing function. Therefore, $g_{Rj} = 0$ has at most one root. First suppose that $C_{Rj}(0) < f_R(0) = 1$ so that $g_{Rj} = 0$ has a root. Then, using (3.30) and (3.29) we have that $g_{Rj} \sim b\sqrt{\lambda_I}$ and $g_{Ij} \sim b\sqrt{\lambda_I}$ as $\lambda_I \to +\infty$ for some $b > 0$. In addition, from (3.29b) and the condition $C_{Ij}(0) = 0$, we have that $g_{Rj} < 0$ and $g_{Ij} = 0$ at $\lambda_I = 0$. This implies that $\arg g_j = \pi/4$ as $\lambda_I \to +\infty$, and $\arg g_j = -\pi$ at $\lambda_I = 0$. Since the root to $g_{Rj} = 0$ is unique, this shows that the change in the argument, $[\arg g_j]_{\Gamma_I}$, is either $5\pi/4$ or $-3\pi/4$ depending on the sign of g_{Ij} at the unique root of $g_{Rj} = 0$. This proves (3.32a) and (3.32b). Next, suppose that $C_{Rj}(0) > f_R(0) = 1$. Then, since $g_{Rj}(0) > 0$ and $g'_{Rj}(\lambda_I) > 0$ from (3.29c) and (3.30a), we conclude that $g_{Rj} > 0$ for $\lambda_I \ge 0$. In this case, $\arg g_j = 0$ at $\lambda_I = 0$. Since $g_{Rj} > 0$ for all $\lambda_I > 0$, the result (3.32c) follows. ■

There are many consequences of Propositions 3.5–3.9. The first concerns the stability of the large solution u_+, ν_+.

Proposition 3.10: *For any* $\tau > 0$, $D > 0$, *and* $0 < s < 1$, *the large solution* u_+, ν_+ *is unstable. In this case there are exactly* k *eigenvalues of (3.12) in the right half-plane, and they are all located on the positive real axis in the interval* $0 < \lambda_R < \sigma_0 = 5/4$. *These* k *real eigenvalues have a common leading-order asymptotic behavior*

$$\lambda_R \sim \frac{5}{4} + \delta_1/\tau^{1/2} + \cdots\,, \qquad \text{as} \quad \tau \to \infty\,, \tag{3.33a}$$

where δ_1 is defined by

$$\delta_1 \equiv -\frac{\left(\int_{-\infty}^{\infty} w\phi_{l0}\,dy\right)\left(\int_{-\infty}^{\infty} w^2\phi_{l0}\,dy\right)}{c_\infty \int_{-\infty}^{\infty} w^2\,dy}\,, \qquad c_\infty \equiv \frac{\sqrt{5}}{4s}\left[\tanh\left(\theta_0/k\right)\right]^{-1}\,. \tag{3.33b}$$

Here ϕ_{l0} is the principal eigenfunction of L_0 (see Lemma 3.4), normalized so that $\int_{-\infty}^{\infty}\phi_{l0}^2\,dy = 1$.

Proof: Let $\tau > 0$ and $0 < s < 1$. Since $C_{Rj}(0) = B_j > 1$ for $j = 1,\ldots,k$ from (3.22), we have $g_{Rj}(0) > 0$, and consequently $g_{Rj}(\lambda_I) > 0$ for $\lambda_I \geq 0$. Therefore, for $j = 1,\ldots,k$, condition (3) of Proposition 3.9 applies. From (3.31) this yields that there are $M = k$ eigenvalues in the right half-plane for any $\tau > 0$ and $0 < s < 1$. Next, we show that these eigenvalues are real and positive. For any $0 < s < 1$, (3.21c) and (3.21d) yield that $1 < B_1 < B_2 < \ldots < B_k$, and consequently $1 = f(0) < C_1(0) < \ldots < C_k(0)$. Proposition 3.6 proves that $C_j(\lambda_R)$ is a positive increasing and concave function, while $f(\lambda_R)$ is a positive increasing convex function on $0 \leq \lambda_R < \sigma_0$. Hence, it follows that $g_j(\lambda_R) = 0$ has exactly one root for each $j = 1,\ldots,k$ on the interval $0 \leq \lambda_R < \sigma_0$. Since $f(\lambda_R) < 0$ for $\lambda_R > \sigma_0$ from (3.20c), there can be no roots on $\lambda_R > \sigma_0$. Hence, we have k real positive eigenvalues for (3.12) on the interval $0 < \lambda_R < \sigma_0 = 5/4$. The asymptotic behavior (3.33) is obtained by expanding λ_R and ψ in fractional powers of τ similar to that done in Proposition 3.9 of [38] for the GM model, and noting from (3.19) that $C_j(\lambda_R) \sim c_\infty \tau^{1/2}$ as $\tau \to \infty$. We leave these details to the reader. ■

The next result gives a criterion for the stability of a one-spike small solution u_-, ν_-, and for a k-spike small solution when $D < D_{kL}$, or $\mathcal{A} > \mathcal{A}_{kL}$. Here D_{kL} and $\mathcal{A}_{kL}$ are the thresholds given in (3.27).

Proposition 3.11 *Let $\tau > 0$, $k = 1$, and consider the small solution u_-, ν_-, where $s > 1$. For such a solution, we have $M = 0$ when $\tau \ll 1$ and $M = 2$ when τ is sufficiently large. Moreover, there exists a value $\tau = \tau_{h1}$, depending on $\mathcal{A}$ and D, such that there is a pair of complex conjugate eigenvalues on the imaginary axis. For a multi-spike solution where $k > 1$, suppose that $D < D_{kL}$ or $\mathcal{A} > \mathcal{A}_{kL}$. Then, $M = 0$ when $\tau \ll 1$ and $M = 2k$ when $\tau \gg 1$. For $k \geq 1$, and for τ sufficiently large, these eigenvalues are real and are on the interval $0 < \lambda_R < \sigma_0 = 5/4$. There are k eigenvalues λ_{Bj} that tend to $\sigma_0 = 5/4$ from below as $\tau \to \infty$, and k eigenvalues λ_{Sj} that tend to zero as $\tau \to \infty$. The λ_{Bj} for $j = 1,\ldots,k$ have the common asymptotic behavior (3.33), while the asymptotic behavior of λ_{Sj} is given by*

$$\lambda_{Sj} \sim \frac{\omega_j}{\tau} + O(\tau^{-2})\,, \quad j = 1,\ldots,k\,. \tag{3.34}$$

Here ω_j is the unique positive root of $C_j(\omega_j\tau^{-1}) = 1$.

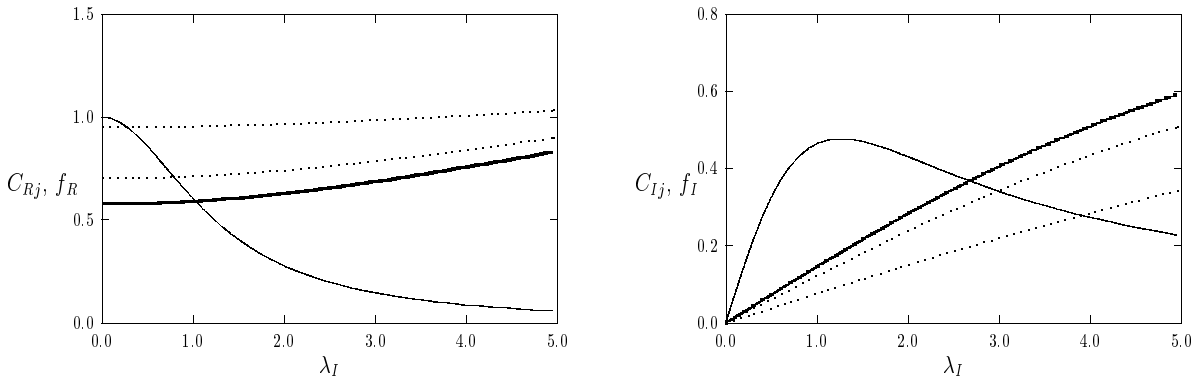

(a) $g_{Rj} = 0$ (b) $g_{Ij} = 0$

Figure 7: Parameter values are $D = 0.75$, $k = 3$, $\mathcal{A} = 9.023$, and $\tau = 2.0$. Left figure: $C_{Rj}(\lambda_I)$, for $j = 1, \ldots, 3$, and $f_R(\lambda_I)$ (solid curve). Right figure: $C_{Ij}(\lambda_I)$ and $f_I(\lambda_I)$ (solid curve). In these figures C_{R1} and C_{I1} are the heavy solid curves.

Proof: Let $\tau > 0$, $s > 1$, and $k \geq 1$. Assume for $k > 1$ that $D < D_{kL}$, or equivalently $\mathcal{A} > \mathcal{A}_{kL}$. We first show that $M = 0$ when $\tau \ll 1$ and $M = 2k$ when $\tau \gg 1$. In this case, we have $C_{Rj}(0) = B_j < f_R(0) = 1$ for $j = 1, \ldots, k$. This, implies that $g_{Rj}(0) < 0$, and so by the monotonicity of g_{Rj}, we have that $g_{Rj} = 0$ has a unique root for each $j = 1, \ldots, k$. Moreover, since C_{Rj} is monotone increasing in λ_I for $\tau > 0$, these roots must lie in the interval $(0, \lambda_{Ic})$, where λ_{Ic} is the unique root of $C_{R1}(0) = f_R(\lambda_I)$. Hence, λ_{Ic} is independent of τ. Since $C_{Ij} \to 0$ uniformly as $\tau \to 0$ for any fixed λ_I from (3.30c), it follows that for $\tau \ll 1$ we have $g_{Ij} < 0$ whenever $g_{Rj} = 0$. Hence, for $\tau \ll 1$ condition (1) in Proposition 3.9 applies. Then, from the winding number criterion (3.31) we get $M = 0$. Alternatively, since at each fixed λ_I, C_{Ij} increases without bound as $\tau \to \infty$ from (3.30b), we have that $g_{Ij} > 0$ at the unique root of $g_{Rj} = 0$. Therefore, for $\tau \gg 1$, condition (2) in Proposition 3.9 holds, and we get $M = 2k$ from (3.31). Next, we show that for $k \geq 1$, and $\tau \gg 1$ that there are $2k$ eigenvalues on the real axis in $0 < \lambda_R < \sigma_0$. Along the real axis, we have from Proposition 3.5 that $f(0) = 1$, and $f(\lambda_R)$ is an increasing, convex, function on $0 < \lambda_R < \sigma_0$. Moreover, $f(\lambda_R) \to +\infty$ as $\lambda_R \to \sigma_0^-$, and $f(\lambda_R) < 0$ for $\lambda_R > \sigma_0$. In contrast, from (3.21b) we have that $C_j(\lambda_R)$ is a monotone increasing concave function, with an unbounded derivative for $\tau \gg 1$. When $D < D_{kL}$, or when $\mathcal{A} > \mathcal{A}_{kL}$, we have that $C_j(0) = B_j < f(0) = 1$ for $j = 1, \ldots, k$. Therefore,

as τ is increased, there must be a critical value $\tau_{mj} > 0$ where $C_j(\lambda_R)$ and $f(\lambda_R)$ first intersect tangentially. For $\tau > \tau_{mj}$ there must be two roots to $g_j(\lambda) = 0$. The values $\tau = \tau_{mj}$ for $j = 1, \ldots, k$ are the values where complex conjugate eigenvalues merge onto the real axis. Clearly, as $\tau \to \infty$, one root of each $g_j(\lambda_R) = 0$ tends to σ_0^- while the other root tends to zero. The precise asymptotic behavior of these roots as $\tau \to \infty$ is obtained in a similar way as in Propositions 3.8 and 3.9 of [38]. We leave these details to the reader. Since for $k = 1$ we have $M = 0$ for $\tau \ll 1$ and $M = 2$ for $\tau \gg 1$, the existence of a Hopf bifurcation value τ_{h1} (possibly non-unique) follows by continuity. ■

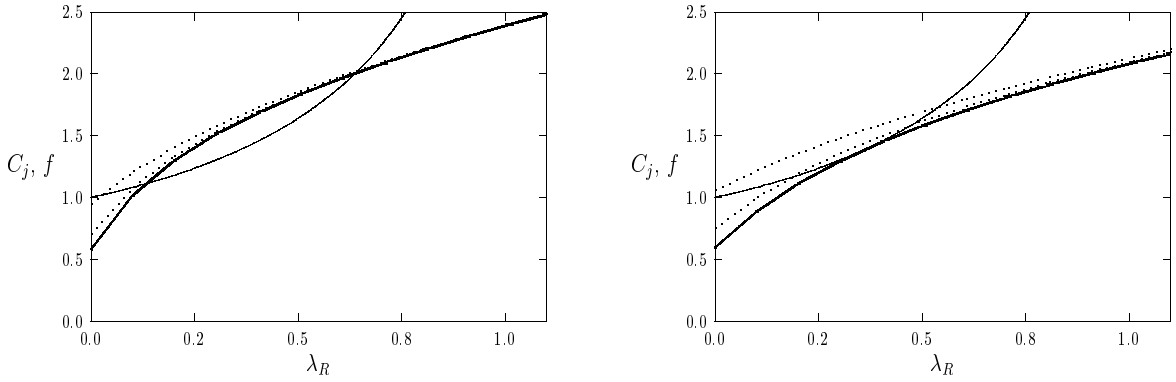

(a) $g_j = 0$ (b) $g_j = 0$

Figure 8: Plots of $C_j(\lambda_R)$, for $j = 1, 2, 3$, and $f(\lambda_R)$ (solid curve). The heavy solid curve is $C_1(\lambda_R)$. Left figure: parameter values are $D = 0.75$, $k = 3$, $\mathcal{A} = 9.023$, and $\tau = 80.0$. Right figure: parameter values are $D = 0.75$, $k = 3$, $\mathcal{A} = 8.357$, and $\tau = 36.93$. For these values, $C_1(\lambda_R)$ intersects $f(\lambda_R)$ tangentially. For this data we have $\mathcal{A}_2 < \mathcal{A} < \mathcal{A}_{3L}$.

To illustrate this result, we take the parameter values $D = 0.75$, $k = 3$, $\mathcal{A} = 9.023$, and $\tau = 2.0$. For these values, we calculate from (3.27b) that $\mathcal{A} > \mathcal{A}_{3L} = 8.686$, so that Proposition 3.11 applies. In Fig. 7(a) we plot the numerically computed $f_R(\lambda_I)$ and $C_{Rj}(\lambda_I)$ for $j = 1, \ldots, 3$. A similar plot of $f_I(\lambda_I)$ and $C_{Ij}(\lambda_I)$, for $j = 1, \ldots, 3$, is shown in Fig. 7(b). For this small value $\tau = 2.0$ it is clear from these figures that whenever $g_{R_j} = 0$ we have $g_{Ij} < 0$. Since condition (1) of Proposition 3.9 holds for each $j = 1, 2, 3$, we get from (3.31) that $M = 0$. Hence, there are no eigenvalues of (3.12) in the right half-plane. In Fig. 8(a) we plot $C_j(\lambda_R)$ and $f(\lambda_R)$ with $\tau = 80.0$, and for the same parameter values given above. For this large value of τ, each $C_j(\lambda_R)$ intersects $f_R(\lambda_R)$ exactly twice.

Hence, we have six real positive eigenvalues on the interval $0 < \lambda_R < 5/4$.

For a one-spike solution, the main limitation of Proposition 3.11 is that we are not able to prove that the Hopf bifurcation value τ_{h1} is unique. In particular, we cannot theoretically rule out the case that there are N, with $N > 1$ and odd, values of τ_{h1} where there are complex conjugate eigenvalues on the imaginary axis. To show that $N = 1$, and hence that τ_{h1} is unique, one would have to prove a strict transversal crossing condition that states that whenever $\tau > \tau_{h1}$ there are two eigenvalues in the right half-plane, so that $M = 2$ for all $\tau > \tau_{h1}$. From all of the numerical experiments that we have performed it appears that such a crossing condition does in fact hold. However, Proposition 3.11 does guarantee that there will be two real positive eigenvalues for all $\tau > \tau_{m1}$.

For the small solution branch, the qualitative difference between the spectrum of (3.12) for a one-spike and for a multi-spike solution is that only for a multi-spike solution can eigenvalues cross through the origin along the real axis $\mathrm{Im}(\lambda) = 0$ as D or $\mathcal{A}$ is varied. However, when $D < D_{kL}$ or $\mathcal{A} > \mathcal{A}_{kL}$, there are no real positive eigenvalues when $\tau \ll 1$. The real eigenvalues that exist when $\tau \gg 1$ have occurred from the merging of complex conjugate pairs of eigenvalues onto the real axis. These complex conjugate eigenvalues arise from a Hopf bifurcation. Notice that since $C_j(0)$ is independent of τ, the eigenvalues of (3.12) can never cross through the origin along the real axis as τ is increased. Therefore, instabilities as τ is increased can only occur from Hopf bifurcations, whereas instabilities that occur as D is increased or $\mathcal{A}$ is decreased occur from real eigenvalues entering the right half-plane.

The next result characterizes the number of eigenvalues in the right half-plane for a multi-spike solution for other ranges of D and $\mathcal{A}$, where there may be positive real eigenvalues when $\tau \ll 1$.

Proposition 3.12: *Let $\tau > 0$, $k > 1$, and consider the multi-spike small solution u_-, ν_-, where $s > 1$. Suppose that there exists a j^* with $2 \le j^* \le k$ such that either $D_{j^*} < D < D_{j^*-1}$, or $\mathcal{A}_{j^*-1} < \mathcal{A} < \mathcal{A}_{j^*}$. Here D_j and $\mathcal{A}_j$ for $j = 2, \ldots, k$ are given in (3.24) and (3.25), respectively. Since there are no thresholds for $j = 1$, we conveniently label $D_1 = \infty$ and $\mathcal{A}_1 = \mathcal{A}_{1e}$, where $\mathcal{A}_{1e}$ is the existence threshold of (2.12). Then, for any $\tau > 0$, the number of eigenvalues M of (3.12) in the right half-plane satisfies the bounds*

$$1 + k - j^* \le M \le k - 1 + j^* . \tag{3.35}$$

Moreover, there are at least $M_R = 1 + k - j^*$ eigenvalues on the positive real axis in the interval $0 < \lambda_R < \sigma_0 = 5/4$ for any $\tau > 0$.

Proof: The proof is simple. For the range of D and $\mathcal{A}$ stated above, we have $C_{Rj}(0) > 1$ for $j = j^*, \ldots, k$, and $C_{Rj}(0) < 1$ for $j = 1, \ldots, j^* - 1$. Hence, $g_{Rj}(\lambda_I) > 0$ for $j = j^*, \ldots, k$, and condition (3) of Proposition 3.9 holds. This yields $[\arg g_j]_{\Gamma_I} = -\pi/4$ for $j = j^*, \ldots, k$ and any $\tau > 0$.

For the other indices, we proceed as in the proof of Proposition 3.11, to get $[\arg g_j]_{\Gamma_I} = -5\pi/4$ for $j = 1, \ldots, j^* - 1$ when τ is sufficiently small, and $[\arg g_j]_{\Gamma_I} = 3\pi/4$ for $j = 1, \ldots, j^* - 1$ when τ is sufficiently large. Substituting these values into the winding number criterion (3.31) we obtain (3.35). It is clear that there are at least $M_R = 1 + k - j^*$ eigenvalues on the real axis when $\tau \ll 1$. This follows since $C_j(0) = B_j > 1 = f(0)$ for $j = j^*, \ldots, k$, and the fact that for any $\tau > 0$ the curve $C_j(\lambda_R)$ must intersect $f(\lambda_R)$ exactly once for each $j = j^*, \ldots, k$. ■

As a special case of this result, we set $j^* = 2$ to obtain $k - 1 < M < k + 1$. Therefore, when $D > D_2$, or when $\mathcal{A} < \mathcal{A}_2$, there will be at least $k - 1$ eigenvalues on the positive real axis. Here D_2 and $\mathcal{A}_2$ are given in (3.24) and (3.25), respectively. This range of the parameters is the near-shadow limit, since we know that a k-spike solution for the shadow problem, obtained by letting $D \to \infty$ in (1.6), will have $k - 1$ eigenvalues on the positive real axis when $\tau = 0$. Hence, this qualitative feature of the spectrum is preserved for finite values of D up until D crosses below D_2.

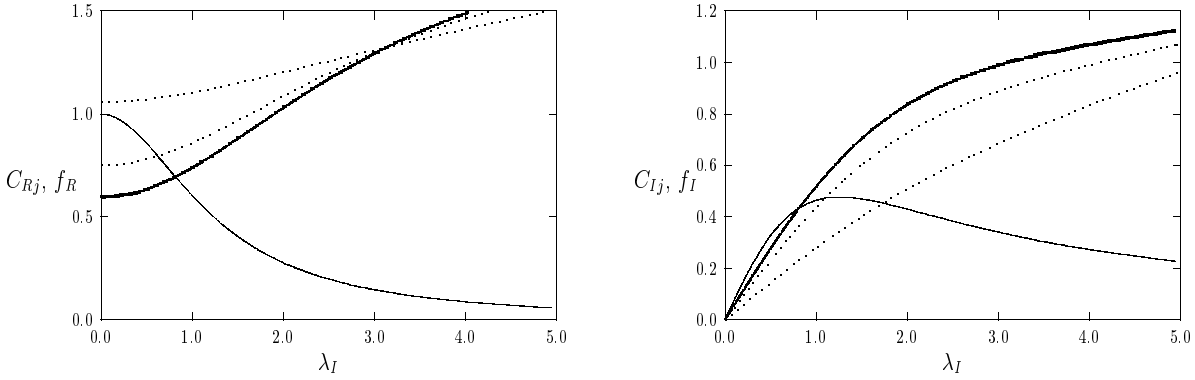

(a) $g_{Rj} = 0$ (b) $g_{Ij} = 0$

Figure 9: Parameter values $D = 0.75$, $k = 3$, $\mathcal{A} = 8.357$, and $\tau = 6.183$. Left figure: $C_{Rj}(\lambda_I)$, for $j = 1, \ldots, 3$, and $f_R(\lambda_I)$ (solid curve). Right figure: $C_{Ij}(\lambda_I)$ and $f_I(\lambda_I)$ (solid curve). In these figures C_{R1} and C_{I1} are the heavy solid curves.

To illustrate Proposition 3.12, we take the parameter values $D = 0.75$, $k = 3$, $\mathcal{A} = 8.357$ and $\tau = 36.93$. For these values, we calculate from (3.25) and (3.27b) that $\mathcal{A}_2 = 6.86$ and $\mathcal{A}_{3L} = 8.686$, so that $\mathcal{A}_2 < \mathcal{A} < \mathcal{A}_{3L}$. Therefore, this corresponds to setting $j^* = k = 3$ in Proposition 3.12 to get $1 \leq M \leq 5$. In Fig. 8(b) we show the graphical determination of the eigenvalues of (3.12) on the

positive real axis by plotting $C_j(\lambda_R)$, for $j = 1, \ldots, 3$, and $f(\lambda_R)$. Since $C_3(0) > 1$, we only get one root of $g_3 = 0$ for any $\tau > 0$. For the value $\tau = 36.93$, we have that C_1 intersects f_R tangentially. For $\tau \gg 1$, it is clear that we will have $M = 5$. For the smaller value $\tau = 6.183$, in Fig. 9(a) we plot $f_R(\lambda_I)$ and $C_{Rj}(\lambda_I)$ for $j = 1, \ldots, 3$. A similar plot of $f_I(\lambda_I)$ and $C_{Ij}(\lambda_I)$, for $j = 1, \ldots, 3$, is shown in Fig. 9(b). For this value of τ, we have $g_{R1} = g_{I1} = 0$. In addition, we have $g_{I2} < 0$ when $g_{R2} = 0$, and that $g_{R3}(\lambda_R) > 0$ for all $\lambda_R > 0$. Therefore, condition (1) and condition (3) of Proposition 3.9 holds for $j = 2$ and $j = 3$, respectively. Then, from (3.31), it is clear that this value of τ corresponds to where (3.12) has complex conjugate eigenvalues on the imaginary axis, together with one positive real eigenvalue.

The method of proof of Proposition 3.12 shows that there exists a value $\tau = \tau_{hj} > 0$ (possibly non-unique) such that $g_{Rj} = g_{Ij} = 0$. At this value of τ, there is a complex conjugate pair of eigenvalues on the imaginary axis. The minimum τ_{hL} of these values determines the stability threshold. Therefore, we define

$$\tau_{hL} \equiv \text{Min}\,(\tau_{hj}\,;\; j = 1, .., k)\;. \tag{3.36}$$

This critical value depends on k, D, and $\mathcal{A}$. The main stability results obtained in this section can now be summarized succinctly as follows.

Proposition 3.13: *Let $\tau > 0$, $k > 1$, and consider the multi-spike small solution u_-, ν_-, where $s > 1$. For $D < D_{kL}$, or $\mathcal{A} > \mathcal{A}_{kL}$, the solution will be stable with respect to the large eigenvalues when $0 < \tau < \tau_{hL}$. Alternatively, suppose that $D > D_{kL}$, or $\mathcal{A}_{ke} < \mathcal{A} < \mathcal{A}_{kL}$, then the solution is unstable for any $\tau > 0$.*

Although we have not been able to prove a strict transversal crossing condition, all of the numerical experiments that we have performed below indicate that the values τ_{hj} are uniquely defined. Specifically, when τ increases past a particular τ_{hj} an additional pair of complex conjugate eigenvalues enters into the right half-plane and remains in this plane for all $\tau > \tau_{hj}$. Therefore, we believe that when $D < D_{kL}$, or when $\mathcal{A} > \mathcal{A}_{kL}$, the multi-spike solution will be unstable for any τ with $\tau > \tau_{hL}$. When $D > D_{kL}$, or when $\mathcal{A} < \mathcal{A}_{kL}$, there is at least one positive real eigenvalue for any $\tau > 0$. In this range of D or $\mathcal{A}$, there may be additional complex conjugate pairs of eigenvalues in the right half-plane if τ is large enough.

Next, we discuss the two types of instabilities that can occur for multi-spike solutions to (1.6). We first discuss **competition instabilities** that occur as a result of eigenvalues on the positive real axis. Suppose that D satisfies $D_{kL} < D < D_{k-1}$, or equivalently $\mathcal{A}_{k-1} < \mathcal{A} < \mathcal{A}_{kL}$. Then, following the idea of the proof of Proposition 3.12, there will be exactly one eigenvalue in the right half-plane for $0 < \tau < \tau_{hL}$, and it is located along the real axis. Therefore, on this parameter range, the $j = k$

mode governs the instability. From Proposition 3.2, the unstable eigenvector is $\boldsymbol{c}_k$ given in (3.11b). This implies that the initial instability of the small k-spike pattern has the form

$$\nu = \nu_- + \delta e^{\lambda_{Rk} t}\phi\,, \qquad \phi(x) = \sum_{n=1}^{k} c_n \Phi\left[\varepsilon^{-1}(x - x_n)\right]\,. \tag{3.37a}$$

Here $\delta \ll 1$, $\lambda_{Rk} > 0$ is the unique root of $g_k(\lambda_R) = 0$, and

$$c_n = \cos\left(\frac{\pi(k-1)}{k}\,(n - 1/2)\right)\,, \quad n = 1, \ldots, k\,. \tag{3.37b}$$

Since $\sum_{n=1}^{k} c_n = 0$, this instability has the effect of locally preserving the sum of the heights of the spikes. Hence, we refer to it as a **competition instability**. As shown in the numerical experiments below, this mode initiates a spike competition process, decreasing the amplitudes of some spikes while increasing the amplitudes of others. Numerically, it is found that this type of instability has the ultimate effect of annihilating spikes.

Next, we discuss the type of oscillatory instability that occurs when $D < D_{kL}$, or $\mathcal{A} > \mathcal{A}_{kL}$, as τ increases past τ_{hL}. The value of j for which the minimum in (3.36) is obtained determines the unstable eigenvector $\boldsymbol{c}_j$ in Proposition 3.2. We now develop a criterion to determine which mode goes unstable first as τ is increased.

To do so, we first try to develop an ordering principle for C_{Rj} and C_{Ij}. From (3.19) and (3.28c), we readily calculate that for $j = 1, .., k-1$ that

$$C_{Rj+1} - C_{Rj} = \beta_j \mathrm{Re}\left[E(\xi)\right]\,, \qquad C_{Ij+1} - C_{Ij} = \beta_j \mathrm{Im}\left[E(\xi)\right]\,. \tag{3.38a}$$

Here $\beta_j > 0$ and $E(\xi)$ are defined by

$$\beta_j \equiv \left(\frac{k}{2\theta_0 s}\right)\left(\frac{\sin\left[\pi(j-1/2)/k\right]\sin\left[\pi/(2k)\right]}{\tanh\left(\theta_0/k\right)}\right) > 0\,, \qquad E(\xi) \equiv \frac{\xi}{\sinh\xi}\,, \tag{3.38b}$$

where

$$\xi \equiv \frac{2\theta_0}{k}\sqrt{1 + i\tau\lambda_I}\,. \tag{3.38c}$$

This leads to the following ordering principle:

Lemma 3.14: *Suppose that* $Re\left[E(\xi)\right] > 0$ *and* $Im\left[E(\xi)\right] < 0$ *at each point on some interval* $0 < \lambda_I < \lambda_*$. *Then, we have the following ordering principle on* $0 < \lambda_I < \lambda_*$:

$$C_{R1}(\lambda_I) < \ldots < C_{Rk}(\lambda_I)\,, \qquad C_{I1}(\lambda_I) > \ldots > C_{Ik}(\lambda_I)\,. \tag{3.39}$$

When this ordering principle holds, the mode that goes unstable first must be the $j = 1$ mode. We state the result as follows.

Proposition 3.15: *Let $\varepsilon \to 0$, $k > 1$ and consider the small solution u_-, ν_-. Let τ_{h1} correspond to the minimum value of τ for which $g_{R1} = g_{I1} = 0$. Label the corresponding root by $\lambda_I = \lambda_{h1}$. Suppose that for the value $\tau = \tau_{h1}$, the ordering principle of Lemma 3.14 holds at each point on the interval $0 < \lambda_I < \lambda_{h1}$. Then, there are either zero or two eigenvalues in the right half-plane for τ in a sufficiently small neighborhood of $\tau = \tau_{h1}$.*

Proof: The proof is simple. Since the ordering principle (3.39) holds when $\tau = \tau_{h1}$, it follows by continuity that it holds in a sufficiently small neighborhood of τ_{h1}. Therefore, we will have $g_{Ij} < 0$ whenever $g_{Rj} = 0$ for $j = 2, .., k-1$. This implies that condition (1) of Proposition 3.9 holds, and so we get $[\arg g_j]_{\Gamma_I} = -5\pi/4$ for $j = 2, \ldots, k$. From (3.31) we obtain $M = 0$ or $M = 2$ depending on whether $[\arg g_1]_{\Gamma_I} = -5\pi/4$ or $[\arg g_1]_{\Gamma_I} = 3\pi/4$. ■

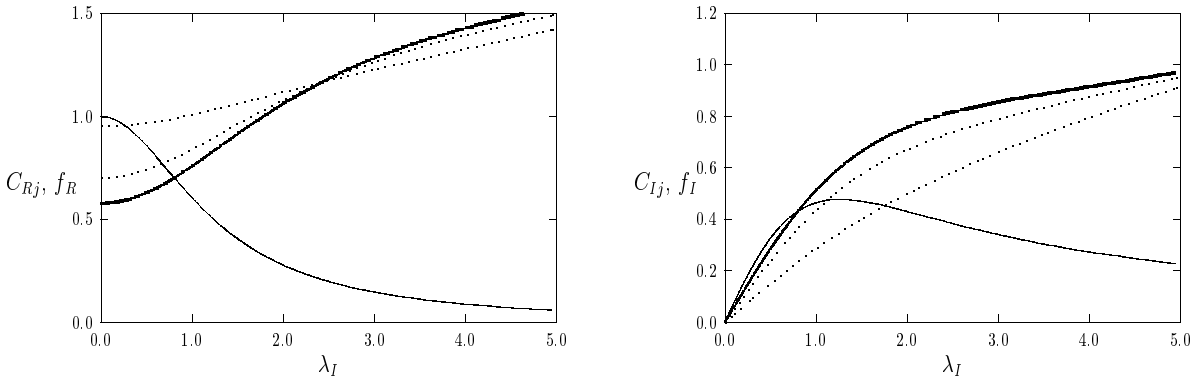

(a) $g_{Rj} = 0$ (b) $g_{Ij} = 0$

Figure 10: Parameter values $D = 0.75$, $k = 3$, $\mathcal{A} = 9.023$, and $\tau = 8.049$. Left figure: $C_{Rj}(\lambda_I)$, for $j = 1, \ldots, 3$, and $f_R(\lambda_I)$ (solid curve). Right figure: $C_{Ij}(\lambda_I)$ and $f_I(\lambda_I)$ (solid curve). In these figures C_{R1} and C_{I1} are the heavy solid curves.

To illustrate Proposition 3.15, we consider the parameter values of Fig. 7 where $D = 0.75$, $k = 3$, and $\mathcal{A} = 9.023 > \mathcal{A}_{3L}$. For $\tau = 8.049$, in Fig. 10(a) we plot the numerically computed $f_R(\lambda_I)$ and $C_{Rj}(\lambda_I)$ for $j = 1, \ldots, 3$. A similar plot of $f_I(\lambda_I)$ and $C_{Ij}(\lambda_I)$, for $j = 1, \ldots, 3$, is shown in Fig. 10(b). For this value of τ it is clear from these figures that the ordering principle (3.39) holds,

and so the $j = 1$ sets the stability threshold. Therefore, for $\tau = 8.049$, it follows that (3.12) has no eigenvalues in the right half-plane, but has a pair of complex conjugate eigenvalues on the imaginary axis determined by the $j = 1$ mode. This is the Hopf bifurcation value.

Under the conditions of Proposition 3.15, it is guaranteed that the $j = 1$ mode goes unstable first. The corresponding eigenvector $\boldsymbol{c}_1$ is given in (3.11b) as $\boldsymbol{c}_1^t = (1, \ldots, 1)$. In this way, we obtain that at $\tau = \tau_{h1}$ the instability takes the form

$$\nu = \nu_- + \delta e^{i\lambda_{h1} t}\phi + \text{c.c}\,, \quad \phi(x) = \sum_{n=1}^{k} c_n \Phi\left[\varepsilon^{-1}(x - x_n)\right]\,, \quad c_n = 1\,, \quad n = 1, .., k\,. \tag{3.40}$$

Here c.c denotes complex conjugate, $\delta << 1$, and λ_{h1} is the root of $g_{R1} = g_{I1} = 0$, which occurs when $\tau = \tau_{h1}$. The key observation is that since $c_n = 1$, for $n = 1, .., k$, the initial form of the instability is to synchronize the amplitudes of the spikes. We refer to this as a **synchronous oscillatory instability**. Therefore, if the ordering principle in Lemma 3.14 holds, the $j = 1$ mode goes unstable first, and the effect is to synchronize the small-scale oscillations in the spike amplitudes.

The critical condition in Lemma 3.14 is to determine the signs of $\text{Re}\,[E(\xi)]$ and $\text{Im}\,[E(\xi)]$. Writing $\xi = \xi_R + i\xi_I$, a simple calculation shows that $\text{Re}\,[E(\xi)] > 0$ if and only if

$$\tanh\xi_R \cos\xi_I + \frac{\xi_I}{\xi_R}\sin\xi_I > 0\,. \tag{3.41a}$$

Similarly, $\text{Im}\,[E(\xi)] < 0$ if and only if

$$\sin\xi_I - \frac{\xi_I}{\xi_R}\tanh\xi_R \cos\xi_I > 0\,. \tag{3.41b}$$

From the definition of ξ in (3.38c), it is clear that both inequalities in (3.41) will hold when $\tau\lambda_I$ is small enough. Therefore, it is natural to look for a condition for which the $j = 1$ governs the instability. The precise condition was stated in Proposition 3.15.

Finally, we remark on the possibility of having an asynchronous small-scale oscillation near the Hopf bifurcation point τ_{hL}. Such an asynchronous instability is governed by the $j = k$ mode which, as discussed above with respect to competition instabilities, has the effect of conserving the amplitude of spikes. The $j = k$ mode will govern the initial instability when both $\text{Re}\,[E(\xi)]$ and $\text{Im}\,[E(\xi)]$ have exactly one zero-crossing on the interval $0 < \lambda_I < \lambda_{hk}$, where $\lambda_I = \lambda_{hk}$ and $\tau = \tau_{hk}$ is the root of $g_{Rk} = g_{Ik} = 0$. Although we show in Example 4 of §3.3 that asynchronous oscillatory instabilities are theoretically possible in a narrow parameter range, we have not been able to realize such oscillations in the Gray-Scott model in the low or intermediate feed-rate regime.

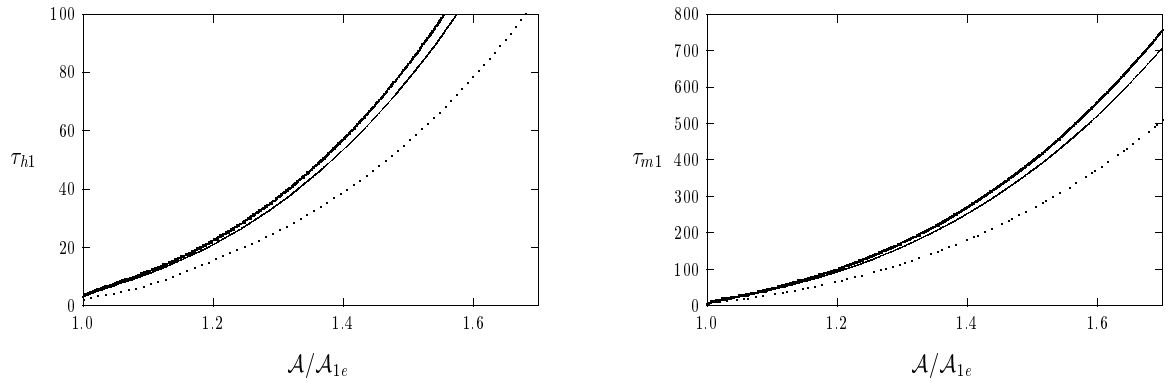

(a) τ_{h1} (b) τ_{m1}

Figure 11: Left figure: the Hopf bifurcation value τ_{h1} versus $\mathcal{A}/\mathcal{A}_{1e}$ for a one-spike solution. Right figure: τ_{m1} versus $\mathcal{A}/\mathcal{A}_{1e}$ where the complex pair of eigenvalues merge onto the positive real axis. The labels are $D = 0.75$ (dashed curve), $D = 0.25$ (solid curve), and $D = 0.1$ (heavy solid curve).

3.3 Numerical Results: Oscillatory and Competition Instabilities

We now give some numerical results for the stability thresholds studied rigorously in §3.2. Here we will only consider instabilities of the small solution. To illustrate our results, we take $D = 0.75$ and $D = 0.1$. For $D = 0.75$, the spike interaction is strong and oscillatory instabilities occur for small values of τ. Moreover, for $D = 0.75$, spike competition instabilities due to positive real eigenvalues can also occur far from the existence threshold $\mathcal{A}_{ke}$. Alternatively, for $D = 0.1$, the inter-spike interaction is relatively weak and the finite domain does not play a very significant role in generating instabilities, unless we have many spikes. More specifically, for $k\sqrt{D} \ll 1$, instabilities due to positive real eigenvalues only occur very close to the existence threshold $\mathcal{A}_{ke}$. Recall also from (1.4), that our formulation of the Gray-Scott model required that $\tau > 1$. All of the stability thresholds for a Hopf bifurcation computed below for $D = 0.75$ and $D = 0.1$ satisfy this requirement.

For a one-spike solution, in Fig. 11(a) we plot the Hopf bifurcation threshold τ_{h1} versus $\mathcal{A}/\mathcal{A}_{1e}$ for $D = 0.75$, $D = 0.25$, and $D = 0.1$. These results suggest that τ_{h1} is an increasing function of $\mathcal{A}/\mathcal{A}_{1e}$, and that the stability threshold τ_{h1} is larger for smaller values of D. This is intuitive since for smaller values of D, the interaction of the spike with the boundaries of the domain is weaker.

In Fig. 11(b) we plot the values τ_{m1} where complex conjugate eigenvalues first merge onto the real axis. In Fig. 12(a) we plot the Hopf bifurcation frequency λ_{h1} versus $\mathcal{A}/\mathcal{A}_{1e}$. This frequency tends to a limiting value $\lambda_{h1} \approx 0.53$ for $\mathcal{A}/\mathcal{A}_{1e} \gg 1$ (see §5).

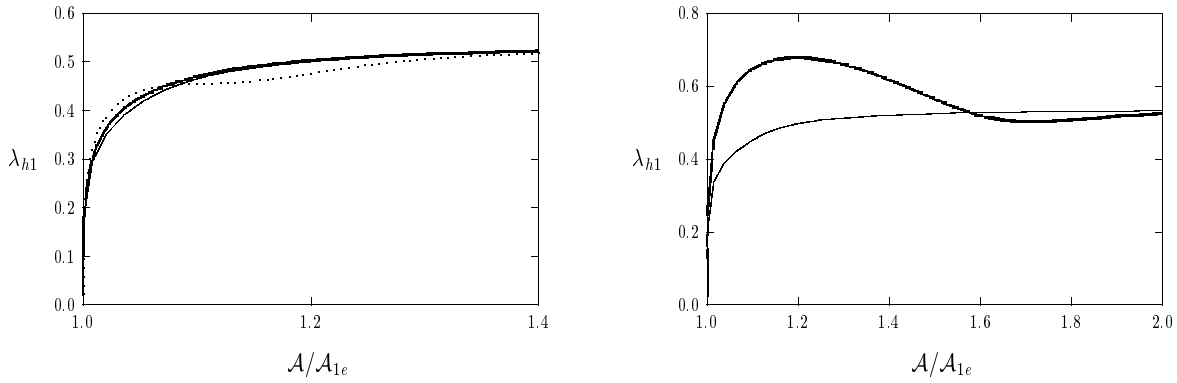

(a) λ_{h1} (b) λ_{h1}

Figure 12: Left figure: the Hopf bifurcation frequency λ_{h1} versus $\mathcal{A}/\mathcal{A}_{1e}$ for a one-spike solution with $D = 0.75$ (dashed curve), $D = 0.25$ (solid curve), and $D = 0.1$ (heavy solid curve). Right figure λ_{h1} for a two-spike solution with $D = 0.75$ (heavy solid curve) and $D = 0.1$ (solid curve).

Next we consider two-spike solutions for $D = 0.75$ and $D = 0.1$. From (2.12) and (3.27b), we calculate the critical values $\mathcal{A}_{2e}$ and $\mathcal{A}_{2L}$ as

$$\mathcal{A}_{2e} = 5.158\,, \quad \mathcal{A}_{2L} = 5.633\,, \quad \text{for} \quad D = 0.75\,; \qquad \mathcal{A}_{2e} = 6.427\,, \quad \mathcal{A}_{2L} = 6.433\,, \quad \text{for} \quad D = 0.1\,. \tag{3.42}$$

In Fig. 13(a) we plot the Hopf bifurcation value τ_{hL} as a function of $\mathcal{A}/\mathcal{A}_{2e}$ for both values of D. This threshold is set by the $j = 1$ mode. In this diagram we have indicated, by a vertical line, the value $\mathcal{A}_{2L}/\mathcal{A}_{2e}$. Recall that below this value there are eigenvalues on the positive real axis for any $\tau > 0$. Since $\mathcal{A}_{2L}$ is very close to $\mathcal{A}_{2e}$ when $D = 0.1$, a competition instability for this value of D occurs only in a narrow parameter regime. The corresponding frequency λ_{h1} is plotted in Fig. 12(b). In Fig. 13(b) we plot a more detailed stability threshold for $D = 0.75$. In this plot we have indicated by a dashed line the threshold τ_{h2} at which an additional pair of complex conjugate eigenvalues enter the right half-plane. Hence, for $\mathcal{A} > \mathcal{A}_{2L}$ and $\tau > \tau_{h2}$ there are four eigenvalues in the right half-plane. From the theory developed earlier, the curve τ_{h2} versus $\mathcal{A}/\mathcal{A}_{2e}$ terminates when $\mathcal{A} \to \mathcal{A}_{2L}^{+}$

since the complex conjugate pair for the $j = 2$ mode coalesce at the origin $\lambda = 0$. One eigenvalue then moves along the positive real axis, while the other moves along the negative real axis as $\mathcal{A}$ is decreased below $\mathcal{A}_{2L}$.

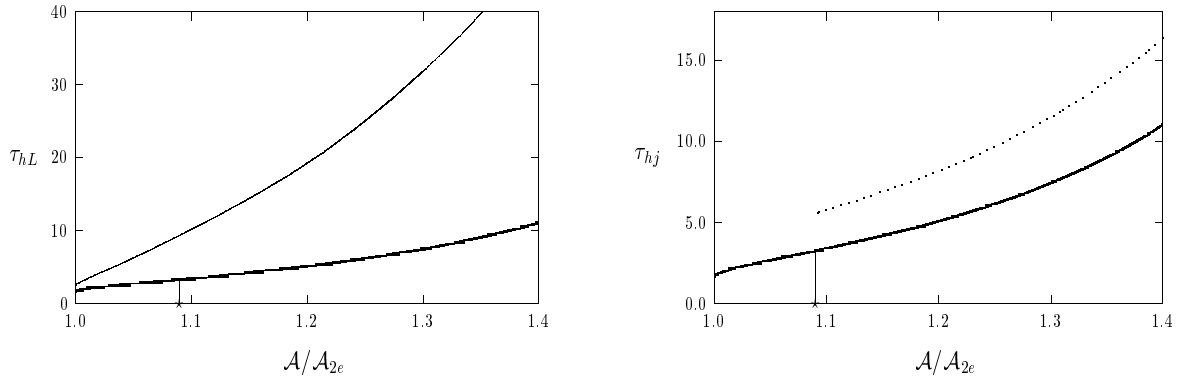

(a) τ_{hL} (b) τ_{hj}

Figure 13: Left figure: the Hopf bifurcation value τ_{hL} versus $\mathcal{A}/\mathcal{A}_{2e}$ for a two-spike solution with $D = 0.75$ (heavy solid curve) and $D = 0.1$ (solid curve). Right figure: τ_{hL} (heavy solid curve) and τ_{h2} (dashed curve) for a two-spike solution with $D = 0.75$.

For three-spike solutions with $D = 0.75$ and $D = 0.1$, we calculate from (2.12), (3.25), and (3.27b), that

$$\mathcal{A}_{3e} = 6.145\,, \quad \mathcal{A}_2 = 6.864\,, \quad \mathcal{A}_{3L} = 8.6857\,, \quad \text{for} \quad D = 0.75\,, \tag{3.43a}$$

$$\mathcal{A}_{3e} = 6.960\,, \quad \mathcal{A}_2 = 6.978\,, \quad \mathcal{A}_{3L} = 7.0904\,, \quad \text{for} \quad D = 0.1\,. \tag{3.43b}$$

Likewise, for four-spike solutions we obtain the thresholds

$$\mathcal{A}_{4e} = 7.023\,, \quad \mathcal{A}_2 = 7.914\,, \quad \mathcal{A}_3 = 10.52\,, \quad \mathcal{A}_{4L} = 12.69\,, \quad \text{for} \quad D = 0.75\,, \tag{3.44a}$$

$$\mathcal{A}_{4e} = 7.589\,, \quad \mathcal{A}_2 = 7.619\,, \quad \mathcal{A}_3 = 7.830\,, \quad \mathcal{A}_{4L} = 8.127\,, \quad \text{for} \quad D = 0.1\,. \tag{3.44b}$$

In Fig. 14(a) and Fig. 15(a) we plot τ_{hL} versus $\mathcal{A}/\mathcal{A}_{ke}$ for three and four-spike solutions when $D = 0.75$ and $D = 0.1$. For the larger value $D = 0.75$, in Fig. 14(b) and Fig. 15(b) we show the detailed stability diagram by plotting τ_{hj} for $j = 2, \ldots, k$. In each case, the stability threshold τ_{hL}

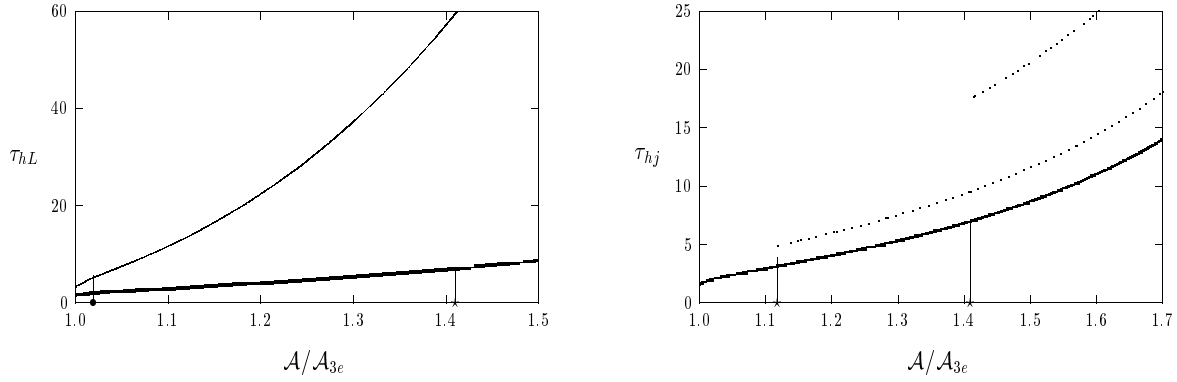

(a) τ_{hL} (b) τ_{hj}

Figure 14: Left figure: the Hopf bifurcation value τ_{hL} versus $\mathcal{A}/\mathcal{A}_{3e}$ for a three-spike solution with $D = 0.75$ (heavy solid curve) and $D = 0.1$ (solid curve). Right figure: τ_{hL} (heavy solid curve) and τ_{hj} (dashed curves) for $j = 2, 3$ for a three-spike solution with $D = 0.75$.

is set by the $j = 1$ mode representing synchronous oscillations. The vertical lines in these figures indicate where positive real eigenvalues enter the right half-plane. The information in Proposition 3.12 is succinctly contained in these detailed stability diagrams. For instance, from Fig. 15(b) for $D = 0.75$, we see that if $\mathcal{A}$ satisfies $7.914 < \mathcal{A} < 10.52$, then there are two real eigenvalues in the right half-plane when $\tau < \tau_{hL}$ and six eigenvalues (at least two real) in the right half-plane when $\tau > \tau_{h2}$.

We now consider some examples of the theory, and we compare the results with full-scale numerical simulations of (1.6). The solution to (1.6) is computed using the routine D03PCF of the NAG library [25] with 1500 uniformly spaced meshpoints. In each of the experiments below, we have taken the initial condition for (1.6) in the form

$$\nu(x,0) = \nu_-(x)\left[1 + 0.01\sum_{j=1}^{k} b_j \cos\left(\frac{\pi(x-x_j)}{\varepsilon}\right) e^{-(x-x_j)^2/(2\varepsilon^2)}\right], \qquad u(x,0) = u_-(x)\,. \tag{3.45}$$

Here $b_j \equiv 1$ if j is odd and $b_j \equiv -1$ if j is even. The k-spike equilibrium solution, ν_-, and u_-, is given in Proposition 2.1.

Example 1: We first consider one-spike solutions to (1.6). In Fig. 16(a) we plot the spike amplitude

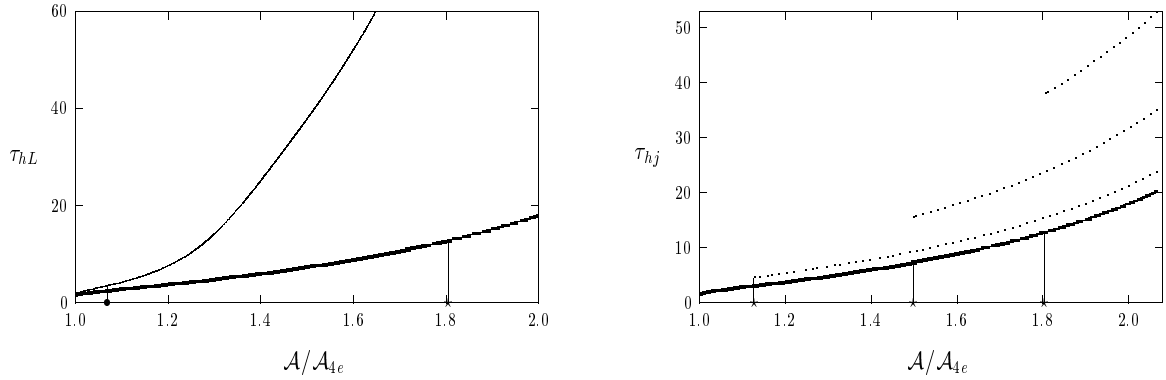

(a) τ_{hL} (b) τ_{hj}

Figure 15: Left figure: the Hopf bifurcation value τ_{hL} versus $\mathcal{A}/\mathcal{A}_{4e}$ for a four-spike solution with $D = 0.75$ (heavy solid curve) and $D = 0.1$ (solid curve). Right figure: τ_{hL} (heavy solid curve) and τ_{hj} (dashed curves) for $j = 2, 3, 4$ for a four-spike solution with $D = 0.75$.

$\nu_m \equiv \nu(0,t)$ versus t for the parameter values $D = 0.75$, $\mathcal{A} = 4.563$, and $\varepsilon = 0.01$. From this figure, we see that when $\tau = 7.5$ we get decaying oscillations, whereas the oscillations grow when $\tau = 7.8$. From the data used to generate Fig. 11(a), we get the Hopf bifurcation value $\tau_{hL} \approx 7.7$. In Fig. 16(b) we plot the spike amplitude $\nu_m \equiv \nu(0)$ versus t for the parameter values $D = 0.1$, $\mathcal{A} = 6.59$, and $\varepsilon = 0.01$. The oscillations are found to decay when $\tau = 8.6$, and they grow when $\tau = 8.8$. The Hopf bifurcation value from Fig. 11(a) is $\tau_{hL} \approx 8.7$. Although our theory correctly predicts the Hopf bifurcation value, it does not explain the large-scale oscillations seen in Fig. 16(b) whereby the instability ultimately leads to the annihilation of the spike.

Example 2: Next, we consider a three-spike solution to (1.6) with $D = 0.75$ and $\varepsilon = 0.1$. We first take the parameter values $\mathcal{A} = 8.6$ and $\tau = 2.0$. Since $\mathcal{A}$ satisfies $\mathcal{A}_2 < \mathcal{A} < \mathcal{A}_{3L}$ from (3.43a), and τ is below the Hopf bifurcation value, we expect a competition instability. In Fig. 17(a) we plot the initial condition (3.45) used for the numerical solution of (1.6). In Fig. 17(b) we show the competition instability that occurs from the unique real positive eigenvalue in the right half-plane. Although we can correctly predict the onset of the competition instability, the nonlinear mechanisms leading to the annihilation of the second spike as seen in Fig. 17(b) is an open problem. Next, we take the slightly larger value $\mathcal{A} = 8.86$, so that now $\mathcal{A} > \mathcal{A}_{3L} = 8.6857$. For this value, the data

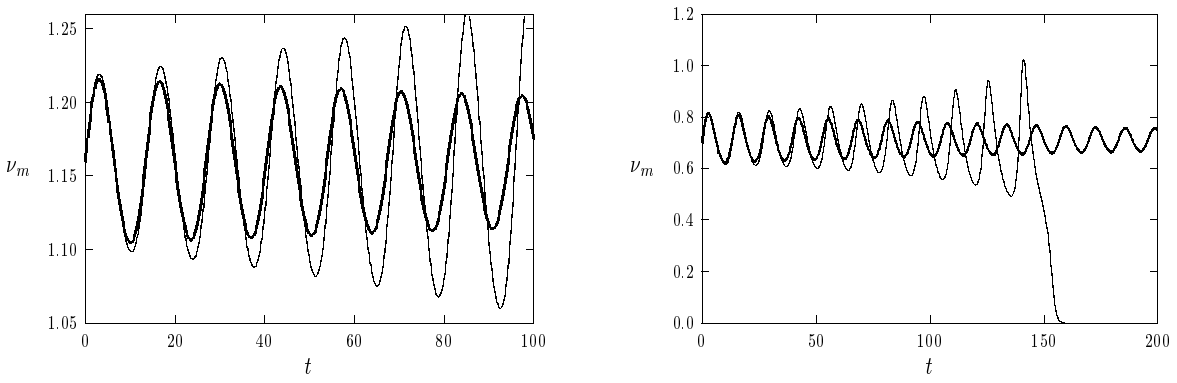

(a) ν_m versus t

(b) ν_m versus t

Figure 16: Example 1: Plots of ν_m versus t for $k = 1$ with $\varepsilon = 0.01$. Left figure: $D = 0.75$ and $\mathcal{A} = 4.563$. The labels are $\tau = 7.5$ (heavy solid curve) and $\tau = 7.8$ (solid curve). Right figure: $D = 0.1$ and $\mathcal{A} = 6.59$. The labels are $\tau = 8.6$ (heavy solid curve) and $\tau = 8.8$ (solid curve).

used to generate Fig. 14(a) yields the Hopf bifurcation value $\tau_{hL} \approx 7.5$. For $\tau = 7.25$, in Fig. 18(a) we show a synchronous decaying oscillation in the spike amplitudes. For the slightly larger value $\tau = 7.6$, in Fig. 18(b) we show both the onset of a synchronous oscillatory instability, and the ultimate simultaneous annihilation of the three spikes.

Example 3: This is the four-spike example for $D = 0.1$ and $\varepsilon = 0.01$ shown in Fig. 2 and Fig. 3 of the introduction §1. Since $\mathcal{A}_3 = 7.83$ and $\mathcal{A}_{4L} = 8.127$ from (3.44b), we will get a competition instability when $\mathcal{A} = 8.0$ and τ is below the Hopf bifurcation value. This is precisely what is seen in Fig. 2(b) where $\tau = 2.0$. For this value of $\mathcal{A}$, from the data used to generate Fig. 15(a) we will have a Hopf bifurcation when $\tau = 3.4$. At this value of τ there is a pair of complex conjugate eigenvalues on the imaginary axis, together with a positive real eigenvalue. Therefore, for $\tau = 3.2$, the instability should be a superposition of a competition instability and a synchronous decaying oscillation in the spike amplitudes. This is shown in Fig. 19. These two types of instabilities lead to an initial synchronization of the oscillations of the spike amplitudes, followed by a spike competition.

Alternatively, suppose we take $\mathcal{A} = 8.3$ so that $\mathcal{A} = 8.3 > \mathcal{A}_{4L}$. From the data used to plot Fig. 15(a) we calculate, for this value of $\mathcal{A}$, that the Hopf bifurcation occurs when $\tau \approx 4.0$. In Fig. 3(a) we show a synchronous decaying oscillation in the spike amplitudes when $\tau = 3.8$. In

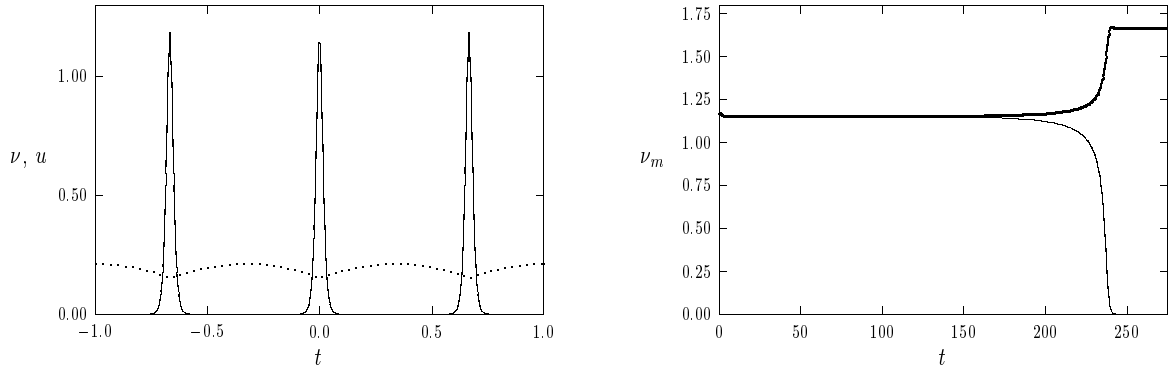

(a) The initial condition

(b) ν_m versus t

Figure 17: Example 2: Here $k = 3$, $D = 0.75$, $\mathcal{A} = 8.6$, $\varepsilon = 0.01$, and $\tau = 2.0$. Left figure: the initial condition for ν (solid curve) and u (dashed curve). Right figure: The spike amplitudes ν_m. The middle spike is annihilated, and the other two spikes have a common amplitude.

Fig. 3(b) we show a synchronous oscillatory instability in the spike amplitudes when $\tau = 4.1$ leading to simultaneous spike annihilation. Since D is small for this example, we might intuitively expect that the inter-spike interaction is very weak. However, for four spikes, the interaction is sufficiently strong so that these instabilities occur rather far from the existence threshold $\mathcal{A}_{4e} = 7.589$.

Example 4: In this example we try to determine asynchronous oscillations of a two-spike solution. We let $D = 0.25$ and we compute the critical values τ_{h1} and τ_{h2} versus $\mathcal{A}/\mathcal{A}_{2e}$ where complex conjugate pairs of eigenvalues enter the right half-plane. The plot is shown in Fig. 20(a). The Hopf bifurcation value τ_{hL} is the minimum of these two values. From this figure we notice that the two curves τ_{h1} and τ_{h2} cross exactly once at some value of $\mathcal{A}/\mathcal{A}_{2e}$, and that they both asymptote to a common limiting behavior as $\mathcal{A}/\mathcal{A}_{2e} \to \infty$. This limiting behavior is analyzed in §5 when we study the intermediate regime. On the range where $\tau_{h1} < \tau_{h2}$ in Fig. 20(a) we expect synchronous oscillations as τ is increased beyond τ_{h1}. Asynchronous oscillations should occur on the narrow range where $\tau_{h2} < \tau_{h1}$ as τ is increased. As a remark, when $D = 0.25$ we compute that $\mathcal{A}_{2e} = 5.614$ and $\mathcal{A}_{2L} = 5.681$. Hence, there will be no competition instabilities due to real eigenvalues crossing into the right half-plane when $\mathcal{A} > 5.681$.

To illustrate the resulting spike dynamics we take $\mathcal{A} = 7.9377$ and $\varepsilon = 0.01$. We compute that

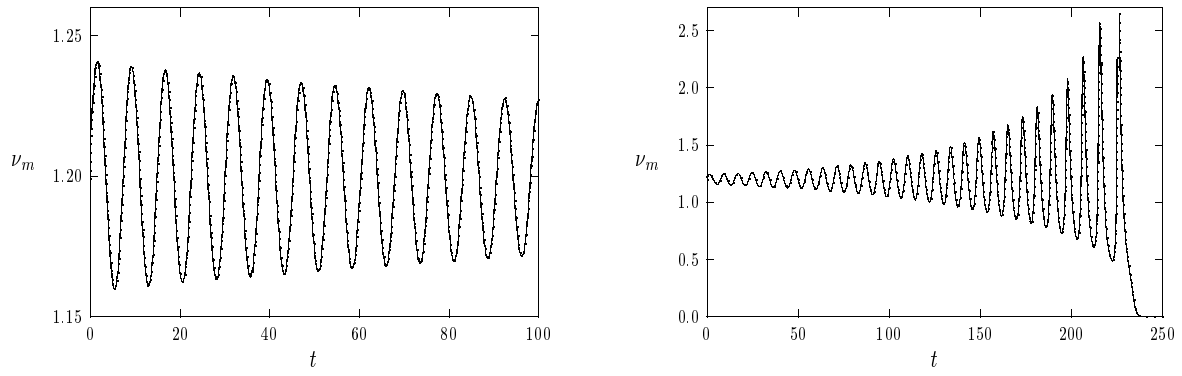

(a) ν_m versus t (b) ν_m versus t

Figure 18: Example 2: The parameters are $k = 3$, $D = 0.75$, $\mathcal{A} = 8.86$, and $\varepsilon = 0.01$. Left figure: synchronous decaying amplitude oscillations when $\tau = 7.25$. Right figure: synchronous oscillatory instability for $\tau = 7.6$, leading to a collapse of the three spikes. The amplitudes of the spikes trace out identical trajectories.

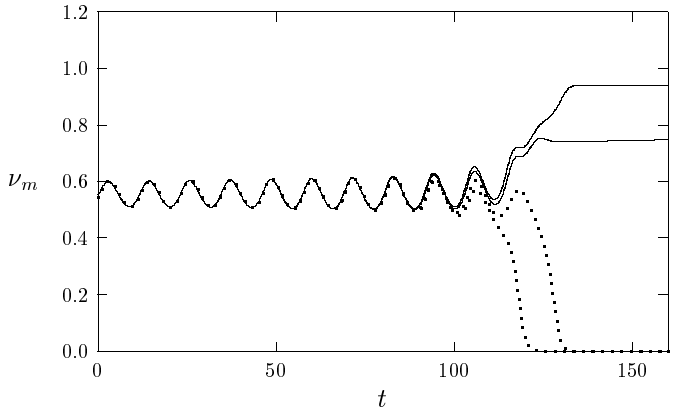

Figure 19: Example 3: The spike amplitudes when $k = 4$, $D = 0.1$, $\varepsilon = 0.01$, $\mathcal{A} = 8.0$ and $\tau = 3.2$. The synchronized oscillations of the spike amplitudes is followed by a competition leading to the annihilation of the second spike and then the fourth spike. Of the two remaining spikes, the third spike has the largest amplitude.

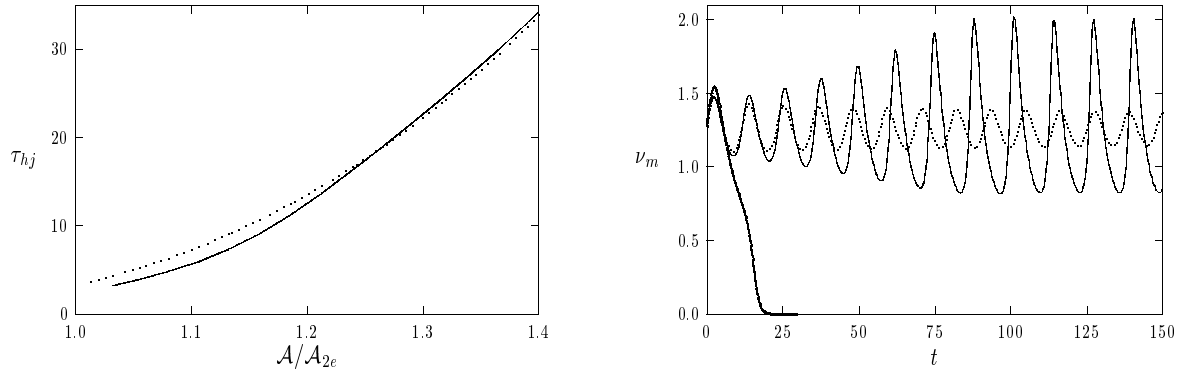

(a) τ_{h1} and τ_{h2} versus $\mathcal{A}/\mathcal{A}_{2e}$

(b) ν_m versus t

Figure 20: Example 4: Left figure: The critical values τ_{h1} (solid curve) and τ_{h2} (dashed curve) versus $\mathcal{A}/\mathcal{A}_{2e}$ for a two-spike solution with $D = 0.25$. Right figure: Spike amplitudes for $D = 0.25$, $\varepsilon = 0.01$, with $\tau = 30$ (dashed curve), $\tau = 34$ (solid curve), and $\tau = 40$ (heavy solid curve).

$\tau_{h1} = 36.1$ and $\tau_{h2} = 35.6$. Hence, the complex eigenvalues that first enter the right half-plane as τ is increased corresponds to the asynchronous mode. In Fig. 20(b) we plot the numerically computed spike amplitudes for three values of τ starting from the asynchronous initial condition (3.45). For each of these values of τ, the spike amplitudes are found to synchronize very quickly in time. For $\tau = 40$, the spike amplitudes both collapse, for $\tau = 34$ they exhibit a large-scale periodic oscillation, and for $\tau = 30$ the oscillations relax back to the equilibrium state as t increases. We have done many other examples to try to determine asynchronous oscillations in the low feed-rate regime without success. However, asynchronous oscillations for the spike amplitudes have been observed in the pulse-splitting parameter regime where $\mathcal{A} = O(\varepsilon^{-1/2})$, or equivalently where $A = O(1)$ (see [16]). There are two possibilities for not observing such oscillations in the low feed-rate regime. One possibility is that the asynchronous mode is unstable in the weakly nonlinear regime. The second possibility results from our observation that whenever $\tau_{hL} = \tau_{hk}$, so that stability is set by the asynchronous mode, the threshold for the synchronous mode τ_{h1} has a numerical value that is typically very close to τ_{hk}. Hence, whenever asynchronous oscillations are theoretically possible as τ is increased, we have typically found that the more dominant synchronous mode is essentially also present.

3.4 The Infinite-Line Problem

Next, we determine the stability threshold for the infinite-line problem where (1.6) is posed on $-\infty < x < \infty$. We will only consider the stability of a one-spike solution centered at $x = 0$. Results for the infinite line problem were obtained using dynamical systems techniques in [4] and [5], and using a formal asymptotic analysis in [24].

The only main modification needed to the analysis leading to Propositions 2.1 and 3.1 is that the Green's function $G(x; x_j)$ in (2.6) must be replaced with $G(x; 0)$, where

$$DG_{xx} - G = -\delta(x)\,, \qquad -\infty < x < \infty\,; \qquad G \to 0 \quad \text{as} \quad |x| \to \infty\,. \tag{3.46}$$

The solution to (3.46) is

$$G(x;0) = \left(\frac{\theta_0}{2}\right) e^{-\theta_0|x|}\,, \qquad \theta_0 = D^{-1/2}\,. \tag{3.47}$$

Since the asymptotic construction of the one-spike equilibrium solution parallels that in §2.1, we only give the result.

Proposition 3.16: *Let $\varepsilon \to 0$, with $\mathcal{A} = O(1)$ and $D = O(1)$ in (1.6) defined now on the infinite line $-\infty < x < \infty$. Then, when $\mathcal{A} > \mathcal{A}_{1e}$, there are two one-spike solutions given asymptotically by*

$$\nu_\pm(x) \sim \frac{1}{\mathcal{A}U_\pm} w\left[\varepsilon^{-1}x\right]\,; \qquad u_\pm(x) \sim 1 - \frac{6}{\mathcal{A}^2 U_\pm} G(x;0)\,. \tag{3.48}$$

We label u_+, ν_+ and u_-, ν_- as the large and small solutions, respectively. In (3.48), w and G satisfy (2.3) and (3.47), respectively. Moreover, $U_\pm$ are given by

$$U_\pm \equiv \frac{1}{2}\left[1 \pm \sqrt{1 - \frac{\mathcal{A}_{1e}^2}{\mathcal{A}^2}}\right]\,, \qquad \mathcal{A}_{1e} \equiv \sqrt{12}D^{-1/4}\,. \tag{3.49}$$

Since the derivation of the nonlocal eigenvalue problem is similar to that done in §3 for a multi-spike solution on the finite interval, we only give the highlights of the derivation. We introduce Φ and η by

$$\nu(x) = \nu_\pm(x) + e^{\lambda t}\Phi\left[\varepsilon^{-1}x\right]\,, \qquad u(x) = u_\pm(x) + e^{\lambda t}\eta(x)\,. \tag{3.50}$$

Substituting (3.50) and (3.48) into (2.17b), we obtain in place of (3.4) that η satisfies

$$D\eta_{xx} - (1 + \tau\lambda)\,\eta = 0\,, \quad -\infty < x < \infty\,; \qquad \eta \to 0\,, \quad \text{as} \quad |x| \to \infty\,, \tag{3.51a}$$

$$[\eta]_0 = 0\,, \qquad [D\eta_x]_0 = \frac{6}{\mathcal{A}^2 U_\pm^2}\eta(0) + \frac{2}{\mathcal{A}}\int_{-\infty}^{\infty} w(y)\Phi(y)\,dy\,. \tag{3.51b}$$

Substituting (3.50) and (3.48) into (2.17a), we obtain in place of (3.8) that $\Phi(y)$ satisfies

$$\Phi'' - \Phi + 2w\Phi + \frac{\eta(0)}{\mathcal{A}U_\pm^2} w^2 = \lambda\Phi\,, \qquad -\infty < y < \infty\,, \tag{3.52}$$

with $\Phi(y) \to 0$ as $|y| \to \infty$. The nonlocal eigenvalue problem analogous to (3.12) is obtained by solving (3.51) for $\eta(0)$, substituting the resulting expression into (3.52), and then using (3.49) for $U_\pm$. In this way, we obtain that $\Phi(y)$ satisfies the conditions of Proposition 3.2, except that now χ in (3.13) is to be replaced with

$$\chi \equiv \frac{2s}{s + \sqrt{1+\tau\lambda}}\,, \qquad s \equiv \frac{1-U_\pm}{U_\pm}\,. \tag{3.53}$$

Notice that the multiplier χ in (3.53) can be obtained by taking the limit $D \to 0$ in the multiplier in (3.13) corresponding to a k-spike symmetric pattern on the finite line. In place of (3.18) and (3.19), we then obtain that the eigenvalues λ are the roots of $g(\lambda) = 0$, where

$$g(\lambda) \equiv C(\lambda) - f(\lambda)\,, \qquad f(\lambda) \equiv \frac{\int_{-\infty}^{\infty} w\,(L_0 - \lambda)^{-1}\, w^2\, dy}{\int_{-\infty}^{\infty} w^2\, dy}\,, \qquad C(\lambda) = \frac{1}{2} + \frac{\sqrt{1+\tau\lambda}}{2s}\,. \tag{3.54}$$

The rigorous spectral approach used in §3.2 can be applied directly to this problem. In this way, we obtain the following result:

Proposition 3.17: *Let $\varepsilon \to 0$ and consider a one-spike solution to (1.6) on the infinite line. The large solution u_+, ν_+, where $0 < s < 1$, is unstable for any $\tau > 0$ as a result of a positive eigenvalue on the real axis. The small solution u_-, ν_-, where $s > 1$, is stable with respect to the large eigenvalues for τ sufficiently small, and is unstable with respect to the large eigenvalues for τ sufficiently large. There exists a value $\tau_h = \tau_h(s)$ (possibly non-unique) where there are complex conjugate eigenvalues on the imaginary axis.*

Using the numerical method described briefly in §3.3, we compute $\tau_h = \tau_h(s)$ numerically. Using (3.49) and $s = (1-U_\pm)/U_\pm$, we get τ_h as a function of $\mathcal{A}/\mathcal{A}_{1e} = (1+s)\,[2\sqrt{s}]^{-1}$. In addition, we can compute the value of τ, labeled by $\tau_m(s)$, where the complex conjugate eigenvalues merge onto the real axis. A simple calculation using (3.53) and the local properties of $f(\lambda)$ as $\lambda \to 0$ given in Propositions 3.5 and 3.7 above, shows that when $s = 1$ we have a double root to $g(\lambda) = 0$ at $\lambda = 0$ and $\tau = 3$. The numerical results for τ_h and τ_m as a function of $\mathcal{A}/\mathcal{A}_{1e}$ are shown in Fig. 21(a). Although we cannot prove that τ_h is unique, numerical evidence suggests that when $\tau > \tau_h$ there are always two eigenvalues in the right half-plane. In Fig. 21(b) we plot the function λ_{Ih} versus $\mathcal{A}/\mathcal{A}_{1e}$ where we have a Hopf bifurcation. In this figure we also plot the function λ_{Rm} versus $\mathcal{A}/\mathcal{A}_{1e}$ where complex conjugate eigenvalues in the right half-plane first merge onto the real axis. From this figure,

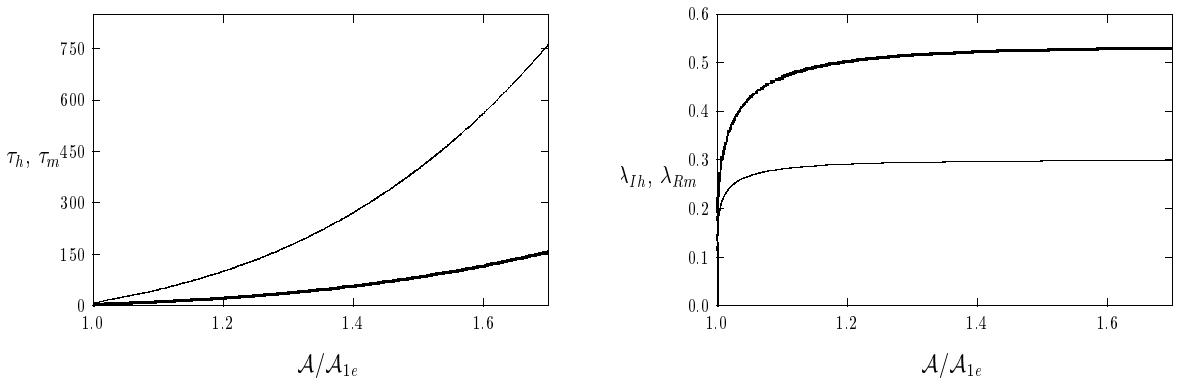

(a) τ_h and τ_m

(b) λ_{Ih} and λ_{Rm}

Figure 21: Left figure: the Hopf bifurcation value τ_h (heavy solid curve) versus $\mathcal{A}/\mathcal{A}_{1e}$. The complex eigenvalues merge onto the positive real axis when $\tau = \tau_m$ (solid curve). Right figure: The corresponding critical values λ_{Ih} (heavy solid curve) and λ_{Rm} (solid curve).

we notice that λ_{Ih} and λ_{Rm} have limiting behaviors for $s \gg 1$. This limiting behavior is analyzed in a more general context in §5.

The critical value τ_h for this infinite-line problem can be obtained by taking the limiting $\sqrt{D}k \ll 1$ in all of the results of §3.2 for the finite domain problem (1.6). Therefore, the results for $D = 0.1$ and $k = 1, \ldots, 3$ computed above in §3.3 should closely approximate those for the infinite-line problem.

Finally, we relate our results for the infinite-line problem with those of [24]. To show the equivalence of our results with those in [24], we integrate (3.12) over $-\infty < y < \infty$ to obtain

$$(2-\chi)\int_{-\infty}^{\infty} w\Phi\, dy = (\lambda+1)\int_{-\infty}^{\infty} \Phi\, dy\,. \tag{3.55}$$

Solving (3.55) for $\int_{-\infty}^{\infty} \Phi\, dy$, we substitute the resulting expression into (3.12) and use $\int_{-\infty}^{\infty} w^2\, dy = 6$ to get

$$L_0\Phi - \frac{\chi(\lambda+1)}{6(2-\chi)} w^2 \int_{-\infty}^{\infty} \Phi\, dy = \lambda\Phi\,. \tag{3.56}$$

Finally, using the definition of χ in (3.53) together with $w(y) = \frac{3}{2}\mathrm{sech}^2(y/2)$, we can write (3.56) for

the small solution as

$$\Phi'' - \Phi + 3\,\mathrm{sech}^2\left(\frac{y}{2}\right)\Phi - \alpha\,\mathrm{sech}^4\left(\frac{y}{2}\right)\int_{-\infty}^{\infty}\Phi\,dy = \lambda\Phi\,, \tag{3.57a}$$

where

$$\alpha = \frac{3\mathcal{A}^2}{8\mathcal{A}_{1e}^2}\frac{(1+\lambda)}{\sqrt{1+\tau\lambda}}\left(1+\sqrt{1-\frac{\mathcal{A}_{1e}^2}{\mathcal{A}^2}}\right)^2\,. \tag{3.57b}$$

The nonlocal eigenvalue problem (3.57) is given in equation (2.13) of [24]. Our plots of τ_h and λ_{Ih} are equivalent to those in Fig. 2.4c and Fig. 2.4d of [24]. In Appendix B of [24], a computer-assisted approach was used to determine qualitative properties of the spectrum for (3.57). Our rigorous approach to the nonlocal eigenvalue problem, with results summarized in Proposition 3.17, provides a simpler alternative proof of the stability properties.

4 Small Eigenvalues: Slow Translational Instabilities for $\mathcal{A} = O(1)$

In this section we determine the conditions for which the small eigenvalues of order $O(\varepsilon^2)$ for (2.17) lie in the stable left half-plane $\mathrm{Re}(\lambda) < 0$. The importance of these eigenvalues is not only that they determine stability thresholds, but that they are also closely related to the existence of the asymmetric patterns constructed in §2. In particular, for $k > 1$, we will show that asymmetric patterns emerge from the symmetric k-spike, small solution, equilibrium branch when $k-1$ small eigenvalues cross through zero.

We will calculate an explicit formula for the small eigenvalues for both the small and large solution branches $u_\pm$, $\nu_\pm$. The first part of the analysis is to reduce (2.17) to the study of a matrix eigenvalue problem. Since this matrix eigenvalue problem is similar to that studied in [14] for the GM model (1.10), we can readily analyze this problem by appealing directly to results from [14].

We begin by writing (2.17) in the form

$$L_\varepsilon\phi + \mathcal{A}\eta\nu_\pm^2 = \lambda\phi\,, \qquad -1 < x < 1\,, \tag{4.1a}$$

$$D\eta_{xx} - \left(1+\tau\lambda+\varepsilon^{-1}\nu_\pm^2\right)\eta = 2\varepsilon^{-1}u_\pm\nu_\pm\phi\,, \qquad -1 < x < 1\,, \tag{4.1b}$$

$$\phi_x(\pm 1) = \eta_x(\pm 1) = 0\,, \tag{4.1c}$$

where

$$L_\varepsilon\phi \equiv \varepsilon^2\phi_{xx} - \phi + 2\mathcal{A}u_\pm\nu_\pm\phi\,. \tag{4.1d}$$

Here $u_\pm$ and $\nu_\pm$ are as given in (2.10) of Proposition 2.1. Since $\lambda = O(\varepsilon^2)$, we observe from (4.1b) that $\tau\lambda \ll 1$ unless $\tau = O(\varepsilon^{-2})$. In the derivation below, we assume that $\tau = O(1)$, and so the small eigenvalues are asymptotically independent of τ when $\tau = O(1)$.

Since $\nu_\pm$ is localized near each spike x_j, the spike pattern is nearly translationally invariant. To show this, we differentiate the equilibrium problem for (1.6a) with respect to x to get

$$L_\varepsilon \nu_{\pm x} = -\mathcal{A} u_{\pm x} \nu_\pm^2 \,. \tag{4.2}$$

For x near x_j, we calculate from (2.10a) that

$$\nu_\pm \sim \frac{1}{\mathcal{A} U_\pm} w_j \,, \qquad \nu_{\pm x} \sim \frac{\varepsilon^{-1}}{\mathcal{A} U_\pm} w_j^{'} \,, \tag{4.3}$$

where we have defined $w_j = w_j(y_j) \equiv w\left[\varepsilon^{-1}(x - x_j)\right]$, and w satisfies (2.3). Substituting (4.3) into (4.2), we obtain

$$L_\varepsilon w_j^{'} \sim -\varepsilon U_\pm^{-1} u_{\pm x} w_j^2 = O(\varepsilon) \,, \tag{4.4}$$

for x near x_j. This suggests that we look for an eigenfunction to (4.1) in the form

$$\phi = \phi_0 + \varepsilon \phi_1 + \cdots \,, \qquad \eta(x) = \varepsilon \eta_0(x) + \cdots \,, \tag{4.5a}$$

where, for coefficients c_j to be determined, we have

$$\phi_0 \equiv \sum_{j=1}^k c_j w_j^{'}\left[\varepsilon^{-1}(x - x_j)\right] \,, \qquad \phi_1 \equiv \sum_{j=1}^k c_j \phi_{1j}\left[\varepsilon^{-1}(x - x_j)\right] \,. \tag{4.5b}$$

Here and below we have defined $\langle \zeta \rangle_j \equiv (\zeta(x_{j+}) + \zeta(x_{j-}))/2$ and $[\zeta]_j \equiv \zeta(x_{j+}) - \zeta(x_{j-})$, where $\zeta(x_{j\pm})$ are the one-sided limits of $\zeta(x)$ as $x \to x_{j\pm}$. In particular, the equilibrium positions for x_j given in (2.1) are such that

$$\langle u_{\pm x} \rangle_j = 0 \,, \qquad j = 1, \ldots, k \,, \tag{4.6}$$

where $u_\pm$ is the outer solution given in (2.10b).

We substitute (4.5a) into (4.1a), and use (4.4) with $\lambda = O(\varepsilon^2)$. For x near x_j, we get that $\phi_{1j}(y)$ satisfies

$$c_j L_\varepsilon \phi_{1j} \sim f(x_j + \varepsilon y_j) w_j^2 \,, \tag{4.7a}$$

where $f(x)$ is defined by

$$f(x) \equiv \frac{c_j u_{\pm x}(x)}{U_\pm} - \frac{\eta_0(x)}{\mathcal{A} U_\pm^2} \,. \tag{4.7b}$$

Substituting (4.5a) into (4.1b), we obtain that η_0 satisfies

$$D\eta_{0xx} - \left(1 + \varepsilon^{-1}\nu_\pm^2\right)\eta_0 = 2\varepsilon^{-2} u_\pm \nu_\pm \left(\phi_0 + \varepsilon \phi_1\right) \,, \qquad -1 < x < 1 \,, \tag{4.8}$$

with $\eta_{0x}(\pm 1) = 0$. Since ϕ_0 is a linear combination of $w_j^{'}$, it follows that the term multiplied by ϕ_0 on the right-hand side in (4.8) behaves like a dipole near $x = x_j$. Hence, for $\varepsilon \ll 1$, this term is a linear combination of $\delta^{'}(x - x_j)$ for $j = 1, .., k$, where $\delta(x)$ is the delta function. Thus, η_0 will be discontinuous across $x = x_j$.

Since η_0 is discontinuous across $x = x_j$, it appears at first glance that $f(x)$ in (4.7b) will also be discontinuous across $x = x_j$. However, this is not the case, as we find that the first term on the right-hand side of (4.7b) cancels this singularity. To see this, we differentiate the equilibrium problem for (1.6b) with respect to x, and subtract appropriate multiples of the resulting equation and (4.8), to find that the dipole term proportional to ϕ_0 cancels exactly. Thus, $f(x)$ is continuous across $x = x_j$, and so $\langle f \rangle_j = f(x_j)$. However, since $\langle u_{\pm x} \rangle_j = 0$ from (4.6), we get from (4.7) that

$$c_j L_\varepsilon \phi_{1j} \sim f(x_j) w_j^2 \,, \qquad f(x_j) = -\frac{\langle \eta_0 \rangle_j}{\mathcal{A} U_\pm^2} \,. \tag{4.9}$$

Then, since $L_\varepsilon w_j = w_j^2 + O(\varepsilon)$, we determine ϕ_{1j} as

$$c_j \phi_{1j} \sim f(x_j) w_j \,. \tag{4.10}$$

Therefore, since ϕ_{1j} has one sign, the term in (4.8) proportional to ϕ_1 behaves like a linear combination of $\delta(x - x_j)$ when $\varepsilon \ll 1$ and, most importantly, is *of the same order* in ε as the dipole term proportional to ϕ_0. This clearly shows that to calculate an eigenvalue of order $O(\varepsilon^2)$, we need to determine the asymptotic eigenfunction for ϕ in (4.5a) to both the $O(1)$ and $O(\varepsilon)$ terms.

Next, we calculate, in the sense of distributions, the effect of the dipole and monopole terms appearing on the right-hand side of (4.8). Using (4.3) for $\nu_\pm$ and $u_\pm \sim U_\pm$ near $x = x_j$, we calculate from (4.5b), (4.9), and (4.10) that, near $x = x_j$,

$$2\varepsilon^{-2} u_\pm \nu_\pm \phi_0 \to \frac{c_j}{\mathcal{A}} \left(\int_{-\infty}^{\infty} w_j^2 \, dy \right) \delta^{'}(x - x_j) = \frac{6 c_j}{\mathcal{A}} \delta^{'}(x - x_j) \,, \tag{4.11a}$$

$$2\varepsilon^{-1} u_\pm \nu_\pm \phi_1 \to \frac{2 f(x_j)}{\mathcal{A}} \left(\int_{-\infty}^{\infty} w_j^2 \, dy \right) \delta(x - x_j) = -\frac{12 \langle \eta_0 \rangle_j}{\mathcal{A}^2 U_\pm^2} \delta(x - x_j) \,, \tag{4.11b}$$

$$\varepsilon^{-1} \nu_\pm^2 \to \frac{6}{\mathcal{A}^2 U_\pm^2} \delta(x - x_j) \,. \tag{4.11c}$$

Substituting (4.11) into (4.8), we obtain that η_0 satisfies

$$D\eta_{0xx} - \left[1 + \frac{6}{\mathcal{A}^2 U_\pm^2} \sum_{j=1}^{k} \delta(x - x_j) \right] \eta_0 = \frac{6}{\mathcal{A}} \sum_{j=1}^{k} c_j \delta^{'}(x - x_j) - \frac{12}{\mathcal{A}^2 U_\pm^2} \sum_{j=1}^{k} \langle \eta_0 \rangle_j \delta(x - x_j) \,, \tag{4.12}$$

with $\eta_{0x}(\pm 1) = 0$. Using (2.9) for $U_\pm$, and the definition of s in (2.15), we can write

$$\frac{6}{\mathcal{A}^2 U_\pm^2} = \frac{s}{a_g}\,, \qquad s = \frac{1-U_\pm}{U_\pm}\,. \tag{4.13}$$

Here a_g is given in (2.8). Substituting (4.13) into (4.12), we get that (4.12) is equivalent to

$$D\eta_{0xx} - \eta_0 = 0\,, \qquad -1 < x < 1\,; \qquad \eta_{0x}(\pm 1) = 0\,, \tag{4.14a}$$

$$[D\eta_0]_j = \frac{6c_j}{\mathcal{A}}\,; \qquad [D\eta_{0x}]_j = \frac{-s}{a_g}\langle \eta_0 \rangle_j\,, \qquad j = 1, \ldots, k\,. \tag{4.14b}$$

Next, we estimate the small eigenvalue. Substituting (4.5) into (4.1a), we then multiply both sides of (4.1a) by $w_j^{'}$. By integrating the resulting equation across the domain, we get

$$\sum_{i=1}^{k} \left(w_j^{'}, c_i L_\varepsilon w_i^{'} \right) + \varepsilon \mathcal{A} \left(\eta_0 \nu_\pm^2, w_j^{'} \right) + \varepsilon \sum_{i=1}^{k} \left(w_j^{'}, c_i L_\varepsilon \phi_{1i} \right) \sim \lambda \sum_{i=1}^{k} c_i \left(w_j^{'}, w_i^{'} \right)\,. \tag{4.15}$$

Here we have defined $(f,g) \equiv \int_{-1}^{1} f(x) g(x)\, dx$. To within negligible exponentially small terms, the dominant contribution to the sums in (4.15) arise from $i = j$, since $w_j^{'}$ is exponentially small away from $x = x_j$. Thus, (4.15) reduces asymptotically to

$$c_j \left(w_j^{'}, L_\varepsilon w_j^{'} \right) + \varepsilon \mathcal{A} \left(\eta_0 \nu_\pm^2, w_j^{'} \right) + \varepsilon \left(w_j^{'}, c_j L_\varepsilon \phi_{1j} \right) \sim \lambda c_j \left(w_j^{'}, w_j^{'} \right)\,. \tag{4.16}$$

We then integrate by parts on the third term on the left-hand side of (4.16). Since L_ε is self-adjoint, we can then use (4.4) for $L_\varepsilon w_j^{'}$ and (2.10a) for $\nu_\pm$. Since the integrands are localized near $x = x_j$, we can write the resulting integrals in terms of $y = \varepsilon^{-1}(x - x_j)$ to get

$$-\frac{\varepsilon^2 c_j}{U_\pm} \int_{-\infty}^{\infty} w^{'} w^2 u_{\pm x}\, dy + \frac{\varepsilon^2}{\mathcal{A} U_\pm^2} \int_{-\infty}^{\infty} w^2 w^{'} \eta_0\, dy - \frac{\varepsilon^3 c_j}{U_\pm} \int_{-\infty}^{\infty} \phi_{1j} w^2 u_{\pm x}\, dy \sim \varepsilon \lambda c_j \left(\int_{-\infty}^{\infty} w^{'2}\, dy \right)\,, \tag{4.17}$$

where w satisfies (2.3). In this expression we have labeled $\eta_0 \equiv \eta_0(x_j + \varepsilon y)$ and $u_{\pm x} \equiv u_{\pm x}(x_j + \varepsilon y)$.

Using (4.10) for ϕ_{1j}, and (4.7b) for $f(x)$, we can write (4.17) more compactly as

$$-\varepsilon^2 \int_{-\infty}^{\infty} w^{'} w^2 f(x_j + \varepsilon y)\, dy - \frac{\varepsilon^3 f(x_j)}{U_\pm} \int_{-\infty}^{\infty} w^3 u_{\pm x}(x_j + \varepsilon y)\, dy \sim \varepsilon \lambda c_j \left(\int_{-\infty}^{\infty} w^{'2}\, dy \right)\,. \tag{4.18}$$

The second integral on the left-hand side of (4.18) is $O(\varepsilon^4)$ since $\langle u_{\pm x} \rangle_j = 0$ from (4.6). The function $f(x)$ in (4.18) is continuous, but not differentiable, at $x = x_j$.

The first term on the left-hand side of (4.18) is calculated by first expanding $f(x_j + \varepsilon y)$ in one-sided Taylor series, and then by integrating the resulting equation by parts. This yields,

$$\int_{-\infty}^{\infty} w' w^2 f(x_j + \varepsilon y)\, dy \sim -\frac{\varepsilon}{3}\langle f' \rangle_j \int_{-\infty}^{\infty} w^3\, dy\,. \tag{4.19}$$

Using (4.7b), and (2.4a), which yields $\langle u_{\pm xx}\rangle_j = (U_\pm - 1)/D$, we calculate

$$\langle f' \rangle_j = \frac{c_j\,(U_\pm - 1)}{U_\pm D} - \frac{1}{\mathcal{A}U_\pm^2}\langle \eta_{0x}\rangle_j\,. \tag{4.20}$$

Then, we substitute (4.20) and (4.19) into (4.18), to get

$$\lambda c_j \sim \frac{\varepsilon^2}{3}\left[\frac{c_j\,(U_\pm - 1)}{U_\pm D} - \frac{\langle \eta_{0x}\rangle_j}{\mathcal{A}U_\pm^2}\right]\left(\frac{\int_{-\infty}^{\infty} w^3 dy}{\int_{-\infty}^{\infty} w'^2\, dy}\right)\,. \tag{4.21}$$

Here $\langle \eta_{0x}\rangle$ is to be calculated from (4.14).

Finally, we re-write (4.21) and (4.14) in a more convenient form by introducing a new variable $\tilde{\eta}_0$ defined by

$$\eta_0 \equiv -\frac{6a_g}{\mathcal{A}}\tilde{\eta}_0\,. \tag{4.22}$$

In addition, we calculate the ratio of the two integrals in (4.21) using $w(y) = \frac{3}{2}\mathrm{sech}^2\,(y/2)$. In this way, we obtain the following problem that determines the small eigenvalues:

Proposition 4.1: *Let $\varepsilon \ll 1$ and $\tau = O(1)$. Then, the eigenvalues of (2.17) of order $O(\varepsilon^2)$ satisfy*

$$\lambda c_j \sim 2\varepsilon^2 s\left[\langle \tilde{\eta}_{0x}\rangle_j - \frac{c_j}{D}\right]\,, \qquad j = 1, \ldots, k\,. \tag{4.23}$$

Here $\langle \tilde{\eta}_{0x}\rangle_j$ is obtained from the solution to the boundary value problem with jump discontinuities

$$D\tilde{\eta}_{0xx} - \tilde{\eta}_0 = 0\,, \qquad -1 < x < 1\,; \qquad \tilde{\eta}_{0x}(\pm 1) = 0\,, \tag{4.24a}$$

$$[D\tilde{\eta}_0]_j = -\frac{c_j}{a_g}\,; \qquad [D\tilde{\eta}_{0x}]_j = \frac{-s}{a_g}\langle \tilde{\eta}_0\rangle_j\,, \qquad j = 1, \ldots, k\,. \tag{4.24b}$$

Here s is defined in (2.15a).

A problem very similar to (4.24) was derived in Proposition 8 of [14] in the context of the GM model (1.10) with exponent set (p, q, m, s), where $\zeta = qm/(p-1) - (1+s)$ and $\zeta > 0$. As was observed in §3 in the study of the large eigenvalues, we also find that (4.24) for the Gray-Scott model is equivalent to the corresponding problem for the GM model with exponent set $(2, s, 2, s)$, where $s = (1 - U_\pm)/U_\pm$.

The system (4.24) can be solved using a lengthy matrix analysis as was done in section 4.2 of [14] for the GM model (1.10). We now only give a brief sketch of that part of the matrix analysis of [14] which is important for describing our results for the Gray-Scott model (1.6). The solution to (4.24) is decomposed as

$$\tilde{\eta}_0(x) = \frac{1}{a_g}\left(\sum_{j=1}^{k} c_j g(x;x_j) + \sum_{j=1}^{k} m_j G(x;x_j)\right), \tag{4.25}$$

for some coefficients m_j, for $j = 1,\dots,k$. Here $G(x;x_j)$ is the Green's function satisfying (2.6), while $g(x;x_j)$ is the dipole Green's function satisfying

$$Dg_{xx} - g = -\delta'(x-x_j), \qquad -1 < x < 1; \qquad g_x(\pm 1;x_j) = 0. \tag{4.26}$$

Define the vectors $\boldsymbol{m}^t \equiv (m_1,\dots,m_k)$ and $\boldsymbol{c}^t \equiv (c_1,\dots,c_k)$, where t denotes transpose. Then, satisfying the jump conditions in (4.24b), we get a matrix problem for $\boldsymbol{m}$ in terms of $\boldsymbol{c}$ in the form

$$\left(-\frac{s}{a_g}\mathcal{G} + I\right)\boldsymbol{m} = \frac{s}{a_g}\mathcal{P}_g\mathbf{c}. \tag{4.27}$$

Here $\mathcal{G}$ and $\mathcal{P}_g$ are matrices associated with G and g, defined by

$$\mathcal{G} \equiv \begin{pmatrix} G(x_1;x_1) & \cdots & G(x_1;x_k) \\ \vdots & \ddots & \vdots \\ G(x_k;x_1) & \cdots & G(x_k;x_k) \end{pmatrix}, \qquad \mathcal{P}_g \equiv \begin{pmatrix} \langle g(x_1;x_1)\rangle_1 & \cdots & g(x_1;x_k) \\ \vdots & \ddots & \vdots \\ g(x_k;x_1) & \cdots & \langle g(x_k;x_k)\rangle_k \end{pmatrix}. \tag{4.28}$$

The angle brackets in (4.28) again denote the average of the right and left-sided limits. This problem (4.27) determines $\boldsymbol{m}$ in terms of $\boldsymbol{c}$.

In (4.23) we must calculate $\langle\tilde{\boldsymbol{\eta}}_{0\boldsymbol{x}}\rangle^t \equiv (\langle\tilde{\eta}_{0x}\rangle_1,\dots,\langle\tilde{\eta}_{0x}\rangle_k)$. To do so, we use (4.25) to get

$$\langle\tilde{\boldsymbol{\eta}}_{0\boldsymbol{x}}\rangle = \frac{1}{a_g}\left(\mathcal{G}_g\boldsymbol{c} + \mathcal{P}\boldsymbol{m}\right), \tag{4.29}$$

where $\mathcal{G}_g$ and $\mathcal{P}$ are two additional Green's function matrices defined by

$$\mathcal{G}_g \equiv \begin{pmatrix} g_x(x_1;x_1) & \cdots & g_x(x_1;x_k) \\ \vdots & \ddots & \vdots \\ g_x(x_k;x_1) & \cdots & g_x(x_k;x_k) \end{pmatrix}, \qquad \mathcal{P} \equiv \begin{pmatrix} \langle G_x(x_1;x_1)\rangle_1 & \cdots & G_x(x_1;x_k) \\ \vdots & \ddots & \vdots \\ G_x(x_k;x_1) & \cdots & \langle G_x(x_k;x_k)\rangle_k \end{pmatrix}. \tag{4.30}$$

Next, we define σ in terms of λ by

$$\lambda = \frac{2\varepsilon^2 s}{a_g}\sigma. \tag{4.31}$$

Combining (4.23), (4.29), and (4.31), we obtain a matrix eigenvalue problem for σ and $\boldsymbol{c}$ given by

$$\mathcal{G}_g \boldsymbol{c} + \mathcal{P}\boldsymbol{m} = \left(\sigma + \frac{a_g}{D}\right)\boldsymbol{c}\,, \tag{4.32}$$

where $\boldsymbol{m}$ is determined in terms of $\boldsymbol{c}$ by (4.27).

Since the matrices $\mathcal{G}$, $\mathcal{G}_g$, $\mathcal{P}$, and $\mathcal{P}_g$, appearing in (4.27) and (4.32) are in general full, it appears to be difficult to determine σ explicitly. However, it was shown in [14] that the inverses of $\mathcal{G}$ and $\mathcal{G}_g$ are in fact tridiagonal matrices, which can be written explicitly as

$$\mathcal{G} = \frac{\mathcal{B}_{00}^{-1}}{\sqrt{D}}\,, \qquad \mathcal{G}_g = \frac{\mathcal{B}_g^{-1}}{D^{3/2}}\,. \tag{4.33}$$

Here $\mathcal{B}_{00}$ is the matrix defined by setting $\tau = 0$ in the matrix $\mathcal{B}_0$ of (3.7). The matrix $\mathcal{B}_g$ has exactly the same tridiagonal form as in (3.7), except that the coefficients d, e, and f, in (3.7b) are to be replaced with

$$d \equiv \coth(2\theta_0/k) + \coth(\theta_0/k)\,, \qquad e \equiv 2\coth(2\theta_0/k)\,, \qquad f \equiv -\mathrm{csch}(2\theta_0/k)\,, \qquad \theta_0 = D^{-1/2}\,. \tag{4.34}$$

A key condition in the analysis of [14] is that we can solve (4.27) for $\boldsymbol{m}$ in terms of $\boldsymbol{c}$. This requires a certain invertibility condition. Since (4.33) relates $\mathcal{G}$ to a matrix $\mathcal{B}_{00}$ whose spectrum was calculated in (3.11) of §3, the invertibility condition is that

$$\frac{-s}{\kappa_{0j}\sqrt{D}a_g} + 1 \neq 0\,, \qquad j = 1, \ldots, k\,, \tag{4.35}$$

where κ_{0j} is an eigenvalue of $\mathcal{B}_0$ when $\tau = 0$. Using (3.11) for κ_{0j}, and (2.8) for a_g, we see that this invertibility condition is equivalent to

$$\frac{1}{2} + \frac{1}{2s\tanh(\theta_0/k)}\left(\tanh\left(\frac{\theta_0}{k}\right) + \frac{[1-\cos\left(\pi(j-1)/k\right)]}{\sinh\left(2\theta_0/k\right)}\right) \neq 1\,. \tag{4.36}$$

From the analysis in §3, we see that the left hand-side of this expression is simply C_j at $\lambda = 0$, where C_j is defined in (3.19). Recall from §3 that $C_j = 1$ implies that there is a zero large eigenvalue. Hence, we conclude that our invertibility condition is precisely equivalent to the condition that the parameters s, k, and D, do not correspond to a zero large eigenvalue. For the large solution branch u_+, ν_+, the invertibility condition (4.36) always holds, since from Proposition 3.10 all of the large eigenvalues are real and positive. For the small solution branch where $1 < s < \infty$, the invertibility condition (4.36) always holds when $k = 1$. For $k > 1$, a sufficient condition for (4.36) to hold is that $\mathcal{A} > \mathcal{A}_{kL}$ (or equivalently $D < D_{kL}$), where $\mathcal{A}_{kL}$ and D_{kL} are given in (3.27).

The eigenvalues ξ_j and the associated normalized eigenvectors $\boldsymbol{v}_j$ of $\mathcal{B}_g$ are essential to the main result below. They were calculated in Proposition 9 of [14] as

$$\xi_j = 2\coth\left(\frac{2\theta_0}{k}\right) - 2\mathrm{csch}\left(\frac{2\theta_0}{k}\right)\cos\left(\frac{\pi j}{k}\right) \qquad j = 1,\ldots,k\,, \tag{4.37a}$$

$$\boldsymbol{v}_k^t = \frac{1}{\sqrt{k}}\left(1,-1,1,\ \ldots\ ,(-1)^{k+1}\right)\ ; \quad \boldsymbol{v}_{l,j} = \sqrt{\frac{2}{k}}\sin\left(\frac{\pi j}{k}\,(l-1/2)\right), \quad j = 1,\ldots,k-1\,. \tag{4.37b}$$

Here $\boldsymbol{v}^t$ denotes transpose and $\boldsymbol{v}_j^t = (v_{1,j},\ldots,v_{k,j})$.

The next step in the analysis is to calculate σ and $\boldsymbol{c}$ explicitly. This was done in (4.37a)–(4.58) of [14]. We will not repeat that calculation here. In this way, we obtain the following explicit main result for the small eigenvalues of (2.17):

Proposition 4.2: *Let $\varepsilon \ll 1$ and $\tau = O(1)$. Assume that the invertibility condition (4.36) holds. Then, the eigenvalues of (2.17) of order $O(\varepsilon^2)$ are given explicitly by*

$$\lambda \sim -\frac{2\varepsilon^2 s}{D}\left[\frac{1-\cos\left(\pi j/k\right) - z_j\left(\cosh\left(2\theta_0/k\right)-1\right)}{\cosh\left(2\theta_0/k\right)-\cos\left(\pi j/k\right)}\right], \qquad j = 1,\ldots,k\,. \tag{4.38a}$$

Here z_j is defined in terms of $s = (1-U_\pm)/U_\pm$ by

$$z_j \equiv \frac{s}{s - \xi_j a_g\sqrt{D}}\,\mathrm{csch}^2\left(\frac{2\theta_0}{k}\right)\sin^2\left(\frac{\pi j}{k}\right), \quad j = 1,\ldots,k\,, \tag{4.38b}$$

where ξ_j and a_g are defined in (4.37a) and (2.8) respectively. The corresponding eigenfunction ϕ from (4.5) is given explicitly as

$$\phi(x) \sim \sum_{j=1}^{k}\left(c_j w'\left[\varepsilon^{-1}(x-x_j)\right] + \varepsilon s\langle\tilde{\eta}_0\rangle_j w\left[\varepsilon^{-1}(x-x_j)\right]\right), \tag{4.39a}$$

where

$$\langle\tilde{\boldsymbol{\eta}}_{\mathbf{0}}\rangle = \frac{1}{a_g}\left[I + \frac{s}{a_g\sqrt{D}}\left(\mathcal{B}_{00} - \frac{s}{a_g\sqrt{D}}I\right)^{-1}\right]\mathcal{P}_g\boldsymbol{c}\,. \tag{4.39b}$$

Here $\mathcal{B}_{00}$ is the matrix $\mathcal{B}_0$ in (3.7) evaluated at $\tau = 0$, and $\mathcal{P}_g$ is the matrix defined in (4.28). The vectors $\boldsymbol{c}_j = (c_1,\ldots,c_k)$ are precisely the eigenvectors $\boldsymbol{v}_j$ defined in (4.37b).

Next, we determine the sign of λ_j with respect to the parameters D, $\mathcal{A}$, and k. Since $z_k = 0$ in (4.38b) it follows that $\lambda_k < 0$ for any k, D and $\mathcal{A}$. Therefore, there is always one negative eigenvalue. Hence, there is always one stable direction for translational perturbations of the equilibrium solution.

Repeating the analysis from (4.60)–(4.64) of [14] we conclude that $\lambda_j < 0$ for $j = 1, \ldots, k-1$ if and only if

$$1 - s + \operatorname{csch}^2\left(\frac{\theta_0}{k}\right) < 0\,. \tag{4.40}$$

For the large solution u_+, ν_+, where $0 < s < 1$, the left hand-side of (4.40) is always positive, and so there are $k-1$ positive small eigenvalues λ_j, for $j = 1, \ldots, k-1$. For the small solution where $s > 1$, we can calculate stability thresholds from (4.40). This yields the following main result:

Proposition 4.3: *Let $\varepsilon \ll 1$, and $\tau = O(1)$. For $k = 1$, both the large and small solutions $u_\pm$ $\nu_\pm$ are always stable with respect to the small eigenvalue. For $k > 1$, and for the large solution u_+, ν_+, there are always $k-1$ positive small eigenvalues and one negative eigenvalue λ_k. Similarly, for $k > 1$, we also have $\lambda_k < 0$ for the small solution u_-, ν_-. However, the other small eigenvalues λ_j, for $j = 1, \ldots, k-1$ are negative at a fixed value of $\mathcal{A}/\mathcal{A}_{ke}$ if and only if D satisfies,*

$$D < D_{kS} \equiv \frac{4}{k^2\left[\ln\left(r + \sqrt{r^2-1}\right)\right]^2}\,, \qquad r \equiv \left[1 - \frac{\mathcal{A}_{ke}^2}{\mathcal{A}^2}\right]^{-1/2}\,. \tag{4.41}$$

When $D = D_{kS}$, then $\lambda = 0$ is an eigenvalue of algebraic multiplicity $k-1$.

We can readily obtain a similar criterion with respect to the parameter $\mathcal{A}$. This leads to the next result.

Proposition 4.4: *Let $\varepsilon \ll 1$ and $\tau = O(1)$. For the small solution u_-, ν_-, the small eigenvalues λ_j, for $j = 1, \ldots, k-1$ are negative at a fixed value of D if and only if $\mathcal{A}$ satisfies*

$$\mathcal{A} > \mathcal{A}_{kS} \qquad \mathcal{A}_{kS} \equiv \mathcal{A}_{ke}\left[\tanh\left(\frac{2\theta_0}{k}\right)\right]^{-1}\,. \tag{4.42}$$

Here $\mathcal{A}_{ke}$ are the existence thresholds of (2.12).

Qualitatively, we summarize our results as follows. For a one-spike solution, the entire small solution branch u_-, ν_- is stable with respect to the small eigenvalues for any $D > 0$ and $\mathcal{A} > \mathcal{A}_{1e}$. For a multi-spike pattern with $k > 1$, the small solution branch is stable with respect to the small eigenvalues if and only if, at a fixed $\mathcal{A}_{ke}/\mathcal{A}$, the diffusion coefficient D is below the threshold D_{kS}, or equivalently, at a fixed value of D, the constant $\mathcal{A}$ exceeds $\mathcal{A}_{kS}$. Notice that when $D \ll 1$, we have $\mathcal{A}_{kS} - \mathcal{A}_{ke} \to 0^+$. The large solution branch is always stable with respect to the small eigenvalues when $k = 1$, but is always unstable when $k > 1$.

Propositions 4.3 and 4.4 show that $k-1$ small eigenvalues cross through zero as either D crosses through D_{kS} or as $\mathcal{A}$ crosses through $\mathcal{A}_{kS}$. Comparing (4.42) with the result in Proposition 2.4, we obtain the next result.

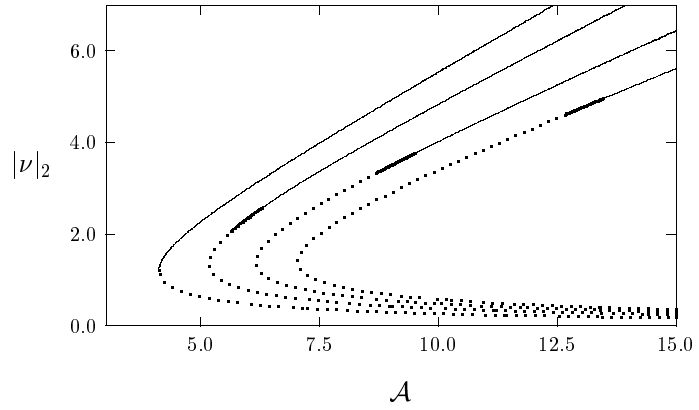

Figure 22: Bifurcation diagram of $|\nu|_2$, defined in (2.14), versus $\mathcal{A}$ for $D = 0.75$. The dashed portions are unstable for any $\tau \geq 0$. The heavy solid portions are stable with respect to the large eigenvalues when $\tau < \tau_{hL}$, but not the small eigenvalues. The solid portions are stable with respect to both the large and small eigenvalues when $\tau < \tau_{hL}$.

Proposition 4.5: *For $\varepsilon \ll 1$, and $k > 1$, the asymmetric k-spike equilibrium solution branch constructed in §2 bifurcates off of the symmetric k-spike equilibrium branch at precisely the parameter value $\mathcal{A} = \mathcal{A}_{kS}$ where $k-1$ small eigenvalues associated with the small solution u_-, ν_- cross through zero.*

Finally, we compare the stability thresholds D_{kS} and $\mathcal{A}_{kS}$ with the thresholds D_{kL} and $\mathcal{A}_{kL}$ calculated in §3 that guaranteed that the small solution was stable whenever τ is sufficiently small. The thresholds D_{kL} and $\mathcal{A}_{kL}$ signified the onset of competition instabilities. A simple calculation shows that D_{kS} and $\mathcal{A}_{kS}$ can be obtained by setting $j = k+1$ in (3.24) and (3.25), respectively. This observation readily implies the following inequalities:

$$\mathcal{A}_{kS} > \mathcal{A}_{kL}\,, \qquad D_{kS} < D_{kL}\,. \tag{4.43}$$

Therefore, the stability thresholds with respect to the small eigenvalues are more stringent than those for the large eigenvalues when τ is small. The next result yields the main stability conclusion for the small solution branch u_- and ν_-.

Proposition 4.6: *Let $\varepsilon \ll 1$ and consider the small solution branch u_-, ν_- of Proposition 2.1. Suppose that $\tau < \tau_{hL}$, where τ_{hL} corresponds to the Hopf bifurcation value given in (3.36). Then, the k-spike symmetric solution branch is stable with respect to both the large and the small eigenvalues*

when either $D < D_{kS}$, or equivalently when $\mathcal{A} > \mathcal{A}_{kS}$. For D satisfying $D_{kS} < D < D_{kL}$, or when $\mathcal{A}_{kL} < \mathcal{A} < \mathcal{A}_{kS}$, the solution is stable with respect to the large eigenvalues but is not stable with respect to the small eigenvalues.

To illustrate our main result graphically, in Fig. 22 we plot the norm $|\nu|_2$ defined in (2.14) versus $\mathcal{A}$ for the parameter values $D = 0.75$ and $k = 1, \ldots, 4$. The stability information of Proposition 4.6 is shown by different shadings of different portions of these branches. For smaller values of D, we still have $\mathcal{A}_{ke} < \mathcal{A}_{kL} < \mathcal{A}_{kS}$ for $k \geq 2$, but in this case $\mathcal{A}_{kS}$ is close to $\mathcal{A}_{ke}$.

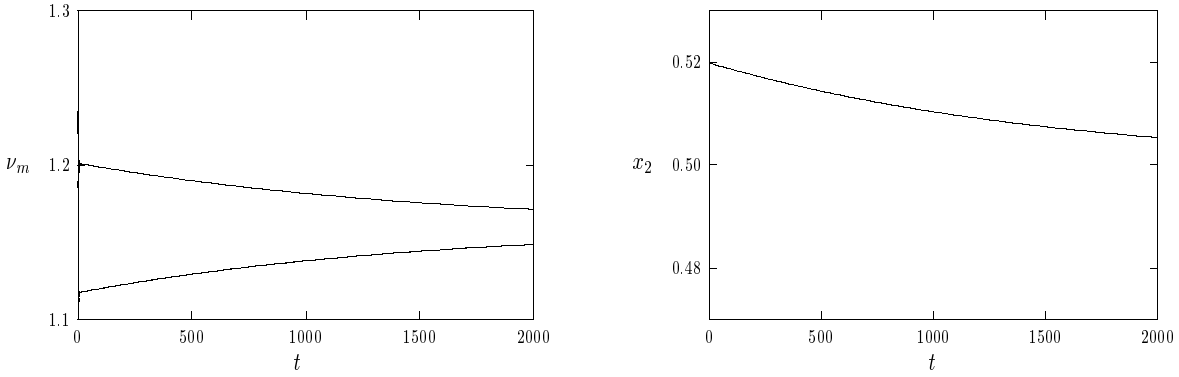

(a) ν_m versus t

(b) x_j versus t

Figure 23: Numerical solution to (1.6) with $D = 0.75$, $k = 2$, $\varepsilon = 0.03$, $\tau = 2.0$, and $\mathcal{A} = 6.5$. Left figure: plot of the spike amplitudes ν_m of ν_- versus t. Right figure: plot of the spike location x_2 versus t.

Although our analysis has only considered the stability of symmetric k-spike equilibrium solution branches, the results above suggest local stability properties near the bifurcation point $\mathcal{A}_{kS}$ for the emergence of asymmetric k-spike branches. Since $k-1$ small eigenvalues for the symmetric branch cross into the stable left half-plane as $\mathcal{A}$ increases past $\mathcal{A}_{kS}$, we conjecture that, locally, the asymmetric branches are always unstable with respect to the small eigenvalues. However, since the symmetric branch is stable with respect to the large eigenvalues at $\mathcal{A} = \mathcal{A}_{kS}$ when $\tau < \tau_{hL}$, we would expect from continuity that, locally, the asymmetric solution branch is stable with respect to the large eigenvalues when τ is below some threshold.

Example: To illustrate our theory, and to show another significance of these small eigenvalues, we

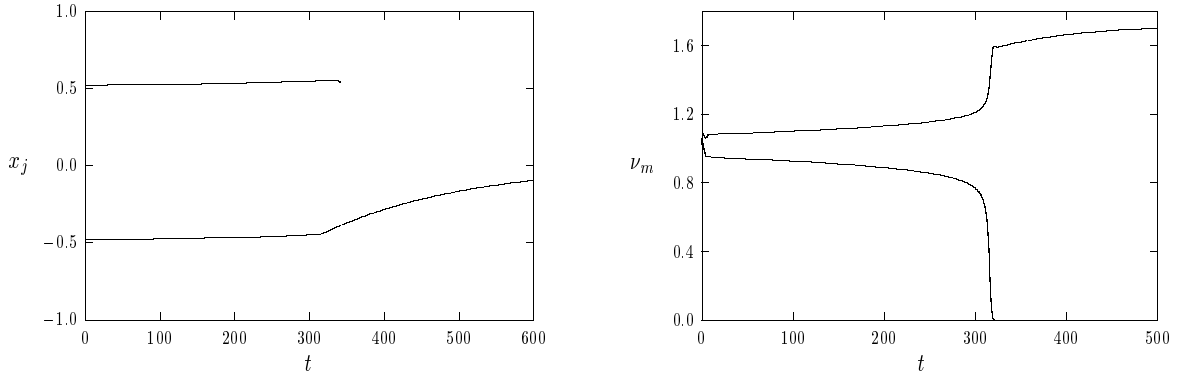

(a) ν_m versus t

(b) x_j versus t

Figure 24: Numerical solution to (1.6) with $D = 0.75$, $k = 2$, $\varepsilon = 0.03$, $\tau = 2.0$, and $\mathcal{A} = 6.0$. Left figure: plot of spike locations x_j versus t. Right figure: plot of the spike amplitudes ν_m versus t.

consider a specific example. In the full numerical simulations of (1.6), we take $D = 0.75$, $k = 2$, $\varepsilon = 0.03$, and $\tau = 2.0$. For this two-spike example, we calculate $\mathcal{A}_{2S} = 6.296$ and $\mathcal{A}_{2L} = 5.633$. Since τ is below the stability threshold there is no Hopf bifurcation for the equilibrium profile. For the initial condition for (1.6), we take the equilibrium solution of Proposition 2.1, with initial spike locations $x_j(0)$, for $j = 1, 2$, slightly offset from their equilibrium values of ± 0.5. The solution to (1.6) is computed using the routine D03PCF of the NAG library [25] with 1500 uniformly spaced meshpoints.

We first take $\mathcal{A} = 6.5 > \mathcal{A}_{2S}$, and $x_1(0) = 0.52$, $x_2(0) = -0.48$. For this value of $\mathcal{A}$, the two small eigenvalues are negative. Therefore, the solution should be stable with respect to translations of the profile. In Fig. 23(a) we plot the spike amplitudes $\nu_m = \nu_-(x_j)$, for $j = 1, 2$, as a function of time showing the convergence towards a symmetric two-spike equilibrium solution over a long time-scale. In Fig. 23(b) we plot x_2 versus t showing that $x_2 \to 0.5$ as t increases. A similar plot can be made for x_1.

Next, we take $\mathcal{A} = 6.0$, so that $\mathcal{A}_{2L} < \mathcal{A} < \mathcal{A}_{2S}$. We also take $x_1(0) = 0.52$, $x_2(0) = -0.48$. In Fig. 24(a) we plot the locations of the two spikes as a function of time showing the divergence away from the two-spike equilibrium locations ± 0.5. In Fig. 24(b) we plot the spike amplitudes ν_m for the two spikes as a function of time. The solution ν_- versus x is shown in Fig. 25(a) at different

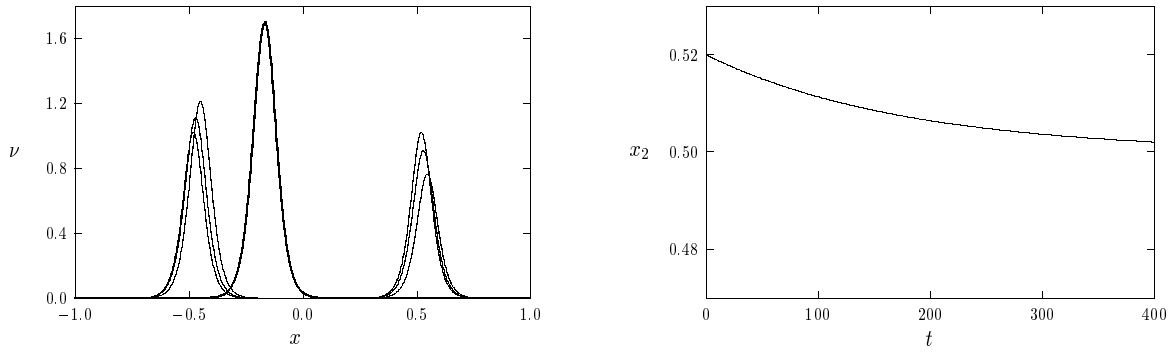

(a) ν versus x

(b) x_j versus t

Figure 25: Left figure: plot of numerical solution to (1.6) at different times for the parameter values of Fig. 24. The clustered solid curves correspond to $t = 0, 150, 300$, and the heavy solid curve corresponds to $t = 500$. Right figure: plot of the spike location x_2 versus t for the parameter values of Fig. 24, except now with symmetric initial locations $x_1(0) = 0.52$ and $x_2(0) = -0.52$.

times. This example suggests the following scenario. For this value of $\mathcal{A}$, the equilibrium two-spike solution is stable with respect to profile instabilities (large eigenvalues), but is unstable with respect to translations (small eigenvalues). Therefore, the locations of the two spikes diverge away from ± 0.5. During their evolution, a competition instability occurs on a $O(1)$ time scale as a result of a large eigenvalue crossing into the right half-plane. Recall that we have only analyzed profile instabilities associated with *equilibrium* spike solutions, and not quasi-equilibrium solutions. This competition kills one of the spikes, and the other spike then tends to the stable one-spike equilibrium solution centered at the origin. Since $\lambda_k < 0$ in Proposition 4.3, a one-spike equilibrium solution is always stable with respect to translations.

Finally, we again take $\mathcal{A} = 6.0$, but we now introduce a symmetric perturbation in the initial spike locations so that $x_1(0) = -0.52$ and $x_2(0) = 0.52$. Although, the equilibrium solution is unstable with respect to translations of the profile, the spike location x_2 is shown, seemingly paradoxically, in Fig. 25(b) to approach its equilibrium value. An identical convergence occurs for x_1. To explain this, we recall from Proposition 4.3 that, although $\lambda_1 > 0$ for this value of $\mathcal{A}$, we always have that $\lambda_2 < 0$. Therefore, we have a saddle-structure for the two-spike equilibrium. From Proposition 4.3, and from the form of the stable eigenvector $\boldsymbol{v}_2$ in (4.37b), we note that symmetric perturbations of

the initial spike locations such as given in this example are, locally, on the stable manifold of the saddle point. Therefore, with sufficient numerical resolution it is possible that we can approach the saddle point as t increases. This is what is observed in Fig. 25(b).

5 The Intermediate Regime: $O(1) \ll \mathcal{A} \ll O(\varepsilon^{-1/2})$

The derivations of the spectral problems in Propositions 3.2 and 4.1 were based on linearizing (1.6) around the solution constructed in Proposition 2.1. A crucial feature of this solution is that the leading-order inner problems for $u_\pm$ and $\nu_\pm$ decouple near each spike. In particular, this implies that $u_\pm = U_\pm + O(\varepsilon)$ in the core of each spike. The eigenvalue problems in Propositions 3.2 and 4.1 are valid for the range of $\mathcal{A}$ where such a leading-order decoupling of the inner problems for $u_\pm$ and $\nu_\pm$ can be made. We now show formally that, when $D = O(1)$, this decoupling property holds for the range $O(1) \leq \mathcal{A} \ll O(\varepsilon^{-1/2})$. For the intermediate regime, which we define by $O(1) \ll \mathcal{A} \ll O(\varepsilon^{-1/2})$, we then derive certain scaling laws for the stability thresholds calculated in §3 and §4.

To construct a k-spike pattern, we proceed as in the study of asymmetric patterns in §2.1 by first constructing a symmetric one-spike equilibrium solution to (1.6) on the interval $-l < x < l$. Then, by setting $l = 1/k$, we obtain the result for a k-spike pattern for (1.6) on $-1 < x < 1$. In the inner region near $x = 0$, we let $y = \varepsilon^{-1}x$, $\nu_i(y) = \nu(\varepsilon y)$, $u_i(y) = u(\varepsilon y)$, and we expand the inner equilibrium solution for (1.6) on $-l < x < l$ as

$$\nu_i(y) = \nu_{i0}(y) + \varepsilon\nu_{i1}(y) + \cdots\,, \qquad u_i(y) = u_{i0}(y) + \varepsilon u_{i1}(y) + \cdots\,. \tag{5.1}$$

Substituting (5.1) into the equilibrium problem for (1.6), we collect powers of ε to get

$$\nu_{i0}'' - \nu_{i0} + \mathcal{A}u_{i0}\nu_{i0}^2 = 0\,; \qquad u_{i0}'' = 0\,, \qquad -\infty < y < \infty\,, \tag{5.2a}$$

$$\nu_{i1}'' - \nu_{i1} + 2\mathcal{A}u_{i0}\nu_{i0}\nu_{i1} = -\mathcal{A}u_{i1}\nu_{i0}^2\,; \qquad Du_{i1}'' = u_{i0}\nu_{i0}^2\,, \qquad -\infty < y < \infty\,. \tag{5.2b}$$

In terms of the solution w to (2.3), the solution to (5.2a) is

$$\nu_{i0}(y) = \frac{1}{\mathcal{A}U}w(y)\,, \qquad u_{i0}(y) = U\,. \tag{5.3}$$

In the outer region, ν is exponentially small and $\varepsilon^{-1}u\nu^2$ can be represented as a Dirac mass, which can be calculated using the leading-order inner solutions u_{i0} and ν_{i0}. Therefore, the outer solution u_0 satisfies,

$$Du_0'' + (1 - u_0) = \frac{6}{\mathcal{A}^2U}\delta(x) \qquad -l < x < l\,; \qquad u_{0x}(\pm l) = 0\,. \tag{5.4}$$

The solution to (5.4) can be written in terms of the Green's function satisfying (2.19) as

$$u_0(x) = 1 - \frac{6}{\mathcal{A}^2 U} G(x;0)\,, \qquad G(x;0) = \frac{\theta_0 \cosh\left[(l-|x|)\theta_0\right]}{2\sinh\left(\theta_0 l\right)}\,, \qquad \theta_0 \equiv D^{-1/2}\,. \tag{5.5}$$

To determine the matching condition for the inner and outer solutions for u, we expand u_0 in (5.5) in right and left-sided limits as $x \to 0^{\pm}$. In this way, we obtain that U satisfies

$$U = 1 - \frac{6G(0;0)}{\mathcal{A}^2 U}\,, \qquad G(0;0) = \left(\frac{\theta_0}{2}\right)\coth\left(\theta_0 l\right)\,, \tag{5.6}$$

and that the solution u_{i1} to (5.2b) must have the far field behavior

$$u_{i1} \sim -\frac{6G_x(0^{\pm};0)}{\mathcal{A}^2 U} y\,, \qquad \text{as} \quad y \to \pm\infty\,. \tag{5.7}$$

Next, we introduce new inner variables $\hat{u}_{i1}$ and $\hat{\nu}_{i1}$ defined by

$$u_{i1} = \frac{1}{D\mathcal{A}^2 U}\hat{u}_{i1}\,, \qquad \nu_{i1} = \frac{1}{D\mathcal{A}^3 U^3}\hat{\nu}_{i1}\,. \tag{5.8}$$

Substituting (5.8) and (5.7) into (5.2), and noting that $G_x(0^{\pm};0) = \mp\theta_0^2/2$, we obtain an explicit two-term inner expansion. The outer expansion is obtained by substituting (5.6) into (5.5). Then, identifying $l = 1/k$, we obtain the following result for a k-spike pattern:

Proposition 5.1: *For $\varepsilon \to 0$, consider a k-spike equilibrium solution to (1.6). Then, when $\mathcal{A} > \mathcal{A}_{ke}$ there are two such solutions; the small solution u_-, ν_-, and the large solution u_+, ν_+. The two-term inner expansions in the core of each spike are*

$$\nu_{i\pm}(y) \sim \frac{1}{\mathcal{A}U_{\pm}}\left[w(y) + \frac{\varepsilon}{\mathcal{A}^2 U_{\pm}^2 D}\hat{\nu}_{i1}(y) + \cdots\right]\,, \qquad u_{i\pm}(y) \sim U_{\pm}\left[1 + \frac{\varepsilon}{\mathcal{A}^2 U_{\pm}^2 D}\hat{u}_{i1}(y) + \cdots\right]\,, \tag{5.9a}$$

where $U_{\pm}$ and $\mathcal{A}_{ke}$ are given by

$$U_{\pm} = \frac{1}{2}\left[1 \pm \sqrt{1 - \frac{\mathcal{A}_{ke}^2}{\mathcal{A}^2}}\right]\,, \qquad \mathcal{A}_{ke} \equiv \sqrt{\frac{12\theta_0}{\tanh\left(\theta_0/k\right)}}\,, \qquad \theta_0 \equiv D^{-1/2}\,. \tag{5.9b}$$

Here $\hat{\nu}_{i1}(y)$ and $\hat{u}_{i1}(y)$ satisfy the parameter-independent inner problems on $-\infty < y < \infty$

$$\hat{\nu}_{i1}'' - \hat{\nu}_{i1} + 2w\hat{\nu}_{i1} = -\hat{u}_{i1}w^2\,, \qquad \hat{\nu}_{i1} \to 0\,, \quad \text{as} \quad |y| \to \infty\,, \tag{5.10a}$$

$$\hat{u}_{i1}'' = w^2\,, \qquad \hat{u}_{i1} \sim 3|y|\,, \quad \text{as} \quad |y| \to \infty\,. \tag{5.10b}$$

The corresponding outer solution for u on $-1 < x < 1$ is

$$u_0(x) = 1 - \frac{(1-U_\pm)}{a_g}\sum_{j=1}^{k} G(x;x_j)\,, \qquad a_g = \left[2\sqrt{D}\tanh\left(\theta_0/k\right)\right]^{-1}\,, \tag{5.11}$$

where $G(x;x_j)$ is the Green's function on $-1 < x < 1$ defined by (2.6).

From (5.9a), we obtain that the leading-order decoupling property for the inner solutions is valid provided that

$$\frac{\varepsilon}{\mathcal{A}^2 U_\pm^2 D} \ll 1\,. \tag{5.12}$$

Since $U_+ \to 1$ as $\mathcal{A} \to \infty$, the condition (5.12) holds uniformly as $\mathcal{A} \to \infty$ for the large solution u_+, ν_+. Alternatively, as $\mathcal{A} \to \infty$, we have for the small solution that

$$U_- \sim \frac{\mathcal{A}_{ke}^2}{4\mathcal{A}^2} + O\left(\frac{\mathcal{A}_{ke}^4}{\mathcal{A}^4}\right)\,, \qquad \text{for} \quad \mathcal{A} \gg 1\,. \tag{5.13}$$

Substituting (5.13) into (5.12), and using (5.9b) for $\mathcal{A}_{ke}$, we obtain that the decoupling condition (5.12) holds when

$$O(1) \le \mathcal{A} \ll 3\varepsilon^{-1/2}\coth\left[\theta_0/k\right]\,, \qquad \theta_0 = D^{-1/2}\,. \tag{5.14}$$

Therefore, for $D = O(1)$, we must have that $\mathcal{A} \ll O(\varepsilon^{-1/2})$. Although, (5.14) appears to hold uniformly in D as $D \to 0$, this is misleading since the existence threshold $\mathcal{A}_{ke}$ in (2.12) yields $\mathcal{A}_{ke} = O(D^{-1/4})$ as $D \to 0$. Hence, for $D \ll 1$, the intermediate regime holds provided that $O(D^{-1/4}) \ll \mathcal{A} \ll \varepsilon^{-1/2}$. This requires that $D \gg O(\varepsilon^2)$. Hence, there is no intermediate range for $\mathcal{A}$ for the parameter regime studied in [29] where $D = O(\varepsilon^2)$.

We now derive certain scaling laws in the intermediate regime where $O(1) \ll \mathcal{A} \ll O(\varepsilon^{-1/2})$ and $D = O(1)$. In particular, in this regime we use (5.13) to obtain that the two-term inner expansion for the small solution in the core of each spike satisfies

$$\nu_{i-}(y) \sim \frac{\mathcal{A}\sqrt{D}}{3\coth\left(\theta_0/k\right)}\left[w(y) + \left(\frac{\varepsilon\mathcal{A}^2}{9\coth^2\left(\theta_0/k\right)}\right)\hat{\nu}_{i1}(y) + \cdots\right]\,, \tag{5.15a}$$

$$u_{i-}(y) \sim \frac{3\coth\left(\theta_0/k\right)}{\mathcal{A}^2\sqrt{D}}\left[1 + \left(\frac{\varepsilon\mathcal{A}^2}{9\coth^2\left(\theta_0/k\right)}\right)\hat{u}_{i1}(y) + \cdots\right]\,. \tag{5.15b}$$

Moreover, for $\mathcal{A} \gg 1$, the outer solution (5.11) has the form

$$u_0(x) \sim 1 - \frac{1}{a_g}\left(1 - \frac{\mathcal{A}_{ke}^2}{4\mathcal{A}^2}\right)\sum_{j=1}^{k} G(x;x_j)\,. \tag{5.16}$$

In the intermediate regime, we can use (5.15a) to calculate the norm $|\nu|_2$ in (2.13) as

$$|\nu|_2 \equiv \left(\varepsilon^{-1} \int_{-1}^{1} \nu^2 \, dx \right)^{1/2} \sim \frac{\sqrt{6Dk}\mathcal{A}}{3 \coth(\theta_0/k)} . \tag{5.17}$$

The expansions (5.15) and (5.16) do suggest the following scalings of the inner and outer solutions in the pulse-splitting regime $\mathcal{A} = O(\varepsilon^{-1/2})$ studied in the companion paper [16]:

$$\nu_i = O(\varepsilon^{-1/2}) , \qquad u_i = O(\varepsilon) , \qquad u_0 = u_{01} + O(\varepsilon) . \tag{5.18}$$

The spectral results of §3 and §4 are valid when the decoupling condition (5.14) holds. We now derive scaling laws for the stability thresholds of the small solution u_-, ν_- in the intermediate regime. Using (5.13), we obtain for $\mathcal{A} \to \infty$ that

$$s \equiv \frac{1 - U_-}{U_-} = \frac{4\mathcal{A}^2}{\mathcal{A}_{ke}^2} - 2 + o(1) , \qquad \text{as} \quad \mathcal{A} \to \infty . \tag{5.19}$$

To calculate the stability threshold D_{kL} for the large eigenvalues, we let $s \to \infty$ in (3.27a). Using (5.19), a simple calculation shows that for $\mathcal{A} \gg 1$ we have

$$D_{kL} = D_{kL}^{\infty} + O(1) , \qquad D_{kL}^{\infty} = \frac{8\mathcal{A}^2}{k^2 \gamma_k \mathcal{A}_{ke}^2} \qquad \text{where} \quad \gamma_k \equiv 1 + \cos\left(\frac{\pi}{k}\right) . \tag{5.20}$$

Hence, $D_{kL}^{\infty} = O(\mathcal{A}^2)$ as $\mathcal{A} \to \infty$.

To determine the thresholds for a Hopf bifurcation in the intermediate regime, we let $s \to \infty$ in (3.19) to get that $C_j = (1/2) + O(s^{-1})$ when $\tau = O(1)$ and $D = O(1)$. In this range of τ and D, where $C_j \sim 1/2$, there are no eigenvalues in the right half-plane (cf. [39]). Therefore, for $D = O(1)$, an instability can only occur when $\tau \gg 1$. The correct scaling law is to introduce a new $O(1)$ parameter τ_0 by

$$\tau = \tau_0 \tanh^2(\theta_0/k) \, s^2 . \tag{5.21}$$

Substituting (5.21) into (3.19), and assuming that $D = O(1)$, we let $s \to \infty$ to get

$$C_j(\lambda) \sim C_{\infty}(\lambda) + O(s^{-2}) , \qquad C_{\infty}(\lambda) \equiv \frac{1}{2}\left[1 + \sqrt{\tau_0 \lambda} \right] . \tag{5.22}$$

Notice that $C_{\infty}(\lambda)$ is independent of j, D, and the number of spikes k. The nonlocal eigenvalue problem in the intermediate regime is then obtained by replacing χ in (3.12) with $\chi = 1/C_{\infty}$. Substituting (5.19) into (5.21), we obtain the key scaling law

$$\tau \sim \tau_{\infty} , \qquad \tau_{\infty} \equiv \frac{16\mathcal{A}^4}{\mathcal{A}_{ke}^4} \tanh^2(\theta_0/k) \, \tau_0 \left(1 - \frac{\mathcal{A}_{ke}^2}{2\mathcal{A}^2} \right)^2 + o(1) . \tag{5.23}$$

Here $\mathcal{A}_{ke}$ are the existence thresholds of (2.12). This leads to the following result for the large eigenvalues in the intermediate regime $O(1) \ll \mathcal{A} \ll O(\varepsilon^{-1/2})$:

Proposition 5.2: *Assume that* $0 < \varepsilon \ll 1$, $D = O(1)$, *and* $O(1) \ll \mathcal{A} \ll O(\varepsilon^{-1/2})$. *Then, with* $\Phi = \Phi(y)$, *the* $O(1)$ *eigenvalues of (2.17) for a symmetric k-spike small solution* u_-, ν_- *satisfy, for each* $j = 1, \ldots, k$, *the following leading-order nonlocal eigenvalue problem:*

$$L_0 \Phi - \chi_\infty w^2 \left(\frac{\int_{-\infty}^{\infty} w\Phi \, dy}{\int_{-\infty}^{\infty} w \, dy} \right) = \lambda \Phi \,, \qquad -\infty < y < \infty \,, \tag{5.24a}$$

with $\Phi \to 0$ *as* $|y| \to \infty$. *Here the local operator* L_0 *is given in (3.12c), and the multiplier* χ_∞ *is*

$$\chi_\infty \equiv \frac{2}{1 + \sqrt{\tau_0 \lambda}} \,. \tag{5.24b}$$

The corresponding global eigenfunction $\phi(x)$, *representing the perturbation in* ν_-, *is*

$$\phi(x) \sim \sum_{i=1}^{k} c_i \Phi \left[\varepsilon^{-1} (x - x_i) \right] \,. \tag{5.25}$$

Here c_i *for* $i = 1, \ldots, k$ *are the components of any one of the k independent eigenvectors in (3.11).*

The eigenvalue problem (5.24) was derived using a dynamical systems approach in [4], and studied in [5]. In [4] and [5], hypergeometric functions were used to numerically compute a winding number criterion for (5.24) over a wedge-shaped region that includes part of the left half-plane. Since the continuous spectrum is on the negative real axis, with the approach in [5] there are many technical difficulties that were overcome to count the number of eigenvalues near the origin. In our approach of §3, by having derived properties of $f(\lambda)$ on the imaginary axis, we do not need to consider the left half-plane and the difficulties with the continuous spectrum intersecting the origin. The only effect of the continuous spectrum with our formulation is that $C_\infty'(0)$ is infinite. Even with this change in the property of C in Proposition 3.6, the theory of §3 applies directly to (5.24), and proves that there is a Hopf bifurcation value τ_{0h} (possibly non-unique) where (5.24) has complex conjugate eigenvalues on the imaginary axis at λ_{Ih}, and that there is another critical value τ_{0m} where complex conjugate eigenvalues in the right half-plane first merge onto the positive real at some λ_{Rm} as τ_0 is increased. The proof is not computer assisted as in [5], since we do not use hypergeometric functions.

In Fig. 26(a) we plot the numerically computed path of the eigenvalues for (5.24) as τ_0 is increased, up until these eigenvalues merge onto the real axis. The corresponding functions $\lambda_R = \lambda_R(\tau)$ and $\lambda_I = \lambda_I(\tau) > 0$ are shown in Fig. 26(b). These numerical computations suggest the stronger result

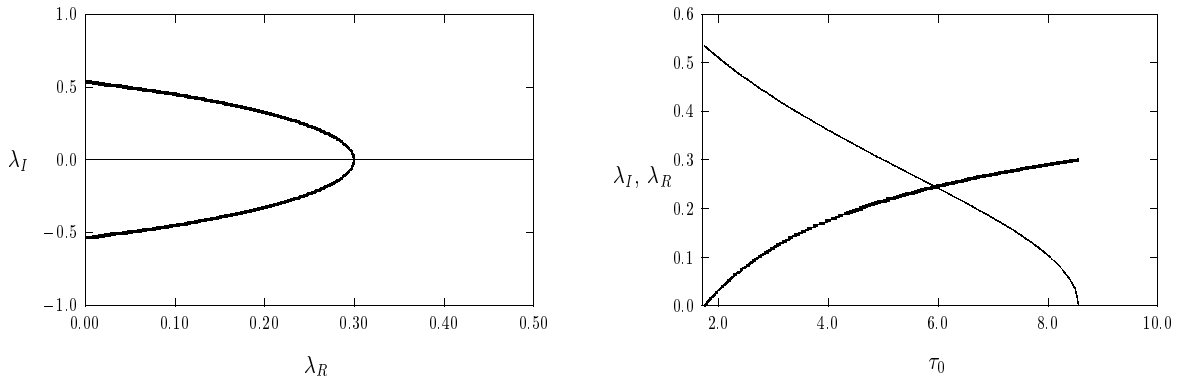

(a) path in complex plane

(b) $\lambda_R(\tau_0)$, $\lambda_I(\tau_0)$

Figure 26: Left figure: plot of the path of $\lambda = \lambda_R \pm i\lambda_I$ as τ_0 increases past $\tau_{0h} = 1.748$ until it merges onto the real axis at $\tau_{0m} = 8.567$. Right figure: λ_R (heavy solid curve) and λ_I (solid curve) versus τ_0.

that τ_{0h} is in fact unique, and that there are always two eigenvalues of (5.24) in the right half-plane when $\tau_0 > \tau_{0h}$. Our computations yield the critical values,

$$\tau_{0h} = 1.748\,, \quad \lambda_{Ih} = 0.534\,; \qquad \tau_{0m} = 8.567\,, \quad \lambda_{Rm} = 0.300\,. \tag{5.26}$$

These values are consistent with those in [4]. To obtain our scaling laws, we substitute (2.12) for $\mathcal{A}_{ke}$ into (5.23). In this way, and in analogy with Proposition 3.15, we can then summarize our stability results for the small solution in the intermediate regime.

Proposition 5.3: *Let $\varepsilon \ll 1$, and consider the intermediate regime $O(1) \ll \mathcal{A} \ll O(\varepsilon^{-1/2})$ for a symmetric k-spike small solution u_-, ν_-. Then, when $D = O(1)$, the solution will be stable with respect to the large eigenvalues when $\tau < \tau_h^\infty$, where*

$$\tau_h^\infty \sim \frac{\mathcal{A}^4 D}{9} \tanh^4(\theta_0/k)\, \tau_{0h} \left(1 - \frac{6\theta_0}{\mathcal{A}^2 \tanh(\theta_0/k)}\right)^2 + o(1)\,. \tag{5.27}$$

Moreover, for $D = O(1)$, there are two eigenvalues on the positive real axis in the interval $0 < \lambda < 5/4$ when $\tau > \tau_m^\infty$, where

$$\tau_m^\infty \sim \frac{\mathcal{A}^4 D}{9} \tanh^4(\theta_0/k)\, \tau_{0m} \left(1 - \frac{6\theta_0}{\mathcal{A}^2 \tanh(\theta_0/k)}\right)^2 + o(1)\,. \tag{5.28}$$

Alternatively, suppose that $D \gg 1$, with $D > D_{kL}^{\infty}$, where D_{kL}^{∞} is defined in (5.20). Then, the small solution u_-, ν_- is unstable for any $\tau > 0$.

This result shows that in the intermediate regime the roots of each $g_j(\lambda) = 0$ for $j = 1, \ldots, k$, where g_j is defined in (3.18), are on the imaginary axis at asymptotically the same value of τ and λ. This suggests a certain complexity in the dynamics near this bifurcation point, since there are k possible eigenfunctions in (5.25) that occur when τ crosses past τ_h^{∞}. Since for a k spike solution each of the k unstable modes crosses into the right half-plane at asymptotically the same value of τ, there is no apriori guarantee that the spike oscillations will be synchronous in the intermediate regime.

The threshold for D can be written more explicitly by using (2.12) for $\mathcal{A}_{ke}$ in (5.20). In this way, we obtain that there are no eigenvalues on the positive real axis when τ is sufficiently small, provided that $D < D_{L\infty}$, where $D_{L\infty}$ is the unique root of

$$\frac{\sqrt{D}}{\tanh\left(\frac{1}{k\sqrt{D}}\right)} = \frac{2\mathcal{A}^2}{3k^2}\,. \tag{5.29}$$

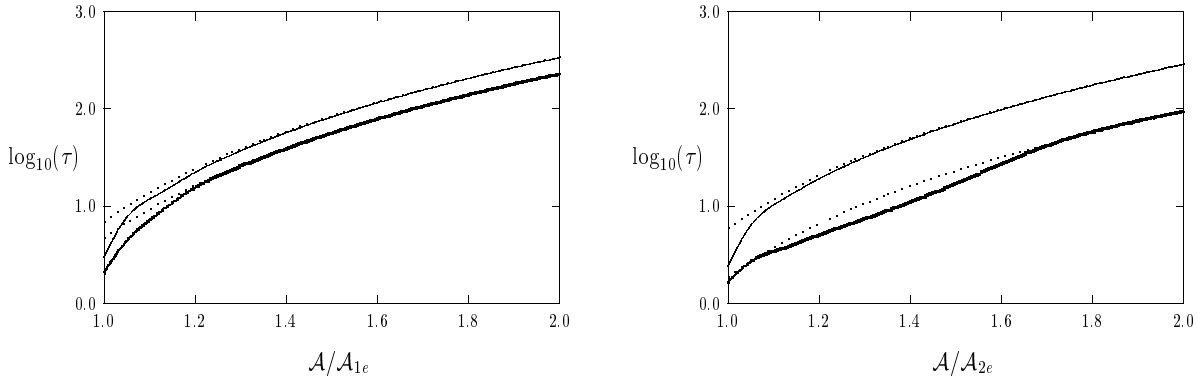

(a) $k = 1$: $\log_{10}(\tau)$ versus $\mathcal{A}/\mathcal{A}_{1e}$

(b) $k = 2$: $\log_{10}(\tau)$ versus $\mathcal{A}/\mathcal{A}_{2e}$

Figure 27: Comparison of numerical Hopf bifurcation value $\log_{10}(\tau_{hL})$ (solid curve is $D = 0.1$, heavy solid curve is $D = 0.75$) with the asymptotic scaling law $\log_{10}(\tau_h^{\infty})$, where τ_h^{∞} given in (5.27) (dashed curves). Left figure: $k = 1$. Right figure: $k = 2$.

In Fig. 27 we compare the scaling law (5.27) for τ for the Hopf bifurcation in the intermediate regime with the corresponding numerical value computed from (3.12). In Fig. 27(a) and Fig. 27(b)

we compare these critical values for $k = 1$ and $k = 2$, respectively. From these figures, we observe that the scaling law τ_h^∞ in (5.27) provides a good approximation to the numerically computed Hopf bifurcation value except near the existence threshold $\mathcal{A}_{ke}$.

As a remark, a similar scaling law for a Hopf bifurcation can be derived for the infinite-line problem studied in §3.4. Letting $s \to \infty$ in (3.53), we obtain that the Hopf bifurcation value τ_h^∞ is given by

$$\tau_h^\infty \sim \frac{\mathcal{A}^4 D}{9}\tau_{0h}\left(1 - \frac{6\theta_0}{\mathcal{A}^2}\right)^2 + o(1)\,, \tag{5.30}$$

where τ_{0h}, computed from (5.24), is given in (5.26). Setting $D = 1$, and writing $A = \varepsilon^{1/2}\mathcal{A}$, we can write the leading term in (5.30) as

$$\tau_h^\infty \sim 0.19422 A^4 \varepsilon^{-2}\,. \tag{5.31}$$

This result for the infinite-line problem is equivalent to equation (2.11) of [24].

Next, we derive a scaling law for the small eigenvalues studied in §4 that determine the stability with respect to translations of a symmetric k-spike small solution u_-, ν_-. We let $s \to \infty$ in the formulae for the small eigenvalues λ_j of (4.38) as well as the corresponding eigenfunction given in (4.39) of Proposition 4.2. Then, letting $s \to \infty$ in (4.41) of Proposition 4.3, we obtain the scaling law for the thresholds D_{kS}. Finally, using (5.19) to relate s to $\mathcal{A}$, and (2.12) for $\mathcal{A}_{ke}$, we obtain the following scaling law behavior for the small eigenvalues:

Proposition 5.4: *Let $\varepsilon \ll 1$, $D = O(1)$, $\tau = O(1)$, and assume that $O(1) \ll \mathcal{A} \ll O(\varepsilon^{-1/2})$. Then, for the small solution u_-, ν_-, the small eigenvalues of (2.17) have the scaling law,*

$$\lambda \sim -\frac{4\varepsilon^2\mathcal{A}^2\theta_0}{3}\tanh\left(\frac{\theta_0}{k}\right)\sin^2\left(\frac{\pi j}{2k}\right)\frac{\left[1 - \operatorname{sech}^2(\theta_0/k)\cos^2(\pi j/(2k))\right]}{\cosh(2\theta_0/k) - \cos(\pi j/k)}\,, \qquad j = 1, \ldots, k\,, \tag{5.32a}$$

where $\theta_0 = D^{-1/2}$. The corresponding eigenfunction ϕ has the scaling behavior

$$\phi(x) \sim \sum_{i=1}^{k}\left(c_i w'\left[\varepsilon^{-1}(x - x_i)\right] - \varepsilon\sqrt{D}\left(\mathcal{B}_{00}\mathcal{P}_g\mathbf{c}\right)_i w\left[\varepsilon^{-1}(x - x_i)\right]\right)\,. \tag{5.32b}$$

Here $\mathcal{B}_{00}$ is the matrix $\mathcal{B}_0$ in (3.7) evaluated at $\tau = 0$, and $\mathcal{P}_g$ is the matrix defined in (4.28). The vectors $\mathbf{c}_j = (c_1, \ldots, c_k)$ are precisely the eigenvectors $\boldsymbol{v}_j$ defined in (4.37b). Finally, the small eigenvalues are negative in the intermediate regime only when $D < D_{kS}^\infty$, where

$$D_{kS}^\infty = \frac{4\mathcal{A}^2}{k^2\mathcal{A}_{ke}^2} + O(1)\,. \tag{5.33}$$

From (5.32), we have that $\lambda_j < 0$ for $j = 1, \ldots, k$ when $D = O(1)$ and $\tau = O(1)$. Therefore, when $D = O(1)$ and $\tau = O(1)$, we have always have stability with respect to the small eigenvalues in the intermediate regime for $\mathcal{A}$. However, stability can be lost when D or τ is asymptotically large. More specifically, using (2.12) to relate $\mathcal{A}_{ke}$ in terms of D, we obtain from (5.33) that the small eigenvalues are all negative provided that $D < D_{S\infty}$, where $D_{S\infty}$ is the unique root of

$$\frac{\sqrt{D}}{\tanh\left(\frac{1}{k\sqrt{D}}\right)} = \frac{\mathcal{A}^2}{3k^2}\,. \tag{5.34}$$

5.1 A Traveling Wave, or Drift, Instability: $\tau = O(\varepsilon^{-2})$

The scaling law for τ given in (5.27) for a Hopf bifurcation in the spike profile in the intermediate regime shows that $\tau = O(\mathcal{A}^4) \gg 1$. In contrast, the instabilities associated with the small eigenvalues studied in §4 only considered the regime where $\tau = O(1)$. Therefore, it is natural to try to extend the analysis for the small eigenvalues to see if an instability can occur on the range where $\tau \gg 1$. If such an instability exists, then in some portion of the intermediate regime for $\mathcal{A}$ one could perhaps observe, as τ is increased, a small eigenvalue instability occurring before the onset of the Hopf bifurcation instability associated with the large eigenvalues. Since, to leading order, the eigenfunction associated with the small eigenvalue is w', this instability, referred to also as a drift instability, suggests the initiation of a traveling wave. In the context of the infinite-line problem, such an idea was explored in [23].

For the finite-line problem, we study the initiation of a traveling wave, or drift, instability for a one-spike small equilibrium solution u_-, ν_- centered at the origin. More specifically, for $\tau \gg 1$, the small eigenvalues can become complex, and we derive a formula for the critical value of τ, with $\tau \gg 1$, where such a traveling wave instability first occurs. For this one-spike solution, we show that at some critical value of τ, with $\tau \gg 1$, a pair of complex small eigenvalues enters the right half-plane through a Hopf bifurcation. This instability with respect to translations in the spike profile leads to oscillations in the spike location, and is distinct from the Hopf bifurcation in the amplitude of the spike profile studied in §3 and §5. As τ is increased past this critical Hopf bifurcation value for the drift instability, the complex conjugate pair of small eigenvalues will eventually merge onto the positive real axis at some further critical value of τ. At this new critical value, the instability with respect to translations leads to a monotonic drift of the spike towards the boundary of the domain.

For $\tau = O(\varepsilon^{-2})$, we now derive a formula for the small eigenvalue associated with a one-spike solution. Repeating the analysis leading to Proposition 4.1, we obtain the following result:

Proposition 5.5: *Let $\varepsilon \ll 1$ and $\tau = O(\varepsilon^{-2})$. Then, the small eigenvalue of (2.17) for a one-spike small solution satisfies,*

$$\lambda \sim 2\varepsilon^2 s \left[\langle \tilde{\eta}_{0x} \rangle_0 - \frac{1}{D} \right] . \tag{5.35}$$

Here $\langle \tilde{\eta}_{0x} \rangle_0$ is to be calculated from

$$D\tilde{\eta}_{0xx} - [1 + \tau\lambda]\,\tilde{\eta}_0 = 0\,, \qquad -1 < x < 1\,; \qquad \tilde{\eta}_{0x}(\pm 1) = 0\,, \tag{5.36a}$$

$$[D\tilde{\eta}_0]_0 = -\frac{1}{a_g}\,; \qquad [D\tilde{\eta}_{0x}]_0 = \frac{-s}{a_g}\langle \tilde{\eta}_0 \rangle_0\,. \tag{5.36b}$$

Here $\langle \zeta \rangle_0 \equiv \frac{1}{2}(\zeta(0^+) + \zeta(0^-))$, $[\zeta]_0 \equiv \zeta(0^+) - \zeta(0^-)$, $s = (1 - U_-)/U_-$, and $a_g = \left[2\sqrt{D}\tanh\theta_0\right]^{-1}$.

An eigenvalue λ with $\mathrm{Re}(\lambda) > 0$ is called a traveling wave instability since, from (5.9) and (4.5), the perturbation in ν has the form

$$\nu_-(x) \sim \frac{1}{\mathcal{A}U_-}\left[w(\varepsilon^{-1}x) + \delta e^{\lambda t} w'(\varepsilon^{-1}x) + \cdots \right] , \tag{5.37a}$$

where $\delta \ll 1$. This can be written as the Taylor series of

$$\nu_-(x) \sim \frac{1}{\mathcal{A}U_-} w(\varepsilon^{-1}\left[x - x_0(t)\right]) , \qquad x_0 \sim -\varepsilon\delta e^{\lambda t}\,. \tag{5.37b}$$

Hence, an instability with $\lambda > 0$ and real leads to a monotonic drift of the spike away from $x = 0$, whereas an instability with $\lambda = \pm i\lambda_I$ leads to oscillations in the spike location around the equilibrium value $x = 0$.

To derive an explicit formula for λ, we first calculate $\langle \tilde{\eta}_{0x} \rangle_0$ explicitly. A simple calculation from (5.36) yields

$$\langle \tilde{\eta}_{0x} \rangle_0 = \frac{\beta}{D}\tanh(\theta_0\beta)\tanh\theta_0\,, \qquad \beta \equiv \sqrt{1 + \tau\lambda}\,. \tag{5.38}$$

Substituting (5.38) into (5.35), we obtain that

$$\lambda \sim \frac{2\varepsilon^2 s}{D}\left[\beta\tanh(\theta_0\beta)\tanh\theta_0 - 1\right] . \tag{5.39}$$

To analyze (5.39), it is convenient to introduce the new variables τ_d, ω, and ξ, defined by

$$\tau = \left(\frac{D}{2s\varepsilon^2}\right)\tau_d\,, \qquad \lambda = \left(\frac{2s\varepsilon^2}{D}\right)\omega\,, \qquad \xi = \tau_d\omega\,. \tag{5.40}$$

Substituting (5.40) into (5.39), we obtain that ξ satisfies $F(\xi) = 0$, where

$$F(\xi) \equiv \frac{\xi}{\tau_d} - G(\xi)\,, \qquad G(\xi) \equiv \beta\tanh\theta_0\tanh(\theta_0\beta) - 1\,, \qquad \beta \equiv \sqrt{1 + \xi}\,, \quad \theta_0 = D^{-1/2}\,. \tag{5.41}$$

In (5.41), the principal value of the square root is taken. In terms of the roots $F(\xi) = 0$, the scaled eigenvalues ω are recovered from $\omega = \xi/\tau_d$.

Below, we will look for complex roots $\xi = \xi_R + i\xi_I$ to $F(\xi) = 0$. We will show that, for each $D > 0$, the equation $F(\xi) = 0$ has a pair of complex conjugate roots on the imaginary axis $\xi_R = 0$ when $\tau_d = \tau_{dh}$. Increasing τ_d past τ_{dh}, this complex conjugate pair of roots merges onto the positive real axis in the ξ plane when $\tau_d = \tau_{dm}$. At this value of τ_d, (5.41) has a double real root. For $\tau_d > \tau_{dm}$, (5.41) is shown to have two positive real roots.

Before analyzing the zeroes of (5.41), we examine the implications for the stability of a one-spike solution in the intermediate regime $O(1) \ll \mathcal{A} \ll O(\varepsilon^{-1/2})$ as τ is increased. Since $s = O(\mathcal{A}^2)$ in the intermediate regime, we obtain from (5.40) that a traveling wave instability will occur when $\tau = \tau_{TW} = O\left(\mathcal{A}^{-2}\varepsilon^{-2}\right)$. In contrast, from (5.27) a Hopf bifurcation in the spike profile will occur when $\tau = \tau_H = O\left(\mathcal{A}^4\right)$. Comparing the asymptotic orders of these two scales, we get

$$\tau_H \ll \tau_{TW}\,, \qquad \text{when} \quad 1 \ll \mathcal{A} \ll O(\varepsilon^{-1/3})\,, \tag{5.42a}$$

$$\tau_{TW} \ll \tau_H\,, \qquad \text{when} \quad O(\varepsilon^{-1/3}) \ll \mathcal{A} \ll O(\varepsilon^{-1/2})\,. \tag{5.42b}$$

For the infinite-line problem, (5.42) was also observed in [23]. Therefore, there is some scaling regime within the intermediate range $O(1) \ll \mathcal{A} \ll O(\varepsilon^{-1/2})$ where, as τ is increased, a traveling wave instability will occur before the Hopf bifurcation value associated with the spike profile.

We first look for roots of $F(\xi) = 0$ along the real axis. These roots correspond to the intersections points of the line ξ/τ_d with $G(\xi)$. A simple calculation using (5.41) shows that

$$G_\xi(\xi) = \frac{\tanh\theta_0}{2\beta}\left[\tanh(\theta_0\beta) + \beta\theta_0\mathrm{sech}^2(\theta_0\beta)\right]\,, \tag{5.43a}$$

$$G_{\xi\xi}(\xi) = \frac{\tanh\theta_0}{4\beta^3}\left[\theta_0\beta\mathrm{sech}^2(\theta_0\beta) - \tanh(\theta_0\beta)\right] - \frac{\theta_0^2}{2\beta}\tanh\theta_0\tanh(\theta_0\beta)\mathrm{sech}^2(\theta_0\beta)\,. \tag{5.43b}$$

Since $z\,\mathrm{sech}^2 z - \tanh z < 0$ for all $z > 0$, it follows that $G(\xi)$ is a monotonically increasing, and concave, function on $\xi \geq 0$. In addition, $G(0) = -\mathrm{sech}^2\theta_0 < 0$. These properties of $G(\xi)$ prove that there are exactly two real roots to $F(\xi) = 0$ when $\tau_d > \tau_{dm}$ and no such roots when $0 < \tau_d < \tau_{dm}$. Here τ_{dm} corresponds to the value of τ_d for which the straight line ξ/τ_d intersects $G(\xi)$ tangentially at some point ξ_m. By combining the equations $F = F_\xi = 0$ for the double root at $\tau_d = \tau_{dm}$ and $\xi = \xi_m$, we obtain that ξ_m is the unique root of

$$\left(\beta^2+1\right)\frac{\tanh(\theta_0\beta)}{\theta_0\beta} - \left(\beta^2-1\right)\mathrm{sech}^2\left(\theta_0\beta\right) = \frac{2}{\theta_0\tanh\theta_0}\,, \qquad \beta = \sqrt{1+\xi}\,. \tag{5.44}$$

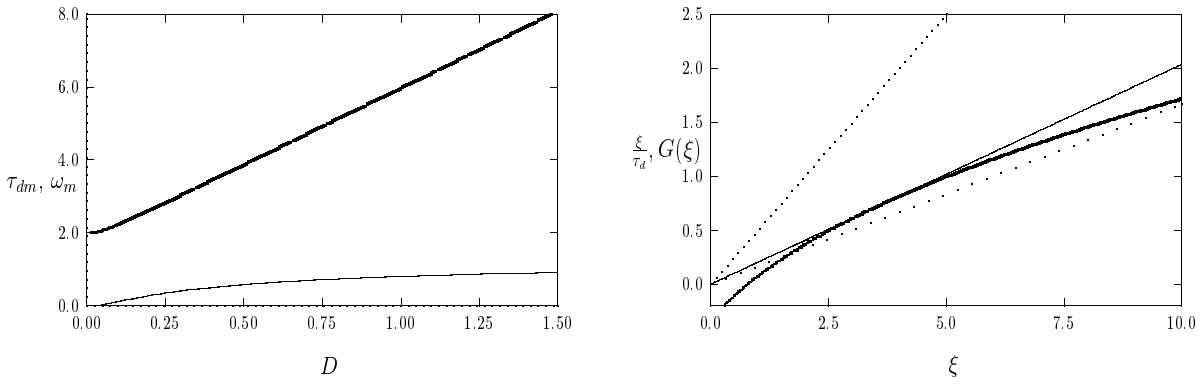

(a) τ_{dm} and ω_m (b) G versus ξ

Figure 28: Left figure: τ_{dm} (heavy solid curve) and ω_m (solid curve) versus D. Right figure: graphical determination of real roots to $F = 0$ when $D = 0.75$: Here $G(\xi)$ (heavy solid curve), and ξ/τ_d are shown for $\tau_d = 2.0$ (dotted curve), $\tau_d = \tau_{dm} \approx 4.91$ (solid curve), and $\tau_d = 6.0$ (widely spaced dots).

This yields ξ_m as a function of $\theta_0 = D^{-1/2}$. In terms of ξ_m, we then calculate τ_{dm} and the eigenvalue ω_m from $\tau_{dm} = \xi_m/G(\xi_m)$ and $\omega_m = \xi_m/\tau_{dm}$.

By solving (5.44) numerically, we plot τ_{dm} and ω_m as a function of D in Fig. 28(a). For $D = 0.75$ and $D = 0.1$, we calculate

$$D = 0.75\,, \quad \tau_{dm} = 4.914\,, \quad \omega_m = 0.717\,; \qquad D = 0.1\,, \quad \tau_{dm} = 2.229\,, \quad \omega_m = 0.116\,. \tag{5.45}$$

For $D = 0.75$, in Fig. 28(b) we plot G versus ξ together with the straight line ξ/τ_d for three different values of τ_d, one of which is the double root value $\tau_d = \tau_{dm}$. From this figure we see that there are two real roots to $F(\xi) = 0$ when $\tau_d > \tau_{dm}$ and none when $0 < \tau_d < \tau_{dm}$.

Fig. 28(a) suggests that τ_{dm} and ω_m have limiting values as $D \to 0$ and $D \to \infty$, respectively. Let $D \to 0$ so that $\theta_0 \to \infty$. In this limit, $\xi_m \to 0$ from (5.44). Therefore, for $D \to 0$, τ_{dm} corresponds to the value of τ_d for which $F(\xi) = 0$ has a double root at the origin. Using (5.41), we set $F(0) = F_\xi(0) = 0$, and let $\theta_0 \to \infty$ to obtain

$$\frac{1}{\tau_{dm}} = \frac{1}{2}\left[\tanh^2\theta_0 + \theta_0 \tanh\theta_0 \,\mathrm{sech}^2\theta_0\right] \to \frac{1}{2} \quad \text{as} \quad \theta_0 \to \infty\,. \tag{5.46}$$

Hence, $\tau_{dm} \to 2$ as $D \to 0$, which is consistent with Fig. 28(a). To determine the limiting behavior

of ω_m as $D \to \infty$, we let $\theta_0 \to 0$ in (5.44) to conclude that $\xi_m \to \infty$. Using $\beta \sim \sqrt{\xi}$ when $\xi \gg 1$, the double root condition for F can be written asymptotically as

$$\frac{\xi}{\tau_d} \sim \sqrt{\xi}\theta_0 \tanh\left(\sqrt{\xi}\theta_0\right) - 1\,, \qquad \frac{1}{\tau_d} \sim \frac{1}{2\sqrt{\xi}}\left[\theta_0 \tanh\left(\sqrt{\xi}\theta_0\right) + \sqrt{\xi}\theta_0^2 \operatorname{sech}^2\left(\sqrt{\xi}\theta_0\right)\right]. \tag{5.47}$$

Assuming that $\sqrt{\xi}\theta_0 \to \mu$ as $\theta_0 \to 0$ for some $\mu = O(1)$, we can combine the equations in (5.47) to get that μ satisfies

$$\mu \tanh\mu - 2 = \mu^2 \operatorname{sech}^2\mu\,. \tag{5.48}$$

The unique root of (5.48) is $\mu = 2.2649$. Then, since $\omega_m = \xi_m/\tau_{dm}$ and $\xi_m \sim D\mu^2$, we conclude that

$$\omega_m \to \mu\tanh\mu - 1 \approx 1.2166\,, \qquad \xi_m \to 5.1298D\,, \qquad \tau_{dm} \to 4.2165D\,, \quad \text{as} \quad D \to \infty\,. \tag{5.49}$$

Hence for $D \gg 1$, τ_{dm} is linear in D. The limiting behavior for ω_m is clearly seen in Fig. 28(a).

Next, we look for roots of $F(\xi) = 0$ on the positive imaginary axis $\xi = i\xi_I$ with $\xi_I \geq 0$. Separating (5.41) into real and imaginary parts, we obtain

$$F_R(\xi_I) = -G_R(\xi_I)\,, \qquad F_I(\xi_I) = \frac{\xi_I}{\tau_d} - G_I(\xi_I)\,, \tag{5.50}$$

where $F_R(\xi_I) = \mathrm{Re}(F(i\xi_I))$, $F_I(\xi_I) = \mathrm{Im}(F(i\xi_I))$, $G_R(\xi_I) = \mathrm{Re}(G(i\xi_I))$, and $G_I(\xi_I) = \mathrm{Re}(G(i\xi_I))$.

Using (5.41), we readily see that for each $D > 0$ we have $G_R(0) = -\operatorname{sech}^2\theta_0 < 0$ and that $G_R(\xi_I)$ is monotonically increasing with $G_R \to +\infty$ as $\xi_I \to \infty$. Therefore, $F_R(\xi_I) = 0$ has a unique root, which we label by ξ_h. Then, setting $F_I(\xi_h) = 0$, we determine the Hopf bifurcation value of τ_d as

$$\tau_{dh} = \left(\frac{\theta_0}{\tanh\theta_0}\right)\frac{\xi_h}{\mathrm{Im}(z\tanh z)}\,, \qquad z \equiv \sqrt{1 + i\xi_h}\,\theta_0\,. \tag{5.51}$$

The corresponding value of ω that determines the frequency of small scale oscillations is $\omega_h = \xi_h/\tau_{dh}$. The resulting numerical values for τ_{dh} and ω_m as a function of D are shown in Fig. 29(a). For $D = 0.75$ and $D = 0.1$, we calculate

$$D = 0.75\,, \quad \tau_{dh} = 2.617\,, \quad \omega_h = 0.772\,; \qquad D = 0.1\,, \quad \tau_{dh} = 1.986\,, \quad \omega_h = 0.115\,. \tag{5.52}$$

Clearly, $\tau_{dh} \to \tau_{dm} \to 2$ as $D \to 0$.

By solving numerically for the roots of $F(\xi) = 0$ with $\xi = \xi_R + i\xi_I$ on the range $\tau_{dh} < \tau_d < \tau_{dm}$ we obtain a path in the complex ξ plane. Setting $\omega = \xi/\tau_d$, in Fig. 29(b) we plot this path in terms of ω for $D = 0.75$ and $D = 0.1$. These numerical results suggest that for each $\tau_d > \tau_{dh}$ there are exactly two small eigenvalues in the right half-plane.

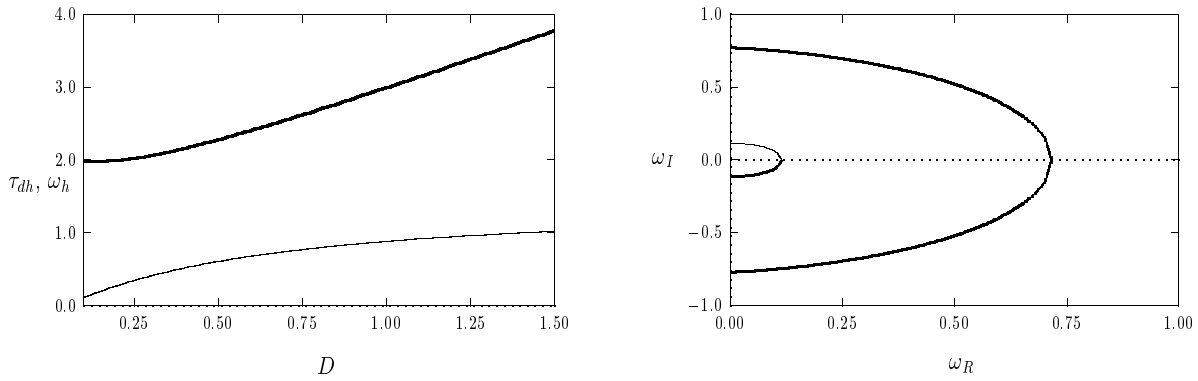

(a) τ_{dh} and ω_h

(b) eigenvalues in right half-plane

Figure 29: Left figure: The Hopf bifurcation values: τ_{dh} (heavy solid curve) and ω_h (solid curve) versus D. Right figure: eigenvalues $\omega = \omega_R + i\omega_I$ in the right half-plane for $\tau > \tau_{dh}$ when $D = 0.75$ (heavy solid curve) and $D = 0.1$ (solid curve).

To prove that, for each $D > 0$, there are exactly two small eigenvalues in the right half-plane when $\tau_d > \tau_{dh}$ we must show that $F(\xi) = 0$ has exactly two roots in $\mathrm{Re}(\xi) > 0$ when $\tau_d > \tau_{dh}$. This is done by calculating the winding number of $F(\xi)$ over the counterclockwise contour composed of the imaginary axis $-iR \le \mathrm{Im}\xi \le iR$ and the semi-circle Γ_R, given by $|\xi| = R > 0$, for $\mathrm{Re}(\xi) > 0$. For any $\tau_d > 0$, we have from (5.41) that $F(\xi) \sim \frac{\xi}{\tau_d}\left[1 + O(\xi^{-1/2})\right]$ as $|\xi| \to \infty$ in the right half-plane. Therefore, the change in the argument of $F(\xi)$ over Γ_R as $R \to \infty$ is π. Since $F(\xi)$ is analytic in the right half-plane, we then use the argument principle, together with $F(\overline{\xi}) = \overline{F(\xi)}$, to obtain that the number M of zeroes of $F(\xi)$ in the right half-plane is

$$M = \frac{1}{2} + \frac{1}{\pi}\left[\arg F\right]_{\Gamma_I} . \tag{5.53}$$

Here $\left[\arg F\right]_{\Gamma_I}$ denotes the change in the argument of $F(\xi)$ along the semi-infinite imaginary axis $\Gamma_I = i\xi_I$, $0 \le \xi_I < \infty$, traversed in the downwards direction.

To calculate M we notice that $F_I = O(\xi_I)$ and $F_R = O(\sqrt{\xi_I})$ as $\xi_I \to \infty$, and that $F_I(0) = 0$ with $F_R(0) > 0$. This implies that $\arg F = \pi/2$ as $\xi_I \to +\infty$, and $\arg F = 0$ at $\xi_I = 0$. Since the root to $F_R(\xi_I) = 0$ is unique, we obtain that the change in the argument, $\left[\arg F\right]_{\Gamma_I}$, is either $3\pi/2$ or $-\pi/2$ whenever $F_I(\xi_I) < 0$ or $F_I(\xi_I) > 0$, respectively, at the unique root of $F_R(\xi_I) = 0$. From

(5.53), we obtain that $M = 2$ or $M = 0$. Finally, since the root ξ_h to $F_R(\xi_I) = 0$ is independent of τ_d, we conclude that $F_I(\xi_I) < 0$ when $\tau_d > \tau_{dh}$ and $F_I(\xi_I) > 0$ when $\tau_d < \tau_{dh}$. This leads to a strict transversal crossing condition at the Hopf bifurcation point. This result is illustrated in Fig. 30(a) and Fig. 30(b) where we show a graphical determination of the roots of $F_R(\xi_I) = 0$ and $F_I(\xi_I) = 0$. We summarize our results as follows:

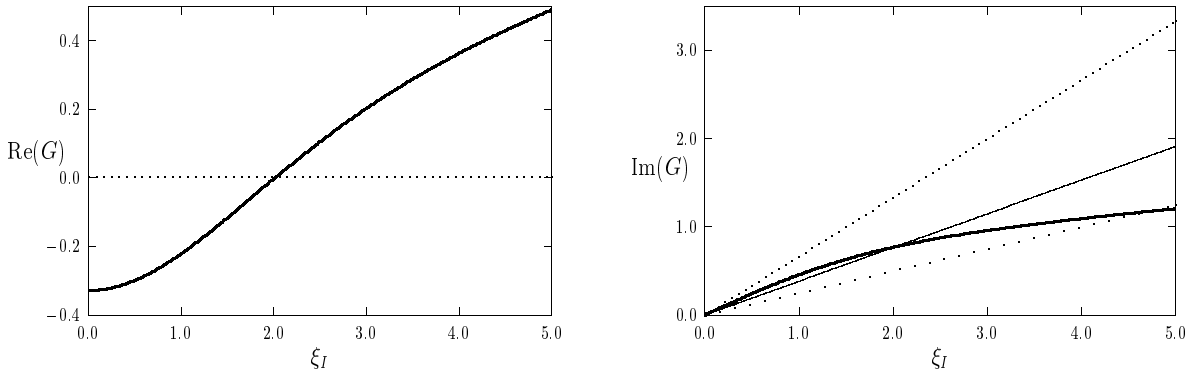

(a) $\mathrm{Re}(G(i\xi_I))$ versus ξ_I

(b) $\mathrm{Im}(G(i\xi_I))$ versus ξ_I

Figure 30: Graphical determination of the roots of $F(i\xi_I) = 0$ when $D = 0.75$. Left figure: $\mathrm{Re}(G(i\xi_I))$ versus ξ_I. Right figure: $\mathrm{Im}(G(i\xi_I))$ versus ξ_I (heavy solid curve). We also plot ξ_I/τ_d for $\tau_d = 1.5$ (dotted curve), $\tau_d = \tau_{dh} = 2.6169$ (solid curve), and $\tau_d = 4.0$ (widely spaced dots).

Proposition 5.6: *Let $\varepsilon \ll 1$ and $\tau = O(\varepsilon^{-2})$, and consider the small eigenvalues with $\lambda = O(\varepsilon^2)$. Then, there is a complex conjugate pair of pure imaginary eigenvalues when $\tau_d = \tau_{dh}$. For any $\tau_d > \tau_{dh}$ there are exactly two eigenvalues in the right half-plane. These eigenvalues have nonzero imaginary parts when $\tau_{dh} < \tau_d < \tau_{dm}$, and they merge onto the positive real axis at $\tau_d = \tau_{dm}$. They remain on the positive real axis for all $\tau_d > \tau_{dm}$.*

We now compare the two thresholds of instability for a one-spike solution. Let τ_H denote the value of τ for an instability due to a Hopf bifurcation in the spike amplitude, and let τ_{TW} denote the value of τ where an instability with respect to oscillations in the spike location is initiated. Then, from (5.21), (5.26), and (5.40), we obtain

$$\tau_H = 1.748 \tanh^2(\theta_0) s^2 , \qquad \tau_{TW} = \frac{D}{2s\varepsilon^2}\tau_{dh} , \tag{5.54a}$$

where

$$s = \frac{1-U_-}{U_-}\,, \quad U_- = \frac{1}{2}\left[1-\sqrt{1-\frac{\mathcal{A}_{1e}^2}{\mathcal{A}^2}}\right]\,, \quad \mathcal{A} = \varepsilon^{-1/2}A\,, \quad \mathcal{A}_{1e} \equiv \sqrt{\frac{12\theta_0}{\tanh(\theta_0)}}\,, \tag{5.54b}$$

and $\theta_0 \equiv D^{-1/2}$. For $D = 0.1$ and $D = 0.75$, in Fig. 31(a) and Fig. 31(b), respectively, we plot $\log_{10}(\tau_H)$ and $\log_{10}(\tau_{TW})$ for two values of ε on the parameter range $\varepsilon^{1/2}\mathcal{A}_{1e} < A < 1$. Notice that this range of A includes the intermediate parameter regime $\varepsilon^{1/2}\mathcal{A}_{1e} \ll A \ll 1$. We observe that when ε is sufficiently small, the curves τ_H and τ_{TW} will cross at some point in the intermediate parameter regime. To determine this crossing point, we set $\tau_H = \tau_{TW}$ and solve for A. Using (5.54) and $s \sim 4\varepsilon^{-1}A^2/\mathcal{A}_{1e}^2$, we obtain that the de-stabilization of a one-spike solution occurs by a traveling wave instability when

$$A > A_{sw} \sim \left(\frac{\varepsilon D\tau_{dh}}{223.744\tanh^2(\theta_0)}\right)^{1/6}\mathcal{A}_{1e}\,. \tag{5.55}$$

Alternatively, a de-stabilization by a Hopf bifurcation in the spike amplitude occurs when $A < A_{sw}$. Although the value of τ where a traveling wave instability first occurs in the intermediate regime is asymptotically large as $\varepsilon \to 0$, this analysis suggests that traveling wave instabilities will occur in the pulse-splitting regime with $A = O(1)$ when $\tau_{TW} = O(\varepsilon^{-1})$. These instabilities are found to play an important role in this regime (see [16]).

We now recover the result of [24] (see section 2.6 of [24]) for the infinite-line problem. To recover this result from (5.55) we let $\theta_0 \to \infty$, $\tilde{\varepsilon} \equiv \varepsilon/\sqrt{D}$, and $\mathcal{A}_{1e} = \sqrt{12\theta_0}$. Also, for $D \to 0$, we found above that $\tau_{dh} \to 2$. Hence, from (5.55), we obtain

$$A_{sw} = 1.578\tilde{\varepsilon}^{1/6}\,, \qquad \tilde{\varepsilon} \equiv \varepsilon/\sqrt{D}\,. \tag{5.56}$$

This limiting result agrees with that derived in [24]. The result (5.55) for the finite domain problem is new. Qualitatively, the effect of the finite domain on the traveling wave instability is to de-stablize a one-spike solution through a Hopf bifurcation leading to a pulsating layer location. This pulsating type of traveling wave instability depends critically on having a finite domain and does not occur for the infinite-line problem.

Example 1: We conclude with a specific example to illustrate the analysis in this section. We take $D = 0.75$, $A = 0.96436$, $\varepsilon = .005$, and the initial condition

$$v(x,0) = 60\text{sech}^2\left[\varepsilon^{-1}(x+.01)\right]\,, \tag{5.57}$$

which represents a layer initially located at $x_0(0) = -0.01$. For $D = 0.75$, we calculate $\tau_{dh} = 2.6169$, and so from (5.54) a traveling wave instability first occurs when $\tau = \tau_{TW} \approx 935.4$. Alternatively,

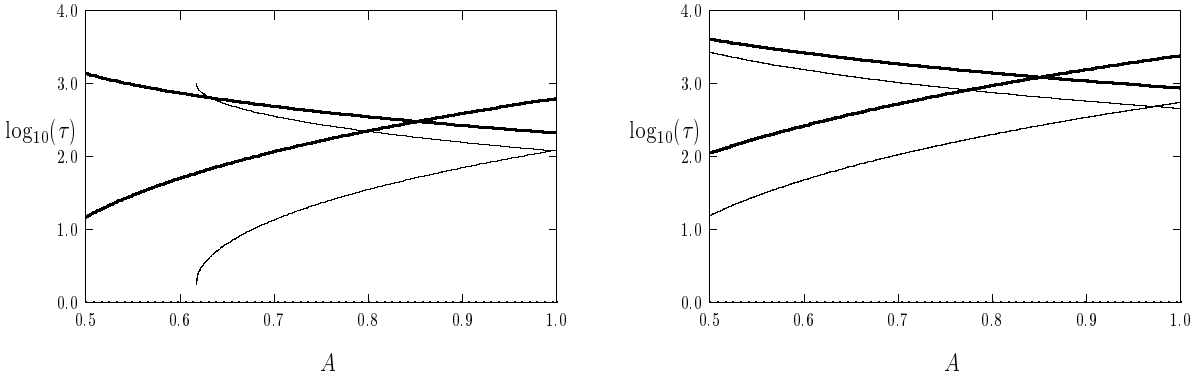

(a) $\log_{10}(\tau)$ for $D = 0.1$

(b) $\log_{10}(\tau)$ for $D = 0.75$

Figure 31: Plots of $\log_{10}(\tau_H)$ (increasing curves) and $\log_{10}(\tau_{TW})$ (decreasing curves) as a function of A on the range $\varepsilon^{1/2}\mathcal{A}_{1e} < A < 1$. The left figure and right figures are for $D = 0.1$ and $D = 0.75$, respectively. The heavy solid curves are for $\varepsilon = 0.005$ and the solid curves are for $\varepsilon = 0.01$.

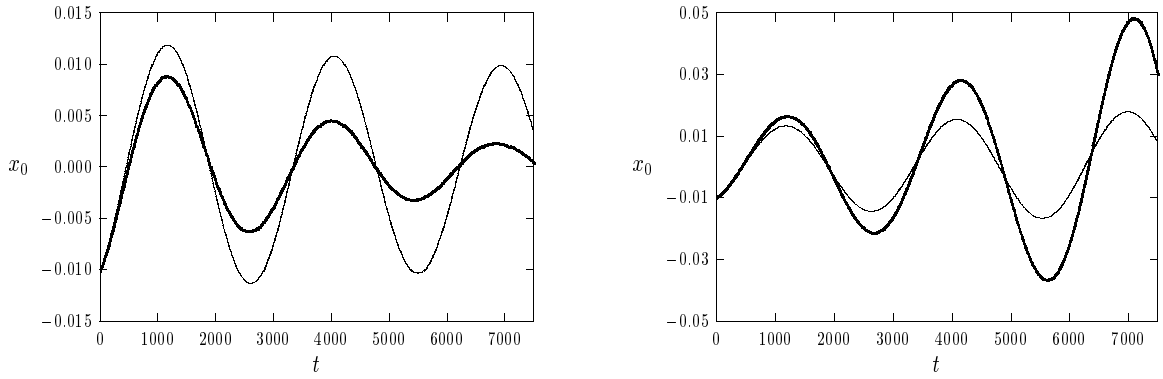

(a) $x_0(t)$ versus t

(b) $x_0(t)$ versus t

Figure 32: Example 1: $D = 0.75$, $A = 0.96436$, and $\varepsilon = 0.005$. Left figure: Plots of $x_0(t)$ versus t for $\tau = 850$ (heavy solid curve) and $\tau = 920$ (solid curve). Right figure: Plots of $x_0(t)$ versus t for $\tau = 950$ (solid curve) and $\tau = 1000$ (heavy solid curve).

the Hopf bifurcation in the spike amplitude occurs when $\tau = \tau_H \approx 2066.0$. For four values of τ, we then compute the numerical solution to (1.3) and output the location of the maximum value of v as a function of t. In Fig. 32(a) where $\tau = 850$ and $\tau = 920 < \tau_{TW}$, we show that the spike location has a decaying oscillation about the equilibrium value $x_0 = 0$. Alternatively, in Fig. 32(b) where $\tau = 950 > \tau_{TW}$ and $\tau = 1000$ the oscillations are found to grow. The ultimate fate of these large-scale oscillations in the spike-layer location is unknown.

6 Discussion and Comparisons

In this section we discuss more precisely the relationship between our results and those in the literature. We also summarize which of our results are rigorous, and we list some open technical problems together with a few interesting areas for further research.

A common dimensionless formulation of the Gray-Scott model (cf. [2], [3], [4], [7], [33], and [34]) takes the form

$$V_T = \mathcal{D} V_{XX} - B_d V + U V^2 \,, \qquad 0 < X < L \,, \quad T > 0 \,, \tag{6.1a}$$

$$U_T = U_{XX} + A_d(1-U) - U V^2 \,, \qquad 0 < X < L \,, \quad T > 0 \,, \tag{6.1b}$$

$$U_X = V_X = 0 \,, \qquad X = 0, L \,. \tag{6.1c}$$

In terms of our dimensionless groupings of (1.3), we have that

$$D \equiv \frac{4}{A_d L^2} \,, \qquad \varepsilon^2 \equiv \frac{4\mathcal{D}}{B_d L^2} \,, \qquad \tau \equiv \frac{B_p}{A_p} \,, \qquad A \equiv \frac{\sqrt{A_d}}{B_d} \,. \tag{6.2}$$

Many of the spectral results in [7] and [4] concern the stability of a one-spike solution for the case where $\mathcal{D} \ll 1$ and $\sqrt{A_d}/B_d \ll 1$. Therefore, the results in these works and in ours should closely correspond in what we have labeled as the intermediate parameter regime and the infinite-line problem.

Therefore, the key difference between our work and that of [4], [5], and [7]), is that in our analysis we allow for $k\sqrt{D} = O(1)$. Hence, both the finite domain and the inter-spike coupling is important in our analysis. In contrast, in [4], [5], and [7], the essential analysis concerns the stability of a one-spike solution on an infinite domain. The spectral properties of this infinite-line problem is equivalent to taking the limit $k\sqrt{D} \ll 1$ in our spectral results for the low and intermediate feed-rate regime. In this limit, we have that $\mathcal{A}_{kS} > \mathcal{A}_{kL} > \mathcal{A}_{ke}$, but with $\mathcal{A}_{kS} \to \mathcal{A}_{ke}$. Therefore, when $k\sqrt{D} \ll 1$, there are no competition instabilities unless $\mathcal{A}$ is very close to the saddle-nose bifurcation value $\mathcal{A}_{ke}$. Moreover, in this limit, the Hopf bifurcation value τ_{hL} for $\mathcal{A} > \mathcal{A}_{kL}$ depends only very weakly on k

and on the effect of the finite domain. In the intermediate parameter regime for $\mathcal{A}$, where both the finite domain and the inter-spike coupling do not play a central role, the universal nonlocal eigenvalue problem derived in Proposition 5.2 has been derived previously in [4], and studied rigorously in [5]. In addition, in [4] a scaling law was derived for the stability of periodic solutions on an infinite domain (see equations (2.7) and (5.16) of [4]). Our scaling law for the Hopf bifurcation value τ on a finite domain given in Proposition 5.3 is a new and more explicit result. In addition, our method to rigorously study the universal nonlocal eigenvalue problem is simpler than in [5] in that we need only analyze the spectrum in the right half-plane. Moreover, our stability proof is not computer assisted as in [5] since we do not rely on computations with hypergeometric functions.

The stability results of [24] for one spatial dimension again correspond to a one-spike solution on the infinite line. As discussed in §3.4, our results for the infinite-line problem are consistent with theirs. An advantage of our approach is that our proof of the existence of a Hopf bifurcation value for the infinite-line problem is not computer-assisted as in [24].

Next, we make some remarks concerning the rigor of our approach. Although we have presented only formal derivations of the nonlocal eigenvalue problem (3.12) for the large eigenvalues and (4.23) for the small eigenvalues in Propositions 3.2 and 4.1, respectively, these derivations can be done rigorously, and with the same result, as was done for the GM model in [40]. All of the spectral results of §3.2 have been rigorously established, and our analysis of the universal eigenvalue problem for the intermediate regime in Proposition 5.2 provides a simple alternative proof to the study in [5] of the existence of a Hopf bifurcation value.

There are some key technical problems that await rigorous proof. The one central problem for both the low feed-rate and intermediate regimes is to prove a strict transversal crossing condition to guarantee that the complex conjugate eigenvalues on the imaginary axis when $\tau = \tau_{hL}$ remain in the right half-plane for any $\tau > \tau_{hL}$. For the low feed-rate regime, a second problem is to study the stability of asymmetric k-spike patterns constructed in §2. We conjecture that there are ranges of parameters where these asymmetric patterns are stable with respect to the large eigenvalues, but we expect that these patterns are always unstable with respect to the small eigenvalues.

There are many open problems concerning large-scale behavior away from bifurcation points. In particular, in the low feed-rate regime $\mathcal{A} = O(1)$, an open problem is to analyze the large-scale synchronous oscillatory instabilities and competition instabilities that occur after they are initiated. Another open problem is to determine a wide parameter regime where asynchronous oscillations in the spike amplitudes are possible. It would also be interesting to characterize the dynamics of quasi-equilibrium patterns in the low and intermediate feed-rate regimes. For this problem, we expect that the asymmetric equilibrium patterns should play an important role. Such an analysis of the

dynamics of quasi-equilibrium patterns was done in [13] and [35] for the GM model (1.10) with $\tau = 0$. A two-spike evolution in the intermediate regime on the infinite line was analyzed in [2] and [3]. Finally, since our analysis does not rely on dynamical systems techniques, much of it is readily extended to treat the stability and dynamics of two-dimensional spot patterns for the Gray Scott model. This work is in progress.

Acknowledgements

T. K. was supported by a PGS-B graduate scholarship from NSERC (Canada). M. J. W. thanks the grant support of NSERC, and the IMS of the Chinese University of Hong Kong where most of this paper was written. J. W. thanks the support of RGC of Hong Kong and a direct grant from CUHK. M. J. W. is most grateful to the University of Washington Applied Math group for the generous use of their computer facilities.

References

[1] U. Ascher, R. Christiansen, R. Russell, *Collocation Software for Boundary Value ODE's*, Math. Comp., **33**, (1979), pp. 659-679.

[2] A. Doelman, W. Eckhaus, T. J. Kaper, *Slowly Modulated Two-Pulse Solutions in the Gray-Scott Model I: Asymptotic Construction and Stability*, SIAM J. Appl. Math., **61**, No. 3, (2000), pp. 1080-1102.

[3] A. Doelman, W. Eckhaus, T. J. Kaper, *Slowly Modulated Two-Pulse Solutions in the Gray-Scott Model II: Geometric Theory, Bifurcations, and Splitting Dynamics*, SIAM J. Appl. Math., **61**, No. 6, (2000), pp. 2036-2061.

[4] A. Doelman, R. A. Gardner, T. J. Kaper, *Stability Analysis of Singular Patterns in the 1D Gray-Scott Model: A Matched Asymptotics Approach*, Physica D, **122**, No. 1-4, (1998), pp. 1-36.

[5] A. Doelman, R. A. Gardner, T. Kaper, *A Stability Index Analysis of 1-D Patterns of the Gray Scott Model*, Memoirs of the AMS, **155**, No. 737, (2002).

[6] A. Doelman, T. Kaper, H. van der Ploeg, *Spatially Periodic and Aperiodic Multi-Pulse Patterns in the One-Dimensional Gierer Meinhardt Model*, Methods and Appl. of Analysis, **8**, No. 3, (2001), pp. 387-414.

[7] A. Doelman, T. J. Kaper, P. Zegeling, *Pattern Formation in the One-Dimensional Gray-Scott Model*, Nonlinearity, **10**, No. 2, (1997), pp. 523-563.

[8] A. Doelman, H. van der Ploeg, *Homoclinic Stripe Patterns*, SIAM J. Appl. Dyn. Systems, **1**, No. 1, (2002), pp. 65-104.

[9] A. Gierer, H. Meinhardt, *A Theory of Biological Pattern Formation*, Kybernetik, **12**, (1972), pp. 30–39.

[10] P. Gray, S. K. Scott, *Autocatalytic Reactions in the Isothermal, Continuous Stirred Tank Reactor: Oscillations and Instabilities in the System* $A + 2B \to 3B$, $B \to C$, Chem. Eng. Sci. **39**, (1984), pp. 1087-1097.

[11] L. Harrison, D. Holloway, *Order and Localization in Reaction-Diffusion Pattern*, Physica A, **222**, (1995), pp. 210-233.

[12] T. Ikeda, Y. Nishiura, *Pattern Selection for Two Breathers*, SIAM J. Appl. Math., **54**, No. 1, (1994), pp. 195-230.

[13] D. Iron, M. J. Ward, *The Dynamics of Multi-Spike Solutions to the One-Dimensional Gierer-Meinhardt Model*, SIAM J. Appl. Math., **62**, No. 6, (2002), pp. 1924-1951. (electronic)

[14] D. Iron, M. J. Ward, J. Wei, *The Stability of Spike Solutions to the One-Dimensional Gierer-Meinhardt Model*, Physica D, **150**, No. 1-2, (2001), pp. 25-62.

[15] B. S. Kerner, V. V. Osipov, *Autosolitions: A New Approach to Problem of Self-Organization and Turbulence*, Kluwer Academic Publishers, Dordrecht, (1994).

[16] T. Kolokolnikov, M. Ward, J. Wei, *The Existence and Stability of Spike Equilibria in the One-Dimensional Gray-Scott Model: The Pulse-Splitting Regime*, submitted, Physica D., (2003).

[17] K. J. Lee, W. D. McCormick, J. E. Pearson, H. L. Swinney, *Experimental Observation of Self-Replicating Spots in a Reaction-Diffusion System*, Nature, **369**, (1994), pp. 215-218.

[18] K. J. Lee, H. L. Swinney, *Lamellar Structures and Self-Replicating Spots in a Reaction-Diffusion System*, Phys. Rev. E., **51**, (1995), pp. 1899-1915.

[19] C. S. Lin, W. M. Ni, I. Takagi, *Large Amplitude Stationary Solutions to a Chemotaxis System*, J. Diff. Eq., **72**, (1988), pp. 1-27.

[20] H. Meinhardt, *Models of Biological Pattern Formation*, Academic Press, London, (1982).

[21] H. Meinhardt, *The Algorithmic Beauty of Sea Shells*, Springer-Verlag, Berlin, (1995).

[22] M. Mimura, N. Nishiura, *Layer Oscillations in Reaction Diffusion Systems*, SIAM J. Appl. Math., **49**, No. 2, (1989), pp. 481-514.

[23] C. Muratov, V. V. Osipov, *Traveling Spike Auto-Solitons in the Gray-Scott Model*, Physica D, **155**, No. 1-2, (2001), pp. 112-131.

[24] C. Muratov, V. V. Osipov, *Stability of the Static Spike Autosolitons in the Gray-Scott Model*, SIAM J. Appl. Math., **62**, No. 5, (2002), pp. 1463-1487.

[25] NAG Fortran library Mark 17, routine D03PCF, Numerical Algorithms Group Ltd., Oxford, United Kingdom (1995).

[26] Y. Nishiura, *Global Bifurcational Approach to the Onset of Spatio-Temporal Chaos in Reaction-Diffusion Systems*, Methods and Appl. of Analysis, **8**, No. 2, (2001), pp. 321-332.

[27] Y. Nishiura, *Coexistence of Infinitely Many Stable Solutions to Reaction-Diffusion Equations in the Singular Limit*, in Dynamics Reported: Expositions in Dynamical Systems Volume 3 (editors: C. K. R. T. Jones, U. Kirchgraber), Springer-Verlag, New York, (1995).

[28] Y. Nishiura, T. Teramoto, K. Ueda, *Scattering and Separators in Dissipative Systems*, Phys. Rev. E., **67**, No. 5, 56210, (2003).

[29] Y. Nishiura, D. Ueyama, *A Skeleton Structure of Self-Replicating Dynamics*, Physica D, **130**, No. 1-2, (1999), pp. 73-104.

[30] Y. Nishiura, D. Ueyama, *Spatio-Temporal Chaos for the Gray-Scott Model*, Physica D, **150**, No. 3-4, (2001), pp. 137-162.

[31] J. E. Pearson, *Complex Patterns in a Simple System*, Science, **216**, (1993), pp. 189-192.

[32] V. Petrov, S. K. Scott, K. Showalter, *Excitability, Wave Reflection, and Wave Splitting in a Cubic Autocatalysis Reaction-Diffusion System*, Phil. Trans. Roy. Soc. London, Series A, **347**, (1994), pp. 631-642.

[33] W. N. Reynolds, S. Ponce-Dawson, J. E. Pearson, *Dynamics of Self-Replicating Patterns in Reaction-Diffusion Systems*, Phys. Rev. Lett., **72**, (1994), pp. 2797-2800.

[34] W. N. Reynolds, S. Ponce-Dawson, J. E. Pearson, *Dynamics of Self-Replicating Spots in Reaction-Diffusion Systems*, Phys. Rev. E, **56**, No. 1, (1997), pp. 185-198.

[35] W. Sun, T. Tang, M. J. Ward, J. Wei, *Numerical Challenges for Resolving Spike Dynamics for Two Reaction-Diffusion Systems*, Studies in Appl. Math., **111**, (2003), pp. 41-84.

[36] D. Ueyama, *Dynamics of Self-Replicating Patterns in the One-Dimensional Gray-Scott Model*, Hokkaido Math J., **28**, No. 1, (1999), pp. 175-210.

[37] M. J. Ward, J. Wei, *Asymmetric Spike Patterns for the One-Dimensional Gierer-Meinhardt Model: Equilibria and Stability*, Europ. J. Appl. Math., **13**, No. 3, (2002), pp. 283-320.

[38] M. J. Ward, J. Wei, *Hopf Bifurcations and Oscillatory Instabilities of Spike Solutions for the One-Dimensional Gierer-Meinhardt Model*, Journal of Nonlinear Science, **13**, No. 2, (2003), pp. 209-264.

[39] J. Wei, *On Single Interior Spike Solutions for the Gierer-Meinhardt System: Uniqueness and Stability Estimates*, Europ. J. Appl. Math., **10**, No. 4, (1999), pp. 353-378.

[40] J. Wei, M. Winter, *The Existence and Stability of N-Peaked Solutions*, submitted, Trans. American Math Society, (2002).